

ELECTROCHEMICAL BIOSENSORS FOR PLANT VOLATILE ORGANIC COMPOUNDS

By

YI FANG

(Under the Direction of Ramaraja P. Ramasamy)

ABSTRACT

The increasing measure of agricultural losses due to plant diseases caused by pathogens and pests is becoming a significant problem worldwide in the recent years. In order to produce enough food to support the population growth, early detection of plant diseases is imperative to reduce the crop spoiled during cultivation and harvest. Although many detection methods are available for diseases, they require either expensive instruments, cumbersome procedures or highly skilled operators. These disadvantages limit the applicability of these methods for on-field detection and confine them to the laboratory. Therefore, an early detection method that is different from the traditional practices is highly desired in the agricultural industry. Volatile organic compounds (VOCs) are largely produced by plants when infected by pathogens and / or infested by pests, and can be used as chemical markers for early detection of the onset of plant diseases. Therefore, electrochemical biosensor devices, which are capable of detecting plant diseases through measurement of VOCs, are proposed and established with the motives validated

by the interviews conducted during a NSF funded I-Corps project. A biosensor for detection of 4-ethylguaiacol, a common VOC, was established using metal oxide (TiO_2 and SnO_2) nanoparticles. Another biosensor based on enzyme tyrosinase-immobilized on an electrode was successfully developed for detection of 4-ethylphenol. Methyl salicylate (MeSA), a VOC that plays important role in plant defense system, could be detected using alcohol oxidase / peroxidase-immobilized bi-enzyme biosensor after chemical hydrolysis. Another version of biosensor for MeSA detection was developed using a different bi-enzyme system involving salicylate hydroxylase and tyrosinase, which improved sensitivity ($30.61 \mu\text{A}\cdot\text{cm}^{-2}\cdot\mu\text{M}^{-1}$) and detection limit (13 nM). In addition, a tri-enzymatic biosensor consisting of an esterase in the electrolyte and salicylate hydroxylase / tyrosinase-immobilized screen-printed electrode were also developed for MeSA detection, yielding a sensitivity of $3.10 \mu\text{A}\cdot\text{cm}^{-2}\cdot\mu\text{M}^{-1}$ and limit of detection of 750 nM. The platform for automatic VOC collection and temperature measurement for MeSA detection were developed using Arduino Uno and MOSFET. Finally, the enzymatic kinetic mechanisms were studied by initial rate measurements, and a mathematical model was developed to simulate the performance of the biosensor under various operating conditions.

INDEX WORDS: Plant disease, Volatile organic compounds, 4-ethylguaiacol, 4-ethylphenol, Methyl salicylate, biosensor, enzyme, Arduino Uno, MOSFET, mathematical modeling, enzyme kinetics

ELECTROCHEMICAL BIOSENSORS FOR PLANT VOLATILE ORGANIC COMPOUNDS

by

YI FANG

B.E., Tianjin University of Science and Technology, China, 2010

M.S., Purdue University, U.S., 2012

A Dissertation Submitted to the Graduate Faculty of the University of Georgia in Partial
Fulfillment of the Requirements for the Degree

DOCTOR OF PHILOSOPHY

ATHENS, GEORGIA

2017

© 2017

Yi Fang

All Rights Reserved

ELECTROCHEMICAL BIOSENSORS FOR PLANT VOLATILE ORGANIC COMPOUNDS

by

YI FANG

Major Professor: Ramaraja P. Ramasamy

Committee: Mark A. Eiteman

Glen C. Rains

William B. Whitman

Electronic Version Approved:

Suzanne Barbour

Dean of the Graduate School

The University of Georgia

August 2017

DEDICATION

To my mother, father and grandparents

ACKNOWLEDGEMENTS

I would like to express my sincere gratitude to my Ph.D. supervisor Dr. Ramaraja P. Ramasamy. Since the day I joined in the lab, he has been supporting me throughout my entire career as a Ph.D. student in College of Engineering at University of Georgia. In addition to his support in my research work, he also guided me in multiple aspects such as manuscript writings, patent applications, and other communication skills. Next, I would like to appreciate the help from my Ph.D. committee members: Dr. William B. Whitman, Dr. Mark A. Eiteman and Dr. Glen C. Rains. It was their experiences, suggestions and sincere help that made my research going smoothly. I would like to express my appreciation to Dr. Sarah Lee and Dr. Hannah Bullock for their help in the experiments during my Ph.D work. I would like to thank Dr. Yogeswaran Umasankar, then post-doc in the laboratory, for helping and guiding the design and conduction of the research work when I lacked of research experiences. Also I would like to thank Stefan R. Schulze for his help during I-Corps program. I am very thankful to my laboratory members whom I spent for more than four years – Narendran Sekar and Yan Zhou for not only offering great help during the research work, but also spending the happiest moment with me. Last but not the least; I would like to appreciate all my other friends for helping and supporting me through the course of my Ph.D. work in the United States and China.

TABLE OF CONTENTS

ACKNOWLEDGEMENTS.....	v
CHAPTER	
1. INTRODUCTION.....	1
1.1 Background and significance.....	3
1.2 New methods for disease detection.....	8
1.3 Specific objectives and organization of chapters.....	15
2. DETECTION OF 4-ETHYLGUIAIACOL USING METAL OXIDE NANOPARTICLE – MODIFIED ELECTRODES.....	18
2.1 Introduction of 4-ethylguaiacol and its detection.....	20
2.2 Materials and methods.....	22
2.3 Results and discussion.....	24
2.4 Conclusion.....	35
2.5 Supplementary data.....	35
3. DETECTION OF 4-ETHYLPHENOL USING TYROSINASE – BASED BIOSENSOR.....	38
3.1 Introduction of 4-ethylphenol and its detection.....	40
3.2 Materials and methods.....	42
3.3 Results and discussion.....	45
3.4 Conclusion.....	57

4. DETECTION OF METHYL SALICYLATE USING ALCOHOL OXIDASE / PEROXIDASE – BASED BIOSENSOR.....	58
4.1 Introduction of methyl salicylate and its detection.....	60
4.2 Materials and methods.....	63
4.3 Results and discussion.....	66
4.4 Conclusion.....	83
5. DETECTION OF METHYL SALICYLATE USING SALICYLATE HYDROXYLASE / TYROSINASE – BASED BIOSENSOR.....	84
5.1 Introduction.....	86
5.2 Materials and methods.....	89
5.3 Results and discussion.....	96
5.4 Conclusion.....	117
5.5 Supplementary data.....	118
6. DIRECT DETECTION OF METHYL SALICYLATE USING ESTERASE / SALICYLATE HYDROXYLASE / TYROSINASE – BASED TRIENZYMATIC BIOSENSOR.....	120
6.1 Introduction.....	121
6.2 Materials and methods.....	125
6.3 Results and discussion.....	127
6.4 Conclusion.....	139
6.5 Supplementary data.....	140
7. COMPUTATIONAL MODELING OF BIENZYMATIC BIOSENSOR.....	143
7.1 Introduction.....	144

7.2 Materials and methods.....	145
7.3 Results and discussion.....	148
7.4 Conclusion.....	159
8. COMMERCIALIZATION POTENTIAL FOR A PORTABLE PLANT DISEASE DETECTION SYSTEM.....	160
8.1 Overview and motivation.....	160
8.2 Discover the customer segments and value propositions.....	164
8.3 Market opportunity.....	168
8.4 Conclusion.....	171
9. CONCLUSIONS AND FUTURE DIRECTION.....	172
REFERENCES.....	177
APPENDICES.....	186

CHAPTER 1

INTRODUCTION

This chapter contains text modified from the following publication:

Yi Fang and Ramaraja P. Ramasamy. 2015. *Biosensors* 5: 537-561.
Reprinted here with permission of the publisher.

Abstract

Food losses due to crop infestations and infections from pathogens such as fungi, bacteria and viruses are persistent issues in agriculture for centuries across the globe. In order to reduce the disease-induced damages in crops during cultivation, harvest and postharvest process, as well as improve the productivity and ensure agricultural sustainability, advanced disease detection and prevention in crops are imperative. This chapter reviews the direct and indirect methods for plant disease identification currently used in agriculture. Laboratory-based techniques such as polymerase chain reaction (PCR), immunofluorescence (IF), fluorescence *in-situ* hybridization (FISH), enzyme-linked immunosorbent assay (ELISA), flow cytometry (FCM) and gas chromatography-mass spectroscopy (GC-MS) are some of the direct detection methods. Indirect methods include thermography, fluorescence imaging and hyperspectral techniques. The chapter also provides a comprehensive overview of biosensors based on highly selective bio-recognition elements such as enzyme, antibody, DNA/RNA and bacteriophage as new tool for the early identification of crop diseases. Finally, the application of volatile organic compounds released by diseased plants for plant disease detection is introduced.

Keywords: Food loss, Plant pathogen, Volatile organic compound, Sensor, Enzyme, Antibody, DNA/RNA, Bacteriophage.

1.1 BACKGROUND AND SIGNIFICANCE

1.1.1 Pathogen / Pest-induced food losses

In 1974, World Food Conference defined the word “food security” as the “availability at all times of adequate world basic food supplies to sustain a steady expansion of food consumption and to offset fluctuations in production and prices” (Clay 2002). Since then, food security, determined by worldwide food supply and consumption has aroused public awareness. The previous reports have indicated that over one billion people were suffering from various type of malnutrition due to lack of food supply while another two billion people do not have access to sufficient nutrients or vitamins that are required for daily life (Conway 2012). The enormous population growth in recent decades has put another challenge for food security. The demand for food will likely continue to increase for another 40 years and additional 70 % production will be required to satisfy the need by 2050 (Godfray, Beddington et al. 2010). In addition to population growth, food scarcity is also attributed to increased farming for biofuel generation and decreased agricultural land for food production due to industrial land use (Vidal 2007, Mason 2013). Although food insufficiency could be attributed to the aforementioned reasons, food damages caused by pest infestations play an important role in agricultural losses throughout the world. In addition to the pest infestation, agricultural losses are also attributed to infection from plant pathogens such as bacteria, viruses and fungi. Just in the United States, pest infestation and plant pathogen cause more than 40 billion dollars of economic losses and 20 % to 40 % of production losses annually (Pimentel, Zuniga et al. 2005, Roberts, Schimmelpfennig et al. 2006, Savary, Ficke et al. 2012). For example, 12 % of maize, barley, rice and soybean, 24 % of groundnuts and potatoes, 50 % to 80 % of wheat and cotton are estimated to be lost to pest infestation and pathogen-induced diseases (Oerke 2006). Apart from the agricultural losses during cultivation,

post-cultivation losses due to plant diseases and sub-standard quality during storage and transportation are estimated to be 30 % to 40 % (Pimentel, Zuniga et al. 2005, Roberts, Schimmelpfennig et al. 2006). Furthermore, pest infestation and pathogen-induced plant diseases not only do damage to the pre- and post-cultivated crops directly, but they also drive the excessive and unnecessary application of chemicals such as pesticides, bactericide and fungicide which increase grower costs and eventually crop prices. Therefore, an early detection method of pest infestation and pathogen-induced diseases is imperative to minimize the damages during crop production and transportation as well as to minimize the spraying of chemicals to enable precision agriculture, decrease the cost of food production and ensure agricultural sustainability.

1.1.2 Current detection methods

Pest infestation and plant disease early detection can be realized through both direct and indirect methods based on the detection target. In direct detection, molecular, biological and serological methods are applied to detect and identify the pathogens such as bacteria, viruses and fungi. On the other hand, indirect methods to detect and identify the diseases through the various parameters and symptoms such as the change of morphology, temperature, transpiration rate and the volatile organic compounds (VOCs) released by plants under infestation and infection have also been investigated widely by various researchers.

1.1.2.1 Direct detection methods

Deoxyribonucleic acid (DNA) is a molecule that carries the genetic instructions used in the growth, development, functioning and reproduction of all organisms including bacteria, viruses and fungi. Therefore, detection and identification of the sequence of pathogenic DNA provide the firsthand information to predict the plant diseases. A Nobel Prize was awarded to Kary Banks

Mullis in 1993 for the development of amplification of nucleic acid sequences using the technique of polymerase chain reaction (PCR). Based on the high fidelity of DNA hybridization and replication, PCR was initially used to identify the bacteria and viruses causing disease (Cai, Caswell et al. 2014). With the development of the technique, advanced PCR-based methods such as reversed-transcription PCR (RT-PCR), multiplex PCR, real-time PCR, have also been introduced for plant pathogen identification due to their high sensitivity and specificity, on-site application and rapid diagnosis (Osioy 1998, Pallisgaard, Hokland et al. 1998, James 1999, Williams, Blake et al. 1999, Nassuth, Pollari et al. 2000, Schaad and Frederick 2002, Lievens, Brouwer et al. 2006).

In addition to PCR, another molecular detection technique called fluorescence *in-situ* hybridization (FISH) has been used to detect bacteria, viruses and fungi (Kempf, Trebesius et al. 2000, Hijri 2009, Klot, Kontsedalov et al. 2014). Single-cell sensitivity can be achieved due to the high affinity and specificity of the DNA probe. Other microscopy-based technique such as immunofluorescence (IF) is reported for the analyses of microbial samples to detect infections in plant tissue. For this technique, specific antibody conjugated with a fluorescent dye is used to visualize the distribution of target molecule throughout the sample (Dewey and Marshall 1996).

Serological technique such as flow cytometry (FCM), a laser-based optical method used for cell counting and sorting, biomarker detection and protein engineering, is also reported for characterization of bacterial DNA and fungal spores (Chitarra and Van Den Bulk 2003).

In addition to aforementioned DNA-based techniques, an antigen-antibody conjugation-based technique such as enzyme-linked immunosorbent assay (ELISA) is also widely used for identification of diseases based on color change in the assay (Clark and Adams 1977). In this method, antibodies conjugated with enzyme are made to bind specifically with the target

epitopes of the antigens from the bacteria, viruses and fungi of interest. The color change upon the conjugation of antibody and targeted antigen is used to visualize the presence of the pathogen. The performance of ELISA has improved significantly with the development of specific monoclonal antibodies, for which J.F. Kohler and C. Milstein were awarded the Nobel Prize in 1984 (Clark and Adams 1977, Gorris, Alarcon et al. 1994, López, Bertolini et al. 2003).

1.1.2.2 Indirect detection methods

Apart from the direct methods discussed above, indirect methods, based on measuring plant stress symptoms that profile plant diseases, have also been developed for identification of biotic stresses (*e.g.* pathogenic diseases) during crop cultivation. In this regard, new types of sensors providing detailed information based on different electromagnetic spectra have been developed for prediction of plant health condition. Thermography, fluorescence imaging and hyperspectral imaging are the most favorable techniques for crop health prediction.

Previous reports have demonstrated that loss of water regulated by stomata is affected by infection, which renders the temperature change of plant leaves. Thermography allows imaging the surface temperature of plant leaves and canopies, which can be scaled up for disease monitoring without external temperature influences (Lindenthal, Steiner et al. 2005, Oerke, Steiner et al. 2006, Chaerle, Leinonen et al. 2007, Stoll, Schultz et al. 2008, Oerke, Fröhling et al. 2011).

In addition to transpiration rate, the photosynthetic apparatus and photosynthetic electron transport chain will also be affected upon plant pathogen infection. Therefore, fluorescence imaging, based on measuring chlorophyll fluorescence of the leaves as a function of the incident light and the change in the fluorescence parameters, can also be used for plant disease prediction.

This technique has already been approved for precise detection of leaf rust and powdery mildew infections in wheat through the analyses of temporal and spatial variations of chlorophyll fluorescence (Lindenthal 2005).

Recently, hyperspectral imaging has been used for plant phenotyping and crop disease identification in large-scale agriculture. Hyperspectral imaging over a wide range of spectrum from 350 to 2500 nm can be used for obtaining useful information about plant health parameters. Furthermore, more accurate and detailed information about plant health across a large crop field can be realized through the hyperspectral imaging camera which facilitates the 3D data collection (Mahlein, Oerke et al. 2012). By measuring the reflectance changes resulting from the changes in biophysical and biochemical characteristics due to infestation and infection, hyperspectral techniques have been widely used for plant disease detection such as *Magnaporthe grisea* infection of rice, *Phytophthora infestans* infection of tomato and *Venturia inaequalis* infection of apple trees (Kobayashi, Kanda et al. 2001, Zhang, Qin et al. 2003, Delalieux, Van Aardt et al. 2007).

1.1.3 Limitations of current detection methods

Although various detection techniques have been developed which have many advantages – robust, rapid and detailed information, *etc.*, the application for on-site detection of plant diseases is still limited to laboratory-based methods due to a variety of reasons. First, many direct detection methods, such as fluorescence *in-situ* hybridization, immunofluorescence, flow cytometry, as well as indirect methods such as thermography, fluorescence imaging and hyperspectral imaging, require expensive instruments which greatly increase the cost of disease detection. Second, the requirement of cumbersome instruments implies that no on-site measurements can be carried out; therefore, real-time information of plant health situation cannot

be provided by those techniques. Additionally, other techniques, such as PCR and ELISA, which do not need cumbersome instruments, still require professional technicians to carry out the detection which further confines their application to laboratory use. Therefore, a portable, robust and user-friendly device to predict plant disease is needed.

1.2 NEW METHODS FOR DISEASE DETECTION

1.2.1 Volatile organic compounds as disease signature

Different from the direct and indirect methods of plant disease detection mentioned above, a non-optical based indirect method by profiling the volatile signatures released by the plant is also reported. Volatile organic compounds (VOCs), as phytohormones for communication and self-defense, will be released by the plant upon infestation and infection. VOCs released by diseased plants are different according to different pathogens as well as from those under healthy condition. Thus, they are highly indicative of biotic stress types experienced by the plants (Fang, Umasankar et al. 2014). For example, an infection by *Phytophthora cactorum*, the fungus that causes crown rot in strawberries, results in the production of two specific VOCs – 4-ethylguaiacol and 4-ethylphenol, in addition to other VOCs that also released under healthy conditions. Other VOCs such as *cis*-3-hexenol, *cis*-hexenyl acetate and hexyl acetate are reported to be released by green leaf plants under pathogenic and mechanical damages (*i.e.* herbivore infestation and lawn mowing) (Umasankar, Rains et al. 2012). Analyses of these VOCs provide the firsthand of information for identifying the nature of the infestations and infections (Fang, Umasankar et al. 2014). Compared to other indirect methods like thermography and fluorescence imaging, the type of released VOCs provides detailed information of the type and severity of infections and infestations.

1.2.2 Current analysis of volatile organic compounds

Gas chromatography (GC), a common type of chromatography used in analytical chemistry for separating and analyzing compounds that can be vaporized without decomposition, has been used for analyzing the presence of the specific VOC that is indicative of a particular disease (Jansen, Hofstee et al. 2009). To enhance the separation and analysis performance of VOCs, the technique mass-spectrometry (MS) is often combined with GC, forming GC-MS to identify unknown compounds in volatile samples produced by diseased plants (Isidorov, Zenkevich et al. 1985, Kesselmeier and Staudt 1999, Perera, Marriott et al. 2002). Compared to other optical-based detection methods, such as thermography and fluorescence, GC-MS provides more detailed and specific information which allows the prediction of certain plant diseases. It also allows the detection of diseases in different evolving stages based on the quantity of specific VOCs that plants produce. However, the application of GC-MS is still confined to the laboratory study due to its non-portability. Even though some portable devices have been developed recently, the requirement of sophisticated operator and analyzer still does not facilitate the use of GC-MS by farmers.

1.2.3 Portable electrochemical biosensors

Unlike the bulky instruments mentioned above, sensors are portable, non-destructive and can provide real-time measurements. Among different types of sensors, the application of sensors has been developed as one of the most potential techniques due to its advantages such as portability, low-cost, high accuracy, rapid detection, real time applicability, robustness, ultra-low limits of detection and high specificity when biosensors are fabricated with electrodes modified by bio-recognition elements (Bakker 2004). Biosensors, with modification of bio-recognition elements

such as DNA and antibody, have been developed for plant disease detection based on the reaction of the bio-recognition elements and the target analyte (Sadanandom and Napier 2010).

1.2.3.1 Antibody-based biosensor

Antibodies are versatile and suitable for diverse immunosensing fabrications. Antibody-based biosensors allow rapid and selective detection of a range of pathogens; therefore, they have been used for food safety monitoring. With the similar mechanism, antibody-based biosensors hold great potential for agricultural plant pathogen detection. The biosensors enable the pathogen detection in air, water, soil and seeds with different platforms for greenhouse, on-field and postharvest storage processes and distributors of crops and fruits (Skottrup, Nicolaisen et al. 2008). The principle of establishing an antibody-based biosensor lies in the coupling of specific antibody with a transducer, which converts the binding event (the binding of the antibody immobilized on the electrode with the antigen of interest) to a signal that can be interpreted. Most antibody-based electrochemical biosensors can be categorized into four types: amperometric, potentiometric, impedimetric and conductometric, which use electric current, potential change, impedance change and conductance change, respectively, as the interpreting signal (Leonard, Hearty et al. 2003, Palchetti and Mascini 2008, Byrne, Stack et al. 2009). Other electrochemical techniques, such as quartz crystal microbalance (QCM) based on the measurement of the change in frequency of a quartz crystal resonator upon specific binding of antibody with antigen, are also reported. In addition to electrochemical techniques, other non-electrochemical transducers for affinity biosensing have been developed and reported such as surface plasmon resonance (SPR) and cantilever. During the past decades, many studies have been published demonstrating the capability of antibody-based biosensors for plant pathogen detection such as *Cowpea mosaic virus*, *Tobacco mosaic virus*, *Lettuce mosaic virus*, *Puccinia*

striiformis, *Phytophthora infestans*, orchid viruses and *Aspergillus niger* (Eun, Huang et al. 2002, Dickert, Hayden et al. 2004, Torrance, Ziegler et al. 2006, Candresse, Lot et al. 2007, Nugaeva, Gfeller et al. 2007, Skottrup, Frøkiær et al. 2007, Skottrup, Hearty et al. 2007).

1.2.3.2 DNA/RNA-based biosensor

Being different from antibody-based biosensors where hydrophobic, ionic and hydrogen bonds play a role in the stabilization of antibody-antigen complex, DNA binding is dependent upon the formation of stable hydrogen bonds between DNA (or RNA) chains. Therefore, a new type of affinity biosensor uses nucleic acid fragments as bio-recognition elements for pathogen detection has been developed. The detection of a specific DNA sequence is of significance in a variety of applications such as clinical genetic disease detection, environmental protection, horticulture, and foodborne disease analysis. Due to the possibility of detection at molecular level and the fidelity of DNA hybridization, DNA-based biosensor enables early detection of diseases before any visual symptoms appear. The application of specific DNA-based biosensors has been widely used for detection of bacteria, viruses and fungi. Similar to antibody-based biosensor, DNA-based biosensor can also be classified by the type of the transducers. The common type of electrochemical biosensor is amperometric, which measures the current change with constant applied potential upon the DNA hybridization. Other types of biosensors, such as piezoelectric DNA biosensors that detect the analyte using a quartz crystal that oscillates at a specific frequency at an applied oscillating potential, have been reported for detection of two orchids viruses – *Cymbidium mosaic virus* (CymMV) and *Odontoglossum ringspot virus* (ORSV) (Eun, Huang et al. 2002). Transducers other than electrochemical are also reported, such as molecular beacons (MB) and surface plasmon resonance (SPR) for the detection of orchid viruses and *Fusarium culmorum* (Eun and Wong 2000, Zezza, Pascale et al. 2006).

1.2.3.3 Applications of enzymatic biosensor

In addition to the affinity biosensor based on the specific combination of DNA and antibody / antigen, enzymes as bio-recognition element can provide highly selective detection of the target analyte due to the high specificity of enzyme-substrate combination. Therefore, the detection of analyte can be realized through the bio-electrocatalytic reaction between the target and electrode, which results in an amperometric signal (*i.e.* current) that can be used for quantitative detection of the analyte. The amperometric signal used for detection can be obtained through the electrode either via directed electron transfer (DET) from the enzyme-electrode interaction or via mediated electron transfer (MET) from the intermediate-electrode interaction (Figure 1.1).

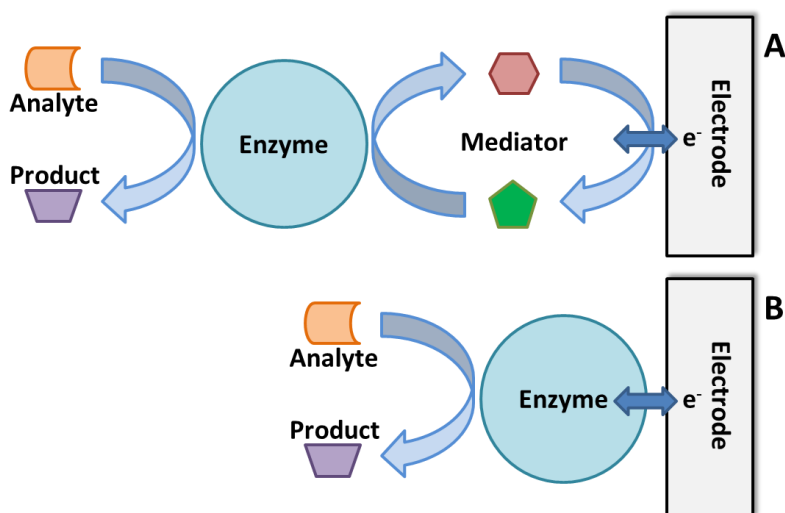


Figure 1.1: Schematic illustration of enzymatic biosensor based on mediated electron transfer (A) and direct electron transfer (B). Not drawn to scale.

Unlike other types of biosensors which are mostly confined in the laboratory, the successful commercialization of glucose biosensor for personal diabetes monitors has marked the real application of electrochemical biosensors (Ronkainen, Halsall et al. 2010). A similar biosensing methodology can be adopted for plant pathogen / infestation detection, food quality control and environmental monitoring (El-Ansary and Faddah 2010). The detection of plant pathogen /

infestation can be realized through the detection of VOCs, as long as the plant VOCs could be solubilized in a compatible liquid electrolyte. Previous research has demonstrated several phytohormones released by the plants upon infections / infestations can react by a redox enzyme to generate electrochemically active compounds (Sponzel and Hedden 2010). In addition to the detection based on analyte-enzyme reaction, enzyme activity can also be deactivated by common phytohormones such as auxin, cytokinins and gibberellins which indicate plant health. For example, GA-2-oxidase can be inhibited by gibberellin which provides the potential for gibberellin biosensor based on the inhibition of the enzyme (Thomas, Phillips et al. 1999).

1.2.3.4 Bacteriophage-based biosensor

Composed of protein capsid that encapsulates DNA or RNA genome, bacteriophage infects bacteria, replicates within the bacterial cell and finally lyses the bacterial host to propagate. Being able to lyse the bacterial, bacteriophages have been widely studied and used in phage therapy to cure bacteria-caused infections and other diseases (Mc Grath and van Sinderen 2007). In addition to phage therapy, bacteriophage also emerges as an alternative bio-recognition element for biosensor development due to its highly specific binding with bacteria (Neufeld, Schwartz-Mittelmann et al. 2003, Brigati and Petrenko 2005, Kretzer, Lehmann et al. 2007). The detection of bacteria can be carried out through the impedance change of charge transfer reactions at the interface of electrode upon specific binding of bacteriophage and target bacteria. Recently, a bacteriophage-based diagnostic assay for detecting and identifying *Pseudomonas cannabina* pv. *Alisalensis* from infected plants was reported by D. A. Schofield (Schofield, Bull et al. 2013).

1.2.4 Application of nanomaterials to biosensor platforms

Recent breakthroughs in nanotechnology enable the preparation of various nanoparticles and other nanostructures with few technical hurdles. Displaying fascinating physical, chemical, electronic, and optical properties, nanoparticles synthesized with different types of materials have been used for electronics and sensing applications (Shipway, Katz et al. 2000). The popularity of nanomaterials for sensor development can be explained by the platform-property provided by the nanomaterials. Nanomaterials such as carbon nanotubes (CNTs) are easy to modify with the cross-linkers, providing the assembly of bio-recognition element (*e.g.* antibody and enzyme introduced above), and eventually increase the specificity of detection. In addition, limit of detection can be improved due to the high surface area and high conductivity resulting from the nanomaterials used for sensor fabrication. The nanomaterials used for biosensor construction include metal oxide nanoparticles, quantum dots, carbon nanomaterials such as CNTs, carbon nanorods, graphene, as well as polymeric nanomaterials. With the development of biosensors based on antibody, DNA and enzyme as recognition molecules as introduced above, the nanomaterials could be used as support materials for recognition molecules and in some cases transducers for the development of biosensors for detecting plant diseases. An example of this is the detection of *Xanthomonas axonopodis*, which causes bacterial spot disease. Other materials such as gold nanoparticles have been widely used due to their high electroactivity and electronic conductivity for electron transfer (Cao, Ye et al. 2011, Mandler and Kraus-Ophir 2011).

1.3 SPECIFIC OBJECTIVES AND ORGANIZATION OF CHAPTERS

Chapter 2: DETECTION OF 4-ETHYLGUAIACOL USING METAL OXIDE NANOPARTICLE – MODIFIED ELECTRODES

- a) Exploration of the application of metal oxide nanoparticles such as titanium oxide (TiO_2) and tin oxide (SnO_2) nanoparticles in sensor development for VOC detections.
- b) Characterization of metal oxide-based sensor for 4-ethylguaiacol detection including sensitivity and limit of detection.
- c) Characterization of the specificity of the sensor through interference study.
- d) Evaluation of the applicability of the sensor through simulated sample study.

Chapter 3: DETECTION OF 4-ETHYLPHENOL USING TYROSINASE – BASED BIOSENSOR

- a) Exploration of the enzyme reaction mechanism of tyrosinase, and its electrochemical mechanism for biosensor application.
- b) Exploration of the application of enzyme cross-linking technique for biosensor fabrication.
- c) Characterization of tyrosinase-based biosensor for 4-ethylphenol detection including sensitivity and limit of detection.
- d) Characterization of the specificity of the biosensor through interference study.
- e) Evaluation of the applicability of the biosensor through simulated sample study.

Chapter 4: DETECTION OF METHYL SALICYLATE USING ALCOHOL OXIDASE / PEROXIDASE – BASED BIOSENSOR.

- a) Exploration of the enzyme reaction mechanism of alcohol oxidase and horseradish peroxidase, and their electrochemical mechanism for biosensor application.
- b) Characterization of alcohol oxidase / peroxidase-based biosensor for methyl salicylate detection including sensitivity and limit of detection.
- c) Characterization of the specificity of the biosensor through interference study.
- d) Evaluation of the applicability of the biosensor through simulated sample study.

Chapter 5: DETECTION OF METHYL SALICYLATE USING SALICYLATE HYDROXYLASE / TYROSINASE – BASED BIOSENSOR

- a) Expression of salicylate hydroxylase from *Escherichia coli* transformed with recombinant plasmid DNA.
- b) Purification of salicylate hydroxylase from the crude extract, and derivation of purification table for enzymatic parameters.
- c) Exploration of the enzyme reaction mechanism of salicylate hydroxylase and tyrosinase, and their electrochemical mechanism for biosensor application
- d) Characterization of salicylate hydroxylase / tyrosinase-based biosensor for methyl salicylate detection including sensitivity and limit of detection.
- e) Characterization of the specificity of the biosensor through interference study.
- f) Evaluation of the applicability of the biosensor through simulated sample study.

Chapter 6: DIRECT DETECTION OF METHYL SALICYLATE USING ESTERASE / SALICYLATE HYDROXYLASE / TYROSINASE – BASED TRIENZYMATIC BIOSENSOR

- a) Exploration the application of esterase for methyl salicylate hydrolysis.

- b) Application of esterase for tri-enzymatic biosensor for direct methyl salicylate detection, and the determination of sensitivity and limit of detection.
- c) Design the computer-controlled platform for pre-concentration system using MOSFET, and the computer hardware Arduino Uno.

Chapter 7: MATHEMATICAL MODELING OF BI-ENZYMATIC BIOSENSOR

- a) Prediction of the mechanisms of the enzyme kinetics.
- b) Derivation and calculation of the enzymatic kinetics parameters for mathematical modeling.
- c) Development of a principle mathematical model to describe the performance of the bi-enzymatic biosensor by incorporating the influence of enzyme activity, concentration of salicylate and other reactants.
- d) Discussion the governing equations, initial conditions and boundary conditions for the modelling.

Chapter 8: COMMERCIALIZATION POTENTIAL FOR A PORTABLE PLANT DISEASE DETECTION SYSTEM.

- a) Development of value proposition and customer segregation on business model canvas.
- b) Preparation of both phone and in-person interviews to validate the value proposition and customer segregation proposed on business model canvas.
- c) Pivots from the results of the interview to re-establish the desired value proposition and potential customer segregation.
- d) Investigation of the potential market of early detection devices for plant disease detection.

Chapter 9: CONCLUSIONS AND FUTURE DIRECTIONS.

CHAPTER 2

DETECTION OF 4-ETHYLGUAIACOL USING METAL OXIDE NANOPARTICLE – MODIFIED ELECTRODES

This chapter contains text modified from the following publication:

Yi Fang, Yogeswaran Umasankar, and Ramaraja P. Ramasamy. 2014. *Analyst* 139: 3804-3810.
Reprinted here with permission of the publisher.

Abstract

Nanoparticles of titanium oxide (TiO₂) or tin oxide (SnO₂) on screen-printed (SP) carbon electrodes have been developed in this chapter for evaluating their potential in the electrochemical sensing of volatiles in fruits and plants. These metal oxide (MO_x) nanoparticle-modified electrodes possess high sensitivity and low limit of detection for the detection of 4-ethylguaiacol, a fingerprint compound present in the volatile signature of fruits and plants infected with a pathogenic fungus *Phytophthora cactorum*. The electroanalytical data obtained using cyclic voltammetry and differential pulse voltammetry showed that both TiO₂ and SnO₂ modified electrodes exhibited high sensitivity (0.17 – 0.19 μA·cm⁻²·μM⁻¹) and low limit of detection (35 – 62 nM) for 4-ethylguaiacol detection. The amperometric detection was highly repeatable with RSD values ranging from 2.48 to 4.85 %. The interference studies show that other common plant volatiles do not interfere in the amperometric detection signal of 4-ethylguaiacol. The results demonstrate that metal oxides are a reasonable alternation to expensive electrode materials such as gold or platinum for amperometric sensor applications.

Keywords: Titanium oxide, Tin oxide, Volatile organic compound, 4-Ethylguaiacol, Sensor, *Phytophthora cactorum*.

2.1 INTRODUCTION OF 4-ETHYLGUAIACOL AND ITS DETECTION

2.1.1 4-Ethylguaiacol in plant diseases

Leather rot, commonly known as crown rot, has been identified as a plant disease caused by pathogenic fungus *Phytophthora cactorum* and results in the infection of a variety of cucurbit crops as well as other crops such as strawberry in the southeastern United States (Jeleń, Krawczyk et al. 2005). It is estimated that up to half of 1.3 million tons of strawberries produced in the United States are affected by this disease which either results in total-loss or down grade of the products every year (Ellis and Grove 1983). Due to the high cost of strawberry cultivation, there is an imperative and ever-increasing demand for advanced crown rot detection prior to the appearance of the symptoms. As many plants, volatile organic compounds (VOCs) with distinctive unpleasant odor will be produced upon infection of *Phytophthora cactorum*. One such symbolic VOC is 4-ethylguaiacol (Jeleń, Krawczyk et al. 2005). Therefore, detection of 4-ethylguaiacol released by strawberries infected by *Phytophthora cactorum* will be a useful indication for confirmation of leather rot disease. However, in order to fulfill the capability of early stage detection, the detection method should possess ultra-low limit of detection for 4-ethylguaiacol.

2.1.2 Current methods for 4-ethylguaiacol detection

A variety of methods have been established for 4-ethylguaiacol detection including gas chromatography-mass spectrometry (GC-MS), head space solid phase microextraction (SPME) and high performance liquid chromatography (HPLC)-diode array detection (DAD)-fluorescence (Pollnitz, Pardon et al. 2000, Martorell, Martí et al. 2002, Caboni, Sarais et al. 2007, Rayne and Eggers 2007). Although a variety of methods have been established for 4-ethylguaiacol detection

as other VOCs introduced in Chapter 1, all those methods require detailed operation conducted by professional technicians, thus cannot be widely used for real-time analysis.

2.1.3 Application of metal oxide nanoparticles for sensor fabrication

Electrochemical sensing of VOCs released from diseased plants is a popular technique for non-destructive, real-time detection of target plant diseases as introduced in Chapter 1. Amperometric electrochemical sensor possesses high sensitivity enables rapid detection, thus, are suitable for the field application. Although application of bio-recognition improved sensitivity, non-enzymatic biosensors that used for plant VOC detection have also been reported before (Zhuang, Su et al. 2008, Suneesh, Chandhini et al. 2013). Gold nanoparticle-based electrochemical sensors for VOCs such as methyl salicylate (MeSA), *cis*-3-hexen-1-ol, hexyl acetate and *cis*-3-hexen-1-yl acetate were reported by Ramasamy's group (Umasankar, Rains et al. 2012, Umasankar and Ramasamy 2013). While gold nanoparticles and carbon nanotubes / rods have been widely used for sensor application, metal oxide (MO_x)-based sensors have not been fully understood for electrochemical transducers. The rationale for adopting metal oxide nanoparticles in this project is due to the advantages over other commonly used materials. The advantages are: (1) metal oxide nanoparticles are catalysts for dehydrogenation of alcoholic compounds (*e.g.* aliphatic alcohols, acetic acid, *etc.*), which could enhance the VOC reaction on the electrode, and further increase the current generated (de Lacy Costello, Ewen et al. 1999), (2) compared to other noble metal materials like gold and silver, metal oxides such as titanium oxide, tin oxide, zinc oxide are inexpensive, which decreased the cost of fabrication (Diebold 2003), (3) some metal oxides have a large band gap (greater than 3.3 eV) which make them suitable for amperometric signal generation in aqueous solution, and (4) compared to other materials, the preparation method for metal oxide nanoparticles in required size and shape is easier. In this

project, two commonly used metal oxides namely titanium (IV) oxide (TiO₂) and tin (IV) oxide (SnO₂) are proposed as electrochemical detection elements for amperometric sensing. The conceptual illustration of the detection mechanism can be found in Figure 2.1. Screen-printed carbon (SP) electrodes are modified with nanoparticles of TiO₂ and SnO₂ and used for electrochemical detection of 4-ethylguaiaicol in simulated fruit volatile samples with three-electrode system.

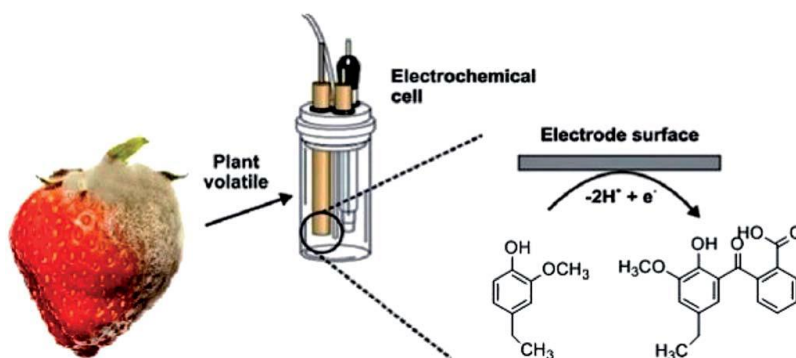


Figure 2.1: Schematic illustration of 4-ethylguaiaicol detection on metal oxide modified screen-printed carbon electrode with three-electrode system. Not drawn to scale.

2.2 MATERIALS AND METHODS

2.2.1 Materials

Tin (IV) oxide (<100 nm) and titanium (IV) oxide (~21 nm) nanoparticles purchased from Sigma-Aldrich were used to prepare nanoparticle suspensions. 4-ethylguaiaicol from Frinton Laboratory, Inc (New Jersey, USA) was used as received. 4-ethylphenol from Sigma-Aldrich and other compounds such as *cis*-3-hexenol, hexyl acetate, *cis*-hexen-1-yl acetate, 3-octanone and 1-octen-3-ol purchased from TCI America (Portland, Oregon, USA) were used as received in interference study and simulated sample studies. All chemicals in the project are of analytical grade. All the aqueous solutions in this project were prepared in 18.2 MΩ nanopure de-ionized

(DI) water. The electrolyte of 0.1 M potassium hydrogen phthalate (KHP), pH 4, was prepared to carry out all electrochemical experiments. All solutions were deoxygenated by purging with nitrogen gas for 15 min prior to each set of experiments.

2.2.2 Apparatus

Cyclic voltammetry (CV) and differential pulse voltammetry (DPV) were performed using a CHI model 920 c potentiostat. A conventional three-electrode cell system was applied for all the electrochemical measurements. Three-electrode system consists of a working electrode, a screen-printed (SP) carbon electrode modified with TiO₂ or SnO₂ nanoparticles, a 3 M Ag/AgCl reference electrode and a platinum wire as a counter electrode. All experiments were carried out at temperature of 25 ± 2 °C.

2.2.3 Electrode preparation

TiO₂ and SnO₂ nanoparticle suspensions were prepared by ultrasonication of 1 mg of the respective nanoparticles in 1 mL DI water. The TiO₂ and SnO₂ nanoparticle-based SP electrodes were prepared by drop-casting 18 μL (three steps of 6 μL addition) of the nanoparticle suspension on the SP electrode, followed by drying up at 70 °C oven. CV and DPV were performed in a 10 mL electrochemical cell containing N₂-saturated 0.1 M KHP solution for TiO₂- or SnO₂-modified SP electrodes. Voltammetry was scanned from -0.1 V to 0.7 V for both CV and DPV. The scan rate for CV is 20 mV/s while the increment, amplitude, pulse width and pulse period are 4 mV, 50 mV, 0.2 s and 0.5 s for DPV.

2.3 RESULTS AND DISCUSSION

2.3.1 Electrochemical response of 4-ethylguaiacol on MO_x -modified SP electrodes

CV was applied to characterize the MO_x -modified electrodes in the presence and absence of 4-ethylguaiacol. Although acidic conditions favor 4-ethylguaiacol oxidation, a pH 4 of electrolyte was used in this project to avoid reaction between metal oxides and electrolyte such as sulfuric acid and hydrochloric acid. The cyclic voltammograms of SnO_2 - and TiO_2 -modified electrodes in the presence and absence of 4-ethylguaiacol are shown in Figure 2.2, and the results demonstrate the better sensitivity of 4-ethylguaiacol detection by MO_x -modified SP electrode compared with an unmodified SP electrode (Figure 2.S1A).

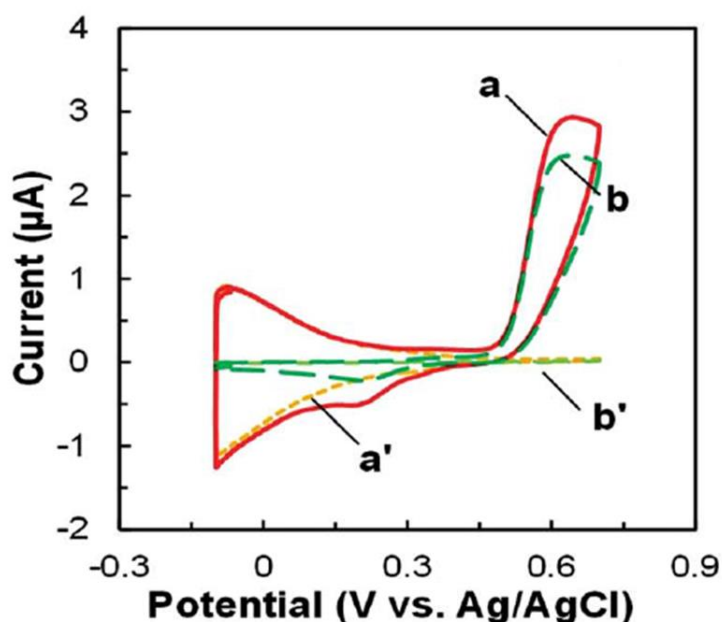
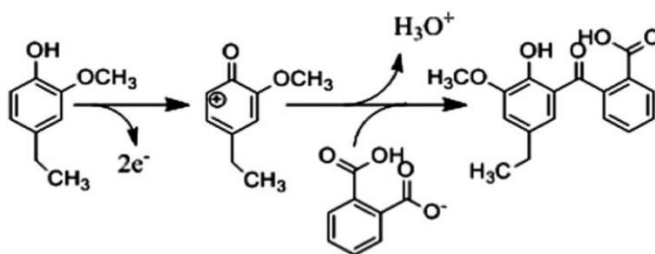


Figure 2.2: CV responses of SnO_2 -SP (a and a') and TiO_2 -SP (b and b') with (a and b) and without (a' and b') the presence of 0.17 mM 4-ethylguaiacol.

In the absence of 4-ethylguaiacol, TiO_2 -SP displayed no redox activity while a significant broad redox peak in the potential window from -0.1 V to 0.4 V was observed, which can be explained

by the adsorption and desorption of phthalate ions, a better known behavior for SnO₂ in KHP electrolyte (Armstrong, Lin et al. 1976, Lian, Zhu et al. 2011). In the presence of 4-ethylguaiacol, both TiO₂- and SnO₂-SP exhibited irreversible redox peaks – oxidation peak at 0.62 V and reduction peak at 0.2 V. As the electrode was scanned with anodic wave, 4-ethylguaiacol underwent a two-step electrochemical reaction as shown below:



With the higher applied potential, 4-ethylguaiacol tends to lose two electrons and forms the phenoxy radical intermediate, which then reacts with phthalate anion in the electrolyte to form a benzoic acid derivative and H₃O⁺ (Sadana and Katzer 1974, Comninellis and Pulgarin 1993). The irreversible reduction peak in the cyclic voltammograms at 0.2 V could be attributed to the reduction of the phenoxy radical to 4-ethylguaiacol. These results demonstrate that the 4-ethylguaiacol is reversible when the potentials are below 0.2 V.

Comparison of the 4-ethylguaiacol oxidation on both TiO₂-SP and SnO₂-SP indicates similar current, thus the effect of 4-ethylguaiacol concentration on both electrodes were studied and reported in Figure 2.3.

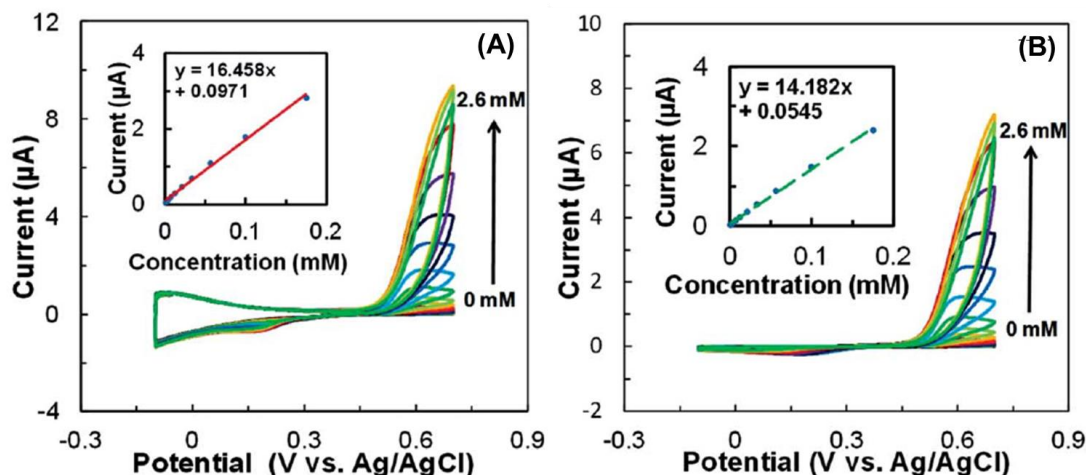


Figure 2.3: Concentration effect of 4-ethylguaiacol at SnO₂-SP (A) and TiO₂-SP (B) electrodes using CV.

The stepwise increase of 4-ethylguaiacol concentration from 0.2 μ M to 2.6 mM in the electrochemical cell was achieved by addition of 4-ethylguaiacol from series of standard concentrations. The lowest concentration was determined based on the noticeable increase in oxidation current upon the incremental addition of 4-ethylguaiacol, and the upper limit was chosen based on the rate of decrease in the oxidation current during subsequent additions of 4-ethylguaiacol. The CV results in Figure 2.3 demonstrate that an increase in the concentration of 4-ethylguaiacol leads to an increase of the oxidation peak current (I_{pa}) of 4-ethylguaiacol oxidation on both SnO₂- and TiO₂-SPs. The initial response to 4-ethylguaiacol additions displayed a potential shift in oxidation peak potential (E_{pa}) from 0.62 V to 0.7 V, which could be explained by the increase in acidity of the electrolyte due to more H₃O⁺ produced during the increase of 4-ethylguaiacol. The electrochemical parameters of the sensors for 4-ethylguaiacol detection such as sensitivity, limit of detection (LOD), and limit of quantification (LOQ) at the signal to noise ratio (S/N ratio) of 3 from both SnO₂- and TiO₂-SP, can be calculated from the following equations.

$$\text{Sensitivity} = \frac{\text{slope of calibration curve (A} \cdot \text{M}^{-1}\text{)}}{\text{Area of electrode (cm}^2\text{)}}$$

$$\text{LOD} = 3.3 \times \frac{\text{Standard deviation of peak current in absence of analyte (A)}}{\text{Slope of calibration curve (A} \cdot \text{M}^{-1}\text{)}}$$

$$\text{LOQ} = 10 \times \frac{\text{Standard deviation of peak current in absence of analyte (A)}}{\text{Slope of calibration curve (A} \cdot \text{M}^{-1}\text{)}}$$

Comparison of the sensitivity values obtained from both SnO₂-SP and TiO₂-SP obtained from cyclic voltammetry are given in Table 2.1 below.

Table 2.1: Comparison of sensitivity, linear range, LOD and LOQ for 4-ethylguaiacol detection at SnO₂-SP and TiO₂-SP electrode using CV and differential pulse voltammetry (DPV).

Electrode	Technique	E_{pc} (V)	Linear range (R^2)	Sensitivity ($\mu\text{A} \cdot \text{cm}^{-2} \cdot \mu\text{M}^{-1}$)	LOD (nM)	LOQ (nM)
SnO ₂ -SP	CV	0.62	0.6 μM – 0.17 mM (0.9954)	0.23	82	249
	DPV	0.54	0.2 μM – 0.1 mM (0.9932)	0.17	62	188
TiO ₂ -SP	CV	0.62	0.6 μM – 0.17 mM (0.9972)	0.20	126	382
	DPV	0.54	0.2 μM – 0.1 mM (0.9934)	0.19	35	106

The results reveal that SnO₂-SP electrode displayed higher sensitivity for 4-ethylguaiacol detection and lower LOD and LOQ compared to TiO₂-SP electrode. Although CV provides a firsthand electrochemical information of the system, the sensor application requires either constant potential amperometry (CPA) or pulse-based electrochemical technique to eliminate the noise caused by the capacitance and resistance in order to improve the detection accuracy (*i.e.* LOD and LOQ) (Settle 1997). Therefore, differential pulse voltammetry (DPV) was used in a

similar matter to CV for 4-ethylguaicol detection between -0.1 V to 0.7 V. Compared to unmodified SP electrode, both SnO₂-SP and TiO₂-SP electrodes displayed a higher sensitivity for 4-ethylguaicol detection (Figure 2.S1B). Similar to CV, DPV also displayed peaks in the absence of 4-ethylguaicol on SnO₂-SP due to the absorption and desorption of phthalate ions. In the presence of 4-ethylguaicol, the oxidation peak was observed at 0.54 V (E_{pa}) with similar I_{pa} 's for both electrodes as shown in Figure 2.4.

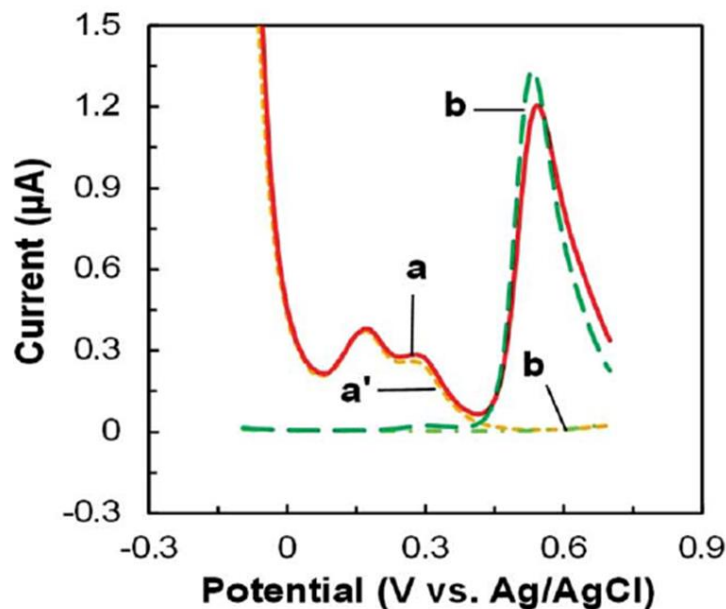


Figure 2.4: DPV responses of SnO₂-SP (a and a') and TiO₂-SP (b and b') with (a and b) and without (a' and b') the presence of 0.17 mM 4-ethylguaicol.

The characteristic oxidation peak of 4-ethylguaicol for both SnO₂- and TiO₂-SP was similar to those of CV with a ~ 0.05 V negative shift due to the applied amplitude (0.05 V) during DPV measurements. The peak currents (I_{pa}) for 4-ethylguaicol oxidation were also observed increased with the concentration increased from 0, 0.2 µM to 1.5 mM on both electrodes as shown in Figure 2.5.

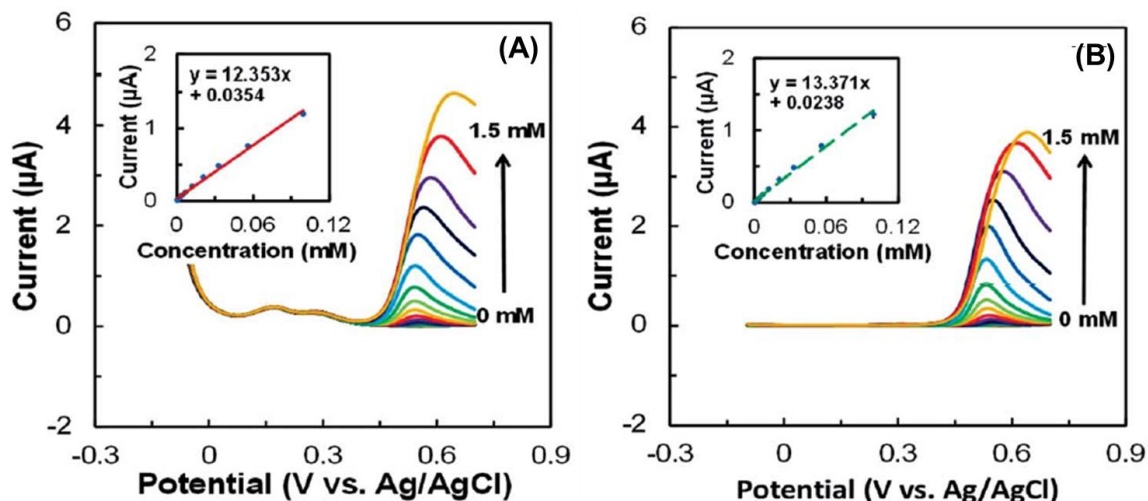


Figure 2.5: Concentration effect of 4-ethylguaiacol on SnO₂-SP (A) and TiO₂-SP (B) electrodes using DPV.

The insets of Figure 2.5 show a linear dependency of I_{pa} on concentration. The empirical electrochemical parameters derived from DPV data are also given in Table 2.1 for comparison with CV. Due to the elimination of capacitance as well as the adsorption-desorption effect in DPV (Figure 2.S2), the results demonstrated lower sensitivity, but better detection and quantification limits for both SnO₂- and TiO₂-SP electrodes for DPV compared to their corresponding CV values. Among the two modified SP electrodes, TiO₂-SP exhibited better sensitivity and limit of detection compared to those of SnO₂-SP according to DPV, although the difference is not significant (Table 2.1). DPV data are better representative of the sensing characteristic of the electrodes due to the elimination of parasitic currents from the true oxidation response of 4-ethylguaiacol. The results demonstrate that both SnO₂- and TiO₂-SP electrodes could be used to fabricate an electrochemical sensor for 4-ethylguaiacol detection at concentrations that relevant to typical infected fruit volatiles.

2.3.2 Repeatability and stability studies

Eight SnO₂- and TiO₂-SP electrodes were prepared using the same protocol introduced and tested for 4-ethylguaiacol oxidation using DPV for repeatability evaluation. The DPV peak currents (I_{pa}) at 0.54 V, for all eight electrodes were measured at a concentration of 2.5 mM. The high concentration was chosen to ensure that even subtle changes in the measured currents can be visualized, and the results (Table 2.S1) showed that the peak currents for all eight electrodes varied between 2.5 % and 4.9 % for SnO₂-SP and TiO₂-SP electrodes, respectively. The low variability indicates the high repeatability from both electrodes.

The stability of SnO₂-SP and TiO₂-SP electrodes was tested in a series of DPV experiments at a 4-ethylguaiacol concentration of 2.5 mM on consecutive days for a period of 15 days. The I_{pa} from the 4-ethylguaiacol oxidation in DPVs was measured on day 1, 2, 3, 4, 5, 6, 10 and 15, and the percentage of current retained compared to the current collected in day 1 was calculated. The results (Table 2.S2) showed a loss of activity of up to 67 % and 81 % for SnO₂-SP and TiO₂-SP electrode, respectively, in 15 days. Though the currents decreased significantly over time, the rate of decrease slowed down after the first two days without large decrease beyond the first week. The loss in stability could be attributed to the formation of surface oxides and other adsorption effects from the ions present in the electrolyte that tend to impact the electrode over the long term.

2.3.3 Interference study of 4-ethylguaiacol detection

The plant volatiles contain other chemical compounds that are non-specific to the infection that are often released in equivalent or even higher concentrations compared to 4-ethylguaiacol. A representative set of such VOCs was selected, and their interference effects on 4-ethylguaiacol

detection were studied using DPV. The compounds including 4-ethylphenol, 3-octanone, 1-octen-3-ol, *cis*-3-hexenol, hexyl acetate and *cis*-hexen-1-yl acetate were tested in the interference study. Among them 4-ethylphenol, 3-octanone and 1-octen-3-ol are present in the chemical signature of the pathogen *Phytophthora cactorum* induced infection (Jeleń, Krawczyk et al. 2005). The other three compounds (*cis*-3-hexenol, hexyl acetate and *cis*-hexen-1-yl acetate) are green leaf volatiles (GLVs) common to most plants (Umasankar, Rains et al. 2012). The fungi-infected plants typically release 0.2 μM of 3-octanone, 0.2 μM of 1-octen-3-ol, 10 μM of *cis*-3-hexenol, 1.2 μM of hexyl acetate and 20 μM of *cis*-hexen-1-yl acetate (Sunesson, Vaes et al. 1995, Umasankar, Rains et al. 2012). Therefore, concentrations higher than those abovementioned were used in our interference study to simulate an extreme case of the production of the interference compounds. The experiments were conducted separately for each of 6 interference compounds where the low concentration of 4-ethylguaiacol (20.8 μM) was used (still within the linear range of the detection obtained from DPV), and the DPV signal was measured as introduced in Section 2.3.1. Then corresponding concentrations of the interference compounds, as shown in Table 2.2 were mixed with 20.8 μM 4-ethylguaiacol and measured using DPV. The currents collected from both pure 20.8 μM 4-ethylguaiacol and 20.8 μM 4-ethylguaiacol with interference compounds were compared for the interference study. The results demonstrated that the characteristic oxidation peak for 4-ethylguaiacol can be found even in the presence of interference compounds as shown in Figure 2.6 for both $\text{SnO}_2\text{-SP}$ and $\text{TiO}_2\text{-SP}$ electrodes.

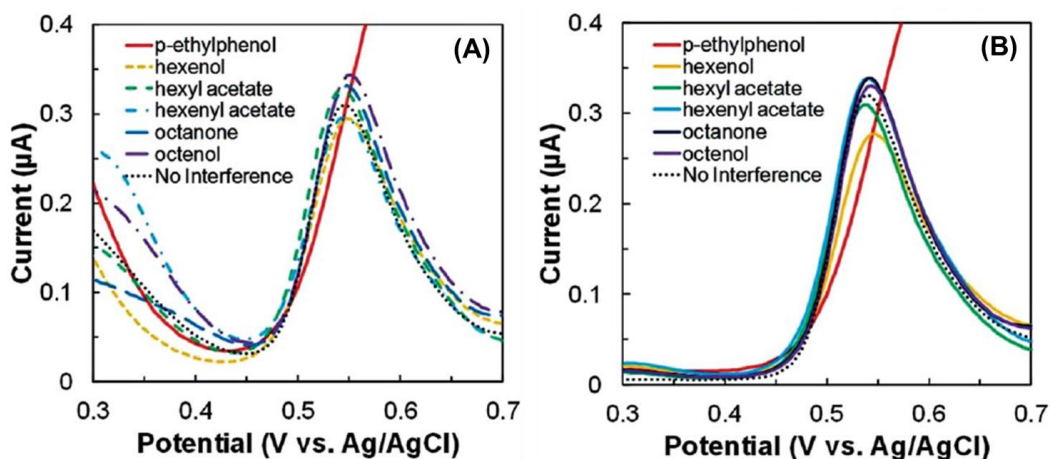


Figure 2.6: Interference study of 20.8 μM 4-ethylguaiacol with 6 different interference compounds: 4-ethylphenol, *cis*-3-hexen-1-ol, hexyl acetate and *cis*-3-hexen-1-yl acetate, 3-octanone and 1-octen-3-ol on $\text{SnO}_2\text{-SP}$ (A) and $\text{TiO}_2\text{-SP}$ (B) electrode by DPV.

For 4-ethylphenol, higher concentration (2.5 mM) was used due to the larger production rate compared to other VOCs to simulate the extreme case. On both $\text{SnO}_2\text{-SP}$ and $\text{TiO}_2\text{-SP}$ electrodes, the addition of 4-ethylphenol significantly changed the DPV wave above 0.55 V but not at the peak oxidation potential (0.54 V) of 4-ethylguaiacol (Figure 2.6), therefore an oxidation peak greater than 0.55 V for 4-ethylphenol can be speculated. As shown by the calculated I_{pa} values in Table 2.2 below, 4-ethylphenol interference was limited to $\pm 6.7\%$ for $\text{SnO}_2\text{-SP}$ and $\text{TiO}_2\text{-SP}$. Less than 2% interference was found on the 4-ethylguaiacol signal on $\text{TiO}_2\text{-SP}$ while up to 12% interference was observed on $\text{SnO}_2\text{-SP}$ with the addition of *cis*-hexen-1-yl acetate. Other compounds such as 3-octanone, 1-octen-3-ol, *cis*-3-hexenol or hexyl acetate did not display any significant interference on 4-ethylguaiacol detection. The interference study above demonstrates that metal oxide-modified SP electrodes can be used for 4-ethylguaiacol detection without significantly affected by the interference compounds.

Table 2.2: Interference study of 20.8 μM 4-ethylguaiacol with 6 different compounds: 4-ethylphenol, *cis*-3-hexen-1-ol, hexyl acetate and *cis*-3-hexen-1-yl acetate, 3-octanone and 1-octen-3-ol by DPV.

	Interference Compound	Conc. of Interference compound	Current w/o Interference compound (μA)	Current with Interference compound (μA)	Found (%)
SnO ₂ -SP	4-ethylphenol	2.5 mM	0.3212	0.3533	110.01
	<i>cis</i> -3-hexen-1-ol	32 μM	0.2906	0.2956	101.73
	hexyl acetate	2 μM	0.3249	0.3274	100.76
	<i>cis</i> -3-hexen-1-yl acetate	32 μM	0.2672	0.2972	111.21
	3-octanone	2 μM	0.3301	0.3320	100.57
	1-octen-3-ol	2 μM	0.3381	0.3436	101.62
TiO ₂ -SP	4-ethylphenol	2.5 mM	0.3459	0.3227	93.30
	<i>cis</i> -3-hexen-1-ol	32 μM	0.2783	0.2782	99.96
	hexyl acetate	2 μM	0.3060	0.3092	101.08
	<i>cis</i> -3-hexen-1-yl acetate	32 μM	0.3336	0.3400	101.91
	3-octanone	2 μM	0.3334	0.3391	101.70
	1-octen-3-ol	2 μM	0.3278	0.3308	100.90

2.3.4 Detection of 4-ethylguaiacol in simulated fruit volatiles

The capability of SnO₂-SP and TiO₂-SP for the determination of 4-ethylguaiacol in real infected samples was evaluated using a simulated chemical mixture that mimics the composition of real fruit volatile signature. As discussed in the interference study section, the chemical compounds released that need to be detected can be both from the volatiles from the pathogen itself and from the green leaf volatiles. Therefore, two sets of samples were used for simulations: (i) only infected fruit volatiles and (ii) both infected fruit volatiles and GLVs. The composition of (i) was 2.5 mM 4-ethylguaiacol, 2.5 mM 4-ethylphenol, 2.5 μM 3-octanone and 2.5 μM 1-octen-3-ol. The composition of (ii) contains all (i) in addition to 10 μM *cis*-3-hexen-1-ol, 1.25 μM hexyl

acetate and 25 μM *cis*-hexen-1-yl acetate. The concentrations were chosen based on the composition of typical VOC signature of *P. cactorum* infection (Sunesson, Vaes et al. 1995, Jeleń, Krawczyk et al. 2005). The experiments were conducted using DPV, and the 4-ethylguaiacol in four different concentrations was measured as control. The currents collected from four concentrations of 4-ethylguaiacol, and from both simulation samples (contains the same concentration of 4-ethylguaiacol as in control), and the calculated recovery are listed in Table 2.3.

Table 2.3: Simulated sample study using typical chemicals released by *P. cactorum* infected plants with same concentration of 4-ethylguaiacol as control.

Electrode	Sample	Currents from 4-ethylguaiacol (μA)	Currents from simulated sample (μA)	Recovery (%)
SnO ₂ -SP	Infected fruit	0.0455	0.0417	91.65
		0.1942	0.1947	100.26
		0.4816	0.4789	99.44
		1.5130	1.5110	99.87
	Infected fruit with plant	0.0455	0.0495	108.79
		0.1942	0.2011	103.55
		0.4816	0.4816	100.00
		1.5130	1.4890	98.41
TiO ₂ -SP	Infected fruit	0.0421	0.0389	92.40
		0.2218	0.2019	91.03
		0.5017	0.5021	100.08
		1.6210	1.6500	101.79
	Infected fruit with plant	0.0421	0.0399	94.77
		0.2218	0.2070	93.33
		0.5017	0.5067	101.00
		1.6210	1.6420	101.30

The results from Table 2.3 shows that the recovery of 4-ethylguaiacol detection from both simulated samples varies from 91 % to 101 % when compared to standard 4-ethylguaiacol control experiments, therefore, demonstrating both electrodes – SnO₂-SP and TiO₂-SP can be used for 4-ethylguaiacol determination during the on-field test in the future.

2.4 CONCLUSION

Both SnO₂-SP and TiO₂-SP electrodes have been demonstrated to exhibit similar detection capabilities for 4-ethylguaiacol based on amperometric determination. Ultra-low limit of detection was achieved by both metal-oxide nanoparticles-based electrodes and DPV measurements. Both electrodes exhibited good repeatability towards 4-ethylguaiacol detection. CV and DPV data along with chemical reactions established here elucidate the electrochemical reaction mechanisms pertaining to the amperometric sensing of 4-ethylguaiacol. The electroanalytical data presented in this chapter can be used for both qualitative and quantitative determination of 4-ethylguaiacol. The synthetic sample studies presented here illustrate the approach for the development of 4-ethylguaiacol detection during the initial stages of *Phytophthora cactorum* infection.

2.5 SUPPLEMENTARY DATA

Table 2.S1: Repeatability of 4-ethylguaiacol (2.5 mM) oxidation at SnO₂-SP and TiO₂-SP electrodes.

	SnO ₂ -SP electrode	TiO ₂ -SP electrode
Electrode 1	7.24	5.66
Electrode 2	7.10	5.39
Electrode 3	6.88	5.68
Electrode 4	7.02	6.01
Electrode 5	7.10	6.22

Electrode 6	7.34	6.16
Electrode 7	7.41	6.13
Electrode 8	7.39	6.14
Average	7.18	5.92
Standard Deviation	0.18	0.29
RSD	2.48 %	4.85 %

Table 2.S2: Stability of SnO₂-SP and TiO₂-SP electrodes for the determination of 2.5 mM 4-ethylguaiacol.

Days	SnO ₂ -SP			TiO ₂ -SP		
	Current retained (%)	Std.	Relative Std. (%)	Current retained (%)	Std.	Relative Std. (%)
1	100			100		
2	72.40	0.92	16.01	60.94	1.21	24.27
3	53.11	1.29	25.60	49.52	1.34	30.81
4	53.80	1.27	27.30	33.11	1.53	40.48
5	40.04	1.39	32.57	22.52	1.67	50.48
6	32.01	1.50	38.24	16.60	1.74	59.57
10	29.49	1.54	42.45	17.41	1.74	65.28
15	32.19	1.53	44.19	18.99	1.70	68.56

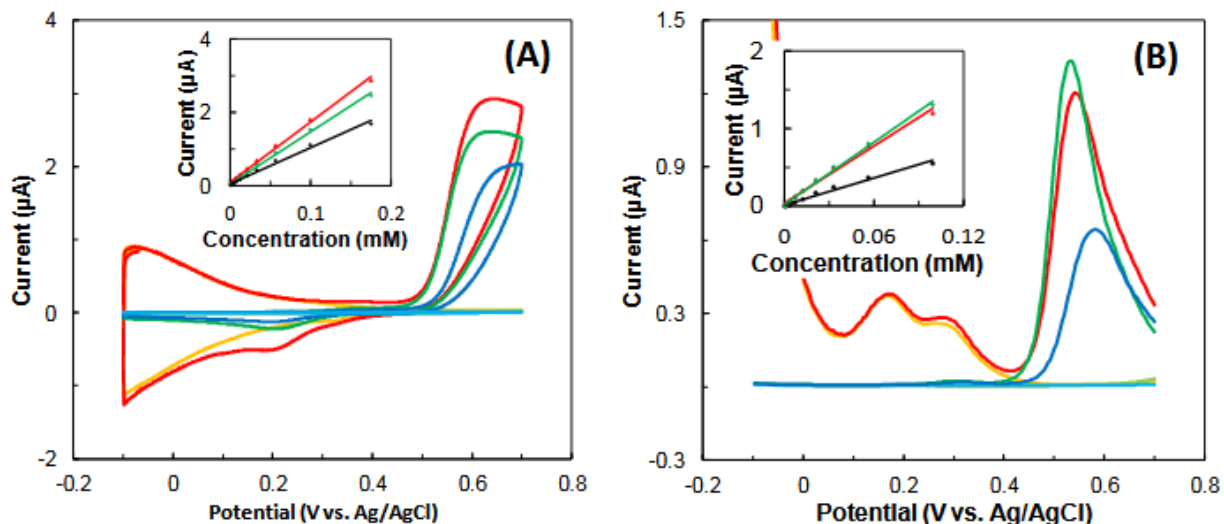


Figure 2.S1: CV (A) and DPV (B) response of 0.17 mM and 0.1 mM 4-ethylguaiacol respectively, at SnO₂-modified (red), TiO₂-modified (green) and unmodified (blue) SP electrodes. The insets display the concentration effect within the linear range of 4-ethylguaiacol oxidation at SnO₂ (red), TiO₂ (green) and unmodified SP (blue).

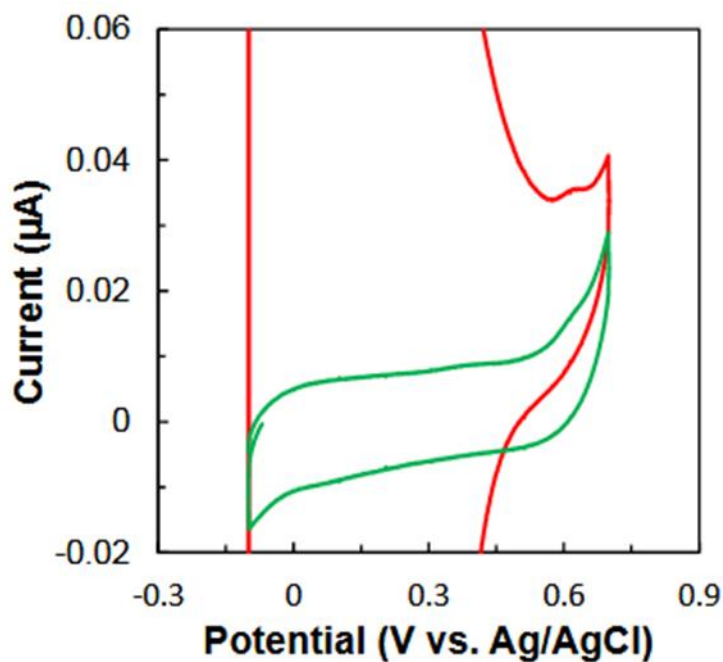


Figure 2.S2: CV response of SnO₂- (red) and TiO₂-modified (green) SP electrodes without 4-ethylguaiacol.

CHAPTER 3

DETECTION OF 4-ETHYLPHENOL USING TYROSINASE – BASED BIOSENSOR

This chapter contains text modified from the following publication:

Yi Fang and Ramaraja P. Ramasamy. 2016. *ECS Journal of Solid State Science and Technology* 5: M3054-M3059.

Reprinted here with permission of the publisher.

Abstract

Volatile organic compounds released by fruits and plants have been suggested as indicators of biotic stress in fruits and plants due to pathogen (fungi, bacteria and viruses) infection. Among the hundreds of volatile organic compounds, 4-ethylphenol has been reported as one of the most important volatile organic compounds released by strawberries upon pathogen infection. Detection of these compounds in a highly selective manner would help in the identification of infected fruits. In this chapter, a novel enzymatic biosensor made of tyrosinase-modified carbon nanotube (CNT) electrode has been developed for the detection of 4-ethylphenol. Cyclic voltammetry and constant potential amperometry were used for 4-ethylphenol detection. High sensitivity of $4.0 \pm 0.5 \mu\text{A}\cdot\text{cm}^{-2}\cdot\mu\text{M}^{-1}$ with measurement range of 0 – 100 μM ($R^2 = 0.9956$) was achieved by constant potential amperometry for the detection of 4-ethylphenol. Limit of detection and limit of quantification were determined as $0.10 \pm 0.02 \mu\text{M}$ and $0.29 \pm 0.07 \mu\text{M}$ respectively. Stability studies showed satisfactory performance of the biosensor for one time disposable use. The biosensor experience little interference from other compounds typically present in strawberry volatile signatures. The studies using synthetic analyte revealed that the biosensor could be reliably used for 4-ethylphenol detection in practical application.

Keywords: Volatile organic compound, 4-Ethylphenol, Enzyme, Tyrosinase, Biosensor, *Phytophthora cactorum*.

3.1 INTRODUCTION OF 4-ETHYLPHENOL AND ITS DETECTION

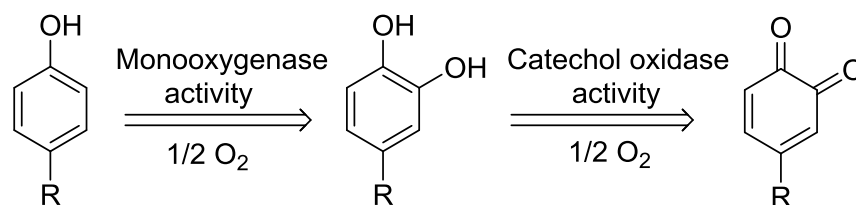
3.1.1 4-Ethylphenol as signature compound for disease detection

As introduced in the Chapter 2, *Phytophthora cactorum* is a very common phytopathogenic fungus that causes leather rot (crown rot) diseases in strawberries and other crops during growth and post-harvesting procedure. In addition to 4-ethylguaiacol released by the infected strawberry plants, the other such characteristic volatile marker or volatile organic compound (VOC) that produced by infected strawberry plants is 4-ethylphenol (Jeleń, Krawczyk et al. 2005, Nieminen, Neubauer et al. 2008, Ubeda, Callejon et al. 2012, Ubeda, San-Juan et al. 2012). Therefore, detection of 4-ethylphenol produced by infected plants in ultra-low quantities could be used as an effective indicator of crown rot stresses of strawberry plants. In the similar situation, GC-MS and other techniques, although provide both qualitative and quantitative measurements for 4-ethylphenol detection, are primarily limited in the laboratory study rather than for real on-field application due to their complicated operation, analysis and requirements for professional technicians to operate.

3.1.2 Application of enzyme tyrosinase as biorecognition element

Although application of nanomaterials, such as metal oxide nanoparticles, are introduced in Chapter 2, bio-recognition element, such as enzyme, is also widely used for sensor development to improve the biosensor performance such as sensitivity, limit of detection (LOD) and specificity due to the catalytic function towards substrate reaction and the enzyme specificity. In this project, we report the successful development of tyrosinase-immobilized biosensor for 4-ethylphenol selective detection. Tyrosinase (TYR) is an effective enzyme that catalyzes catechol, L-dopa and other *o*-phenols to their corresponding *o*-quinone derivatives due to its catechol

oxidase activity (Espín, Varón et al. 2000, de Faria, Rotuno Moure et al. 2007). Additionally, tyrosinase is also able to catalyze monophenols to *o*-phenols due to its monooxygenase activity, and oxidize the *o*-phenol intermediates to *o*-quinones due to its catechol oxidase activity (Rassaei, Cui et al. 2012).



In this project, TYR is used and biochemically oxidized 4-ethylphenol to produce 4-ethyl-1,2-benzoquinone on the electrode surface. The amperometric detection is realized through the electrochemical reduction of 4-ethyl-1,2-benzoquinone to 4-ethyl-1,2-hydroquinone (Cosnier and Innocent 1993). The schematic illustration can be explained by Figure 3.1.

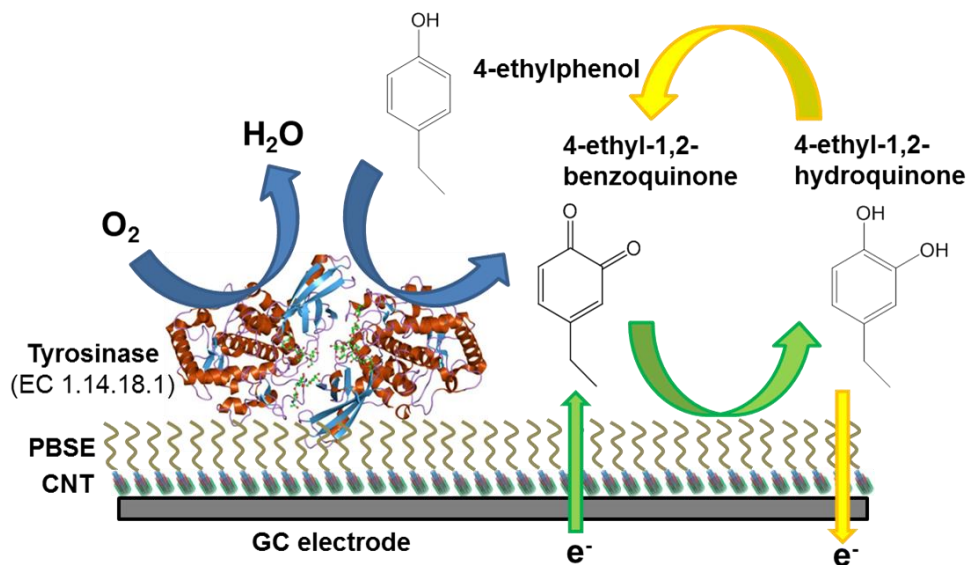


Figure 3.1: Schematic illustration of 4-ethylphenol detection on TYR-immobilized biosensor. Not drawn to scale. 4-Ethylphenol can be oxidized to 4-ethyl-1,2-benzoquinone by TYR and the detection is based on the electrochemical reduction of 4-ethyl-1,2-benzoquinone to 4-ethyl-1,2-hydroquinone (green arrows), the thus formed 4-ethyl-1,2-benzoquinone can be oxidized to 4-ethyl-1,2-benzoquinone (yellow arrows).

TYR catalyzes the conversion of 4-ethylphenol to 4-ethyl-1,2-benzoquinone in the presence of oxygen. The amperometric detection can be realized through the electrochemical reduction of 4-ethyl-1,2-benzoquinone to 4-ethyl-1,2-hydroquinone on the multiwalled carbon nanotubes (MWCNTs) modified on the electrode surface as both enzyme immobilization platform and as amperometric transducer due to its high electrical conductivity and large surface area. TYR is immobilized through a well-developed molecular tethering approach.

3.2 MATERIALS AND METHODS

3.2.1 Materials

Tyrosinase (E.C. 1.14.18.1) purified from mushroom (lyophilized powder, ≥ 1000 U/mg solid) was purchased from Sigma-Aldrich (St. Louis, Missouri, USA) and used as it is. Multiwalled carbon nanotubes (MWCNTs) were obtained from DropSens (Llanera, Spain). Pyrenebutanoic acid succinimidyl ester (PBSE) was obtained from Ana Spec Inc. (Fremont, California, USA) as cross-linker for enzyme immobilization. Dimethylformamide (DMF) and sodium salicylate were purchased from Acros Organics (Pittsburgh, Pennsylvania, USA). 4-ethylphenol was purchased from Aldrich (St. Louis, Missouri, USA). Methanol and ethanol were purchased directly from Fisher Scientific (Pittsburg, Pennsylvania, USA) and Electron Microscopy Sciences (Hatfield, Pennsylvania, USA) respectively. Acetone was obtained from BDH chemicals (London, United Kingdom). 4-ethylguaiacol was obtained from Frinton Laboratories, Inc. (Hainesport, New Jersey, USA). Other chemicals used as interferants such as ethyl butyrate and methyl hexanoate were purchased from Fluka (St. Louis, Missouri, USA) and methyl butyrate, 2-pentanone and 2-heptanone were obtained from Aldrich Chemicals (St. Louis, Missouri, USA). All experiments were carried out in 0.1 M potassium phosphate buffer, pH 6.6 as electrolyte (Bru, Sanchez -

Ferrer et al. 1989). All solutions were prepared in 18.2 M Ω nanopure de-ionized (DI) water. All solutions were oxygenated by purging oxygen for 15 min.

3.2.2 Apparatus

CH Instrument 920 c potentiostat was used to carry out all the experiments including cyclic voltammetry (CV) and constant potential amperometry (CPA). A conventional three-electrode system consisting of a 3M Ag/AgCl as a reference electrode, a platinum wire as a counter electrode, and a glassy-carbon (GC) electrode with diameter of 3 mm obtained from Pine Instruments were used to perform all electrochemical experiments in a custom made 10 mL glass electrochemical reaction cell. All experiments were carried out at the ambient temperature of 25 \pm 2 $^{\circ}$ C.

3.2.3 Electrode preparation

GC electrode was first polished with 0.05 μ m alumina powder for 5 min before each experiment. Polished electrode was then cleaned with ultrasonication for 5 minutes and rinsed with DI water to remove adhered polishing power on the electrode before the modification and immobilization with CNTs and enzymes shown in Figure 3.2. MWCNT suspension was prepared by suspend 1 mg of nanotube in 1 mL of DMF, followed by sonication for an hour with power and frequency of 75 W and 20 kHz.

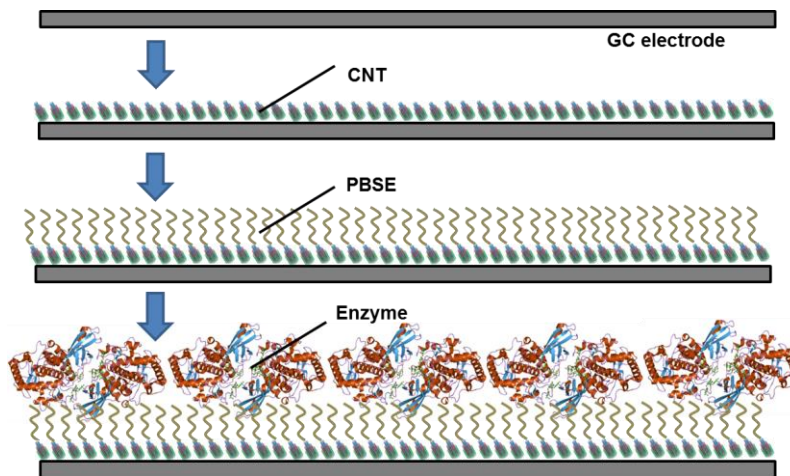


Figure 3.2: Schematic illustration of electrode modification with MWCNT, PBSE and TYR. Not drawn to scale. The GC electrode was first polished and drop-casted with CNT suspension and dried in the oven at the temperature of 70 °C. The electrode is then modified with PBSE as cross-linker before the enzyme is used for the immobilization.

16 μL of CNT suspension were drop-casted on the polished GC electrode (in 8 steps of 2 μL) followed by drying up in 70 °C oven. CNT modified electrode was placed on ice before 2 μL of 10 mM PBSE (in DMF) solution was added. The electrode was then incubated for 15 min to allow non-covalent binding of CNT with pyrene group of PBSE. The electrode was then rinsed with DMF and 0.1 M potassium phosphate buffer, pH 6.6 to remove excessive non-binded PBSE. TYR solution was prepared by dissolving 5 mg of TYR lyophilized powder in 1 mL 20 mM potassium phosphate buffer (PB), pH 6.6. 5 μL of TYR solution was drop-casted on CNT/PBSE modified electrode and the electrode was incubated on ice for 30 min to allow covalent binding of PBSE and TYR. Excessive TYR was rinsed off with 20 mM PB, pH 6.6.

3.2.4 Electrochemical measurement

Cyclic voltammetry (CV) for CNT modified electrode without immobilization of TYR was performed from 0.2 to 0.7 V with scan rate of 20 mV/s and sampling interval of 0.001 V in presence of 0.1 M PB, pH 6.6 as electrolyte. For CNT modified electrode with immobilization of

TYR, CV was performed from -0.2 to 0.4 V with scan rate of 20 mV/s and sampling interval of 1 mV in presence of 0.1 M PB, pH 6.6. Initial potential for both non-TYR immobilized electrode and TYR-immobilized electrode during CPA was set to 0.13 V with sampling interval of 0.1 s. During CPA, the electrodes were stabilized for 2 min before each addition of 4-ethylphenol to the electrolyte in the electrochemical cell with 1 min interval.

3.3 RESULTS AND DISCUSSION

3.3.1 Determination of voltage window for 4-ethylphenol detection

Previous research has already indicated that electrochemical oxidation of para-phenols can be achieved on GC electrode with the window potential between 0.2 and 0.7 V (Enache and Oliveira-Brett 2011). CV was first used to determine the potential window for reliable detection of 4-ethylphenol through the electrochemical reduction of 4-ethyl-1,2-benzoquinone (BQ). The concept is described in Figure 3.1, and the electrochemical effect of modification of CNT on electrode can be explained on Figure 3.3.

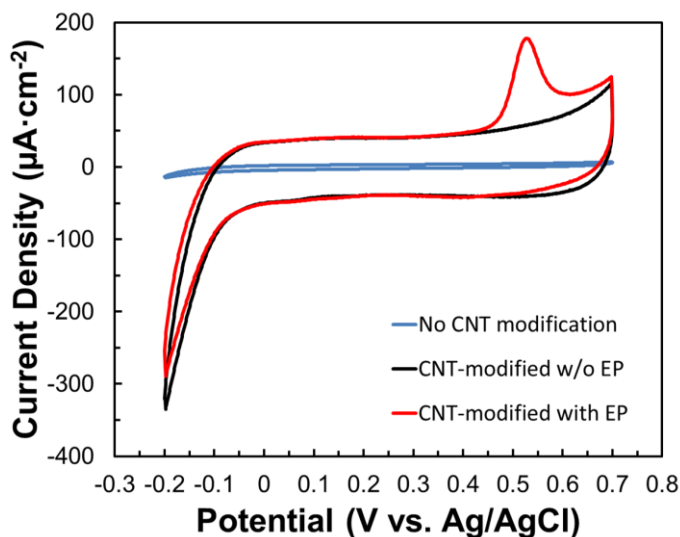


Figure 3.3: CV responses of bare GC electrode without CNT modification and CNT-modified electrode in the presence and absence of 4-ethylphenol.

The increase of non-faradaic current for the CNT-modified electrode compared to bare GC electrode can be attributed to the attachment of CNT on the GC electrode. With the deposition of CNTs on the electrode, electrochemical surface increased, resulting in an increase in the capacitance of the electrode from -0.2 to 0.7 V. With the presence of 4-ethylphenol, the electrochemical oxidation of 4-ethylphenol was observed above 0.45 V during the anodic sweep (from relatively negative to positive potential), and reached its peak around 0.5 V, while corresponding reduction was absent. This result suggests that oxidation of 4-ethylphenol is irreversible. In order to improve the specificity for 4-ethylphenol detection, TYR was used as introduced in Figure 3.1, the direct electrochemical oxidation, in other words, non-specific reactions, need to be avoided when a TYR-immobilized electrode is used for the detection. Therefore, the voltage window was narrowed down to a shorter range from -0.2 V to 0.4 V.

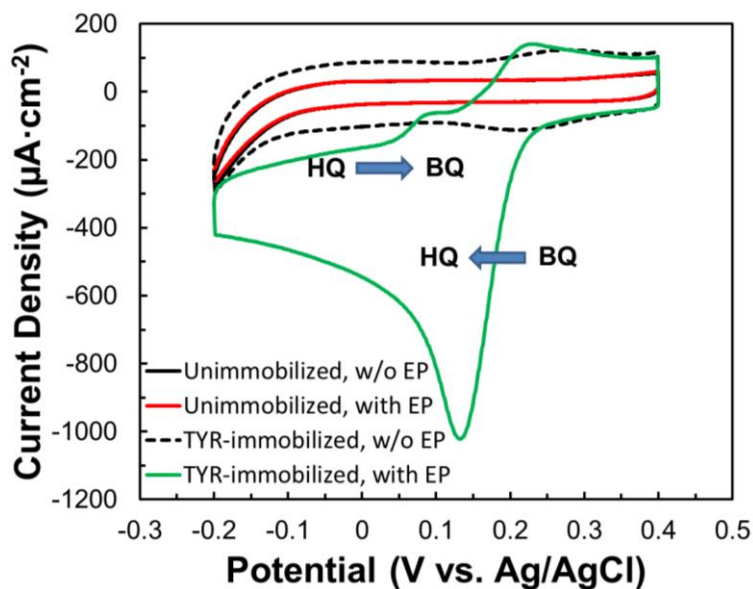


Figure 3.4: CV responses of 0.49 mM 4-ethylphenol on unimmobilized CNT electrode and TYR-immobilized CNT electrode with and without presence of 4-ethylphenol. BQ-4-ethyl-1,2-benzoquinone and HQ-4-ethyl-1,2-hydroquinone.

Figure 3.4 shows the cyclic voltammograms of no TYR-immobilized and TYR immobilized CNT-modified electrodes both in the presence and absence of 4-ethylphenol. The results demonstrate that 4-ethylphenol cannot be directly detected electrochemically within the voltage window between -0.2 and 0.4 V on unimmobilized CNT electrode since no significant oxidation or reduction peak of 4-ethylphenol could be observed within the range. On the other hand, increase of capacitance was observed after the immobilization of TYR, which could be attributed to the crosslinking of TYR on the CNT modified electrode. In addition, upon adding 4-ethylphenol in the electrolyte, 4-ethylphenol was catalyzed and formed the intermediate *o*-phenol (4-ethyl-1,2-hydroquinone) due to the monooxygenase activity of tyrosinase. The intermediate *o*-phenol was further oxidized to *o*-quinone (4-ethyl-1,2-benzoquinone) by catechol oxidase activity (Rassaei, Cui et al. 2012). Due to the monooxygenase activity and catechol oxidase activity, two alternative names – catechol oxidase and monophenol monooxygenase are also proposed for TYR. Therefore, the detection of 4-ethylphenol was realized through the measurement of reduction of 4-ethyl-1,2-benzoquinone (BQ) to 4-ethyl-1,2-hydroquinone (HQ) below 0.2 V during cationic sweep as per the schematic illustration shown as green arrows in Figure 3.1. In addition, two prominent oxidation peaks were also observed as the sweeping potential increases from -0.2 V to 0.1 V during the anodic sweep as shown in Figure 3.4. The peaks can be explained by the two-step electrochemical oxidation of 4-ethyl-1,2-hydroquinone (HQ) as given in yellow arrows in Figure 3.1. In this experiment, it is obvious that about 5-fold increase of the amperometric signal was obtained for 4-ethylphenol from TYR-immobilized electrode (Figure 3.4) compare to the same concentration of 4-ethylphenol from non TYR-immobilized electrode (Figure 3.3), which validates our assumption that TYR-immobilized biosensor cannot only improve specificity, but also increases the sensitivity for 4-ethylphenol detection.

3.3.2 Detection of 4-ethylphenol using tyrosinase-immobilized CNT electrode

The voltammograms of TYR-immobilized CNT electrode at different concentrations of 4-ethylphenol from 0 to 488 μM is shown in Figure 3.5.

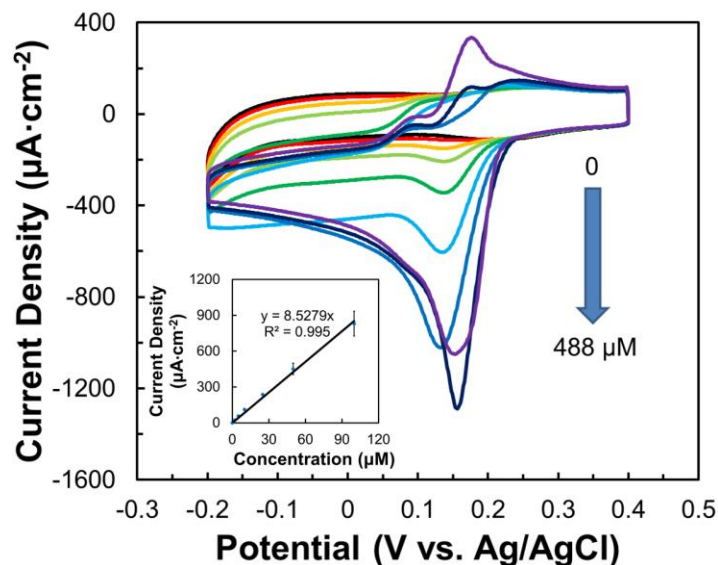


Figure 3.5: CV responses of 4-ethylphenol with TYR-immobilized biosensor. Inset displays linear range of reliable detection, sensitivity and R^2 value.

The reduction current at 0.13 V (reduction of 4-ethyl-1,2-benzoquinone to 4-ethyl-1,2-hydroquinone) increased with the concentration of 4-ethylphenol increased from 0 to 488 μM . The reduction current appeared to reach saturation above 247 μM of 4-ethylphenol, which can be ascribed to the saturation in the enzymatic reaction rate V at high substrate concentration $[S]$ as explained by Michaelis-Menten equation (with K_M as the Michaelis-Menten constant):

$$V = V_{\max}[S]/(K_M + [S])$$

The reduction current density at 0.13 V versus concentration of 4-ethylphenol was plotted as the inset of Figure 3.5. The dependence of the current on concentration was linear from concentration of 0 to 100 μM . The sensitivity for 4-ethylphenol detection with TYR-immobilized

biosensor calculated as the slope of the inset was estimated to be $8.53 \mu\text{A} \cdot \text{cm}^{-2} \cdot \mu\text{M}^{-1}$. The TYR-immobilized CNT electrode also exhibited a limit of detection (LOD) of $0.21 \mu\text{M}$ and limit of quantification (LOQ) of $0.64 \mu\text{M}$ for the detection of 4-ethylphenol (Table 3.1).

Table 3.1: Linear range, R^2 value, sensitivity, LOD and LOQ for TYR-immobilized CNT biosensor for 4-ethylphenol detection by CV and constant potential amperometry (CPA).

Technique	Linear range (μM)	R^2 value	Sensitivity ($\mu\text{A} \cdot \text{cm}^{-2} \cdot \mu\text{M}^{-1}$)	LOD (μM)	LOQ (μM)
CV	0 – 100	0.9950	8.53 ± 0.95	0.21 ± 0.08	0.64 ± 0.25
CPA	0 – 100	0.9956	4.05 ± 0.52	0.10 ± 0.02	0.29 ± 0.07

LOD and LOQ can be calculated by equations below (Long and Winefordner 1983, Armbruster and Pry 2008):

$$\text{LOD } (\mu\text{M}) = 3.3 \times \text{SD } (\mu\text{A} \cdot \text{cm}^{-2}) / \text{Sensitivity} (\mu\text{A} \cdot \text{cm}^{-2} \cdot \mu\text{M}^{-1})$$

$$\text{LOQ } (\mu\text{M}) = 10 \times \text{SD } (\mu\text{A} \cdot \text{cm}^{-2}) / \text{Sensitivity} (\mu\text{A} \cdot \text{cm}^{-2} \cdot \mu\text{M}^{-1})$$

Since CV is commonly a transient method used for steady state quantitative measurements for the evaluation of an electrochemical sensor, a more suitable technique, *i.e.* constant potential amperometry (CPA) was applied for 4-ethylphenol detection. CPA could provide reliable steady state measurements to determine the sensitivity, LOD and LOQ for the analyte detection (Luo, Prabhu et al. 1990, Park, Boo et al. 2006). Additionally, CPA is more convenient to program when building a portable device; and it is easier to carry out the data analysis by computer. The initial potential was set to 0.13 V (the potential at which highest reduction current is obtained from 4-ethyl-1,2-benzoquinone). 4-Ethylphenol was consecutively added to maintain a concentration gradient during the measurement by TYR-immobilized biosensor. The results of the CPA measurements are shown in Figure 3.6.

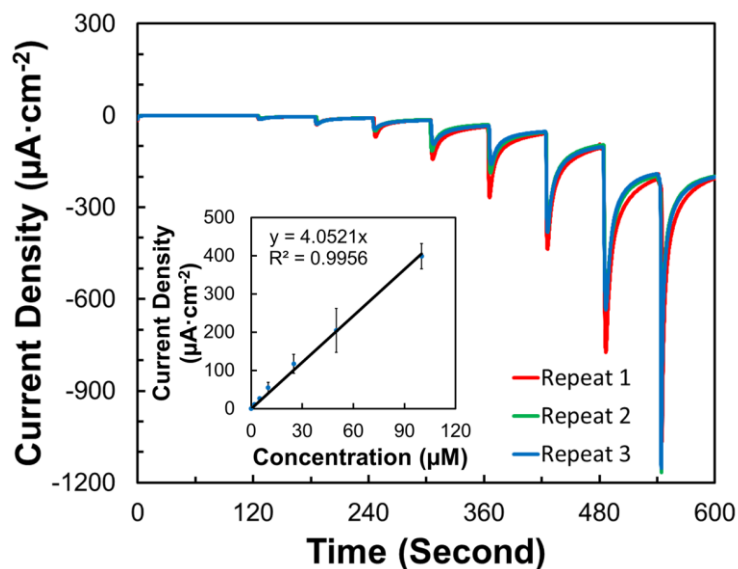


Figure 3.6: CPA responses of 4-ethylphenol with TYR-immobilized biosensor. Inset displays linear range of reliable detection, sensitivity and R^2 value.

As concentration of 4-ethylphenol increased, the reduction current of 4-ethyl-1,2-benzoquinone also increased in all three repetitive trials attempted for this measurement in Figure 3.6. The sensitivity for 4-ethylphenol detection was determined to be $4.05 \mu\text{A}\cdot\text{cm}^{-2}\cdot\mu\text{M}^{-1}$ and LOD and LOQ were determined to be $0.10 \mu\text{M}$ (1.8 ppb) and $0.29 \mu\text{M}$ (5.2 ppb) respectively (Table 3.1). The results indicated that TYR-immobilized biosensor can be reliably used for 4-ethylphenol detection within the concentration between 0 to $100 \mu\text{M}$. In addition, the application of the initial potential of 0.13 V was advantageous compared to the direct electrochemical detection without TYR immobilization, whose oxidation potential is 0.5 V, because the lower potential that applied, the less interference from other compounds will be. Therefore, false positive signal can be avoided by using low detection potential.

3.3.3 Stability of tyrosinase-immobilized biosensor

In addition to sensitivity, LOD and LOQ, stability study of TYR-immobilized biosensor was also carried out to evaluate the stability of the developed biosensor. To fulfill this, the TYR-immobilized electrode was fabricated on the first day (day 1), and its electrochemical responses towards 4-ethylphenol addition were determined using the same procedure introduced above between concentration of 0 and 100 μM . After this, the electrode was rinsed with 0.1 M potassium phosphate buffer (PB), pH 6.6 and stored in 20 mM PB, pH 6.6 with 10 % glycerol at 4 $^{\circ}\text{C}$. The same experiments were repeated on day 2, 4, 6, 8, 10 and 12. Current densities at 4-ethylphenol concentrations of 10, 25, 50 and 100 μM collected on different days are compared in Figure 3.7.

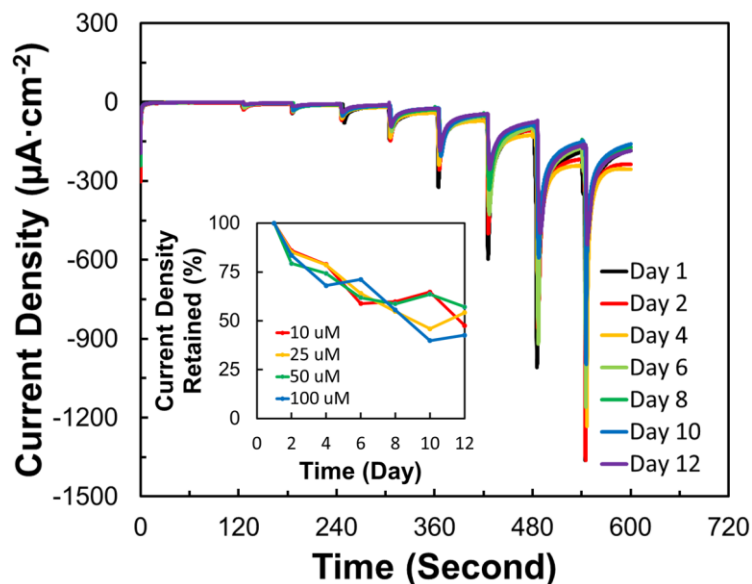


Figure 3.7: Stability of 4-ethylphenol detection in 10, 25, 50 and 100 μM 4-ethylphenol solution on Day 1, 2, 4, 6, 8, 10 and 12. Percentages of current density retained are displayed as inset.

As the results show, the current density for each concentration started to decrease from day 2 (figure 3.7), which could be attributed to the accelerated deterioration of TYR immobilized on

the electrode over time. About 50 % of the current density is retained on day 8. The results suggest that stabilization of enzyme should be carried out pre- or post- immobilization on the electrode surface before the biosensor can be considered for practical use. Developing enzyme stabilization methods to improve the shelf life of the biosensor could be a goal for the future work (Chapter 9).

3.3.4 Biosensor performance in the presence of interference compounds

As we introduced above, high amount of 4-ethylphenol will be produced by strawberry plants upon biotic stresses such as infection of *Phytophthora cactorum*. However, uninfected strawberry plants also produced and released a variety of other VOCs which could pose problems of false positive. Compounds such as ethyl butanoate, methyl hexanoate, ethanol, acetone, methyl butanoate, 2-heptanone and 2-pentanone are mostly produced VOCs by healthy strawberry plants at all times (Hakala, Lapveteläinen et al. 2002). Therefore, the interference from those compounds should be evaluated to avoid false positive signals before the biosensor can be practically used. Different concentrations of the above-mentioned interfering compounds up to 6.67 mM were analyzed using CPA and the results are shown in Figure 3.8.

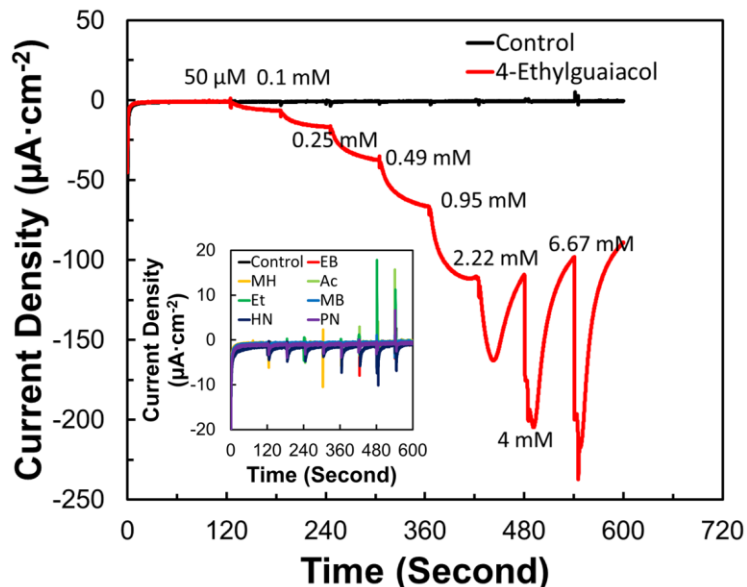


Figure 3.8: CPA responses of interference compounds: ethyl butanoate (EB), methyl hexanoate (MH), acetone (Ac), ethanol (Et), methyl butanoate (MB), 2-heptanone (HN) and 2-pentanone (PN) (Inset) and 4-ethylguaiacol (red) and control (black).

The current densities obtained from the interference VOCs were compared against the amperometric current density obtained from 10 μM 4-ethylphenol, which is a relatively low concentration within the linear range of the biosensor (0 to 100 μM) to mimic the extreme case (*i.e.*, the situation that 4-ethylphenol is produced in small amount while other VOCs are greatly produced simultaneously, mimicking a high noise, low signal scenario). The values for the interference currents obtained from the CPA measurements and the corresponding concentrations are tabulated in Table 3.2.

Table 3.2: Percentage (%) of interference current density resulted from interference compounds compared to 10 μM 4-ethylphenol. ethyl butanoate (EB), methyl hexanoate (MH), acetone (Ac), ethanol (Et), methyl butanoate (MB), 2-heptanone (HN), 2-pentanone (PN) and 4-ethylguaiacol (EG).

Conc. (mM)	EB	MH	Ac	Et	MB	HN	PN	EG
0	0.04	-0.02	0.00	0.03	-0.04	0.13	0.04	-0.02

0.05	0.65	1.24	0.26	0.22	0.35	0.74	0.42	1.37
0.10	0.00	0.16	-0.05	-0.20	-0.18	0.38	0.39	3.56
0.25	0.76	0.73	0.61	0.87	0.44	0.73	0.45	9.04
0.49	0.74	2.38	0.41	0.17	0.44	0.64	0.47	16.37
0.95	0.50	1.23	0.30	0.50	0.41	1.58	0.85	27.75

Among all the interference compounds we tested in different concentration, none of them generates current density greater than 3 % compared to 10 μ M 4-ethylphenol. The results demonstrate that none of the interference compounds tested in this project was able to generate significant interference for 4-ethylphenol detection. Additionally, the spikes collected from each addition of interference compounds can be explained by the disturbance of the sample mixing (Figure 3.8).

In addition to the interference compounds that released by the healthy strawberry plants listed above, 4-ethylguaiacol, another VOC is also produced simultaneously with 4-ethylphenol upon the infection of *Phytophthora cactorum*. Although 4-ethylguaiacol, as another indicator of plants' infection of *Phytophthora cactorum*, has been introduced in Chapter 2, the interference effect of 4-ethylguaiacol was carried out and the results are tabulated in Table 3.2. It is obvious that compared to other compounds, 4-ethylguaiacol generates noticeable interference of 9 % at 250 μ M and up to 28% at 0.95 mM. Although appears to be high, the 4-ethylguaiacol is released in a rate about 5 % to 10 % compared to 4-ethylphenol in typical plant volatile signatures (Jeleń, Krawczyk et al. 2005). Therefore, 4-ethylphenol is not a cause for concern for the tyrosinase-immobilized biosensor.

3.3.5 Evaluation of biosensors using synthetic analyte cocktail

The composition of VOCs released by both healthy and infected strawberry plants has been reported by previous publications (Hakala, Lapveteläinen et al. 2002, Jeleń, Krawczyk et al. 2005). In order to evaluate the application of this biosensor in near-practical conditions, a synthetic cocktail solution was prepared as the analyte to simulate the production of VOCs by healthy strawberries. The cocktail solution was prepared in seven compounds at compositions similar to that found in the volatile signatures of strawberries listed in Table 3.3.

Table 3.3: Composition of the synthetic cocktail solution consisting VOCs released by healthy strawberry plants.

Volatile organic compound	Concentration (mM)
Ethyl butanoate	20.75
Methyl hexanoate	16.62
Acetone	7.42
Ethanol	7.42
Methyl butanoate	13.91
2-Heptanone	9.72
2-Pentanone	3.91

The fabricated TYR-immobilized biosensor was stabilized for 120 seconds in 1 mL, followed by addition of 1 mL of synthetic cocktail solution to mimic the situation that all those VOCs are omnipresent regardless of the healthy condition of strawberry. The mixed stock solution of 20 mM 4-ethylphenol and 20 mM 4-ethylguaiacol was then gradually added at 60-second interval to mimic the release of the two VOCs by infected strawberries in addition to the VOCs released by the healthy plants (*i.e.* cocktails already present in the electrochemical cell). The electrochemical signal collected from the mixture was compared with the control experiment performed by

adding pure 20 mM 4-ethylphenol in the absence of 4-ethylguaiacol and other VOCs shown in Table 3.3. The current densities from both experimental group (different concentration gradients of 4-ethylphenol and 4-ethylguaiacol in the presence of other VOCs in Table 3.3) and control group (only 4-ethylphenol) were plotted in Figure 3.9 with the concentration effect as inset.

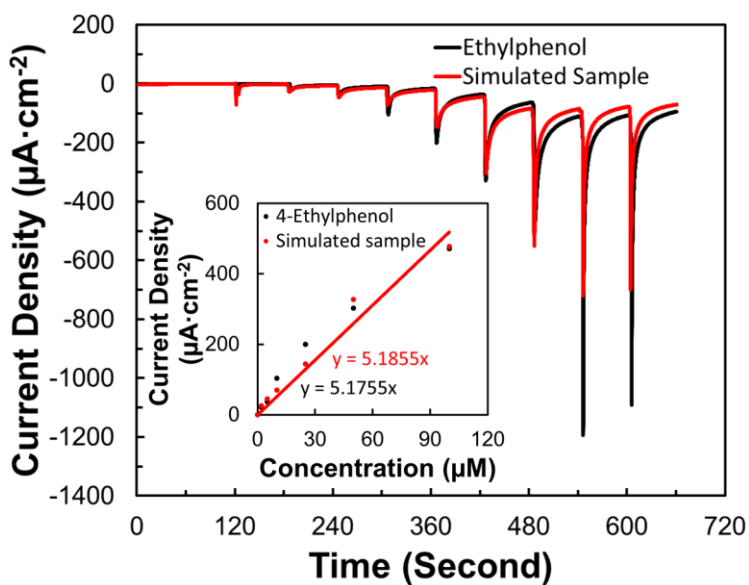


Figure 3.9: CPA comparison of simulated sample and pure 4-ethylphenol as control and sensitivity determination (Inset).

The results in Figure 3.9 indicate that the reduction current collected from 4-ethylphenol in presence of 4-ethylguaiacol and other VOCs released by healthy plants (*i.e.* the cocktail in the electrochemical cell) is similar to that of pure 4-ethylphenol without any interference compounds.

The comparison results in Figure 3.9 demonstrate that the TYR-immobilized biosensor can be used for reliable detection of 4-ethylphenol from a real plant volatile signature with presence of interference from healthy plants. In the future work, collection bag will be used for VOC collection and micro air-pump will be used to pump the headspace VOCs from the collection bag

to electrolyte for enrichment, and therefore, realize the detection of 4-ethylphenol using the biosensor developed above.

3.4 CONCLUSION

In this chapter, a novel TYR-based biosensor for 4-ethylphenol detection was developed with CNTs. The newly developed biosensor exhibited high sensitivity, ultra-low LOD and LOQ for 4-ethylphenol detection. The biosensor also displayed satisfactory stability although the enzyme still needs pre-stabilization before immobilization. Other VOCs have been tested and no significant interference was observed at reasonable concentration. Synthetic analyte consisting of 4-ethylphenol and other types of VOCs produced by both healthy and infected strawberry plants have been used for evaluating the near-practical application and the sensor exhibited reliable detection of 4-ethylphenol in the synthetic analyte sample. This project provides a platform for the development of enzymatic biosensors for plant disease detection through VOCs that signify plant diseases, therefore allows the detection of more VOCs in the future work.

CHAPTER 4

DETECTION OF METHYL SALICYLATE USING ALCOHOL OXIDASE / PEROXIDASE – BASED BIOSENSOR

This chapter contains text modified from the following publications:

Yi Fang, Yogeswaran Umasankar, and Ramaraja P. Ramasamy. 2016. *Biosensors and Bioelectronics* 81: 39-45.

Reprinted here with permission of the publisher.

Abstract

An amperometric biosensor based on a bi-enzyme-immobilized electrode was developed for detection of methyl salicylate, a volatile organic compound released by pathogen-infected plants via systemic response. The detection is based on cascading conversion reactions that result in an amperometric electrochemical signal. The bi-enzymatic electrode is made of alcohol oxidase and horseradish peroxidase enzymes immobilized on to a carbon nanotube matrix through a molecular tethering method. Methyl salicylate undergoes hydrolysis to form methanol, which is consumed by alcohol oxidase to generate formaldehyde while simultaneously reducing oxygen to hydrogen peroxide. The hydrogen peroxide will be further reduced to water by horseradish peroxidase, which results in an amperometric signal via direct electron transfer. The bi-enzymatic biosensor was evaluated by cyclic voltammetry and constant potential amperometry using hydrolyzed methyl salicylate as the analyte. The sensitivity of the bi-enzymatic biosensor as determined by cyclic voltammetry and constant potential amperometry were 0.11 and 0.28 $\mu\text{A}\cdot\text{cm}^{-2}\cdot\mu\text{M}^{-1}$ respectively, and the corresponding limits of detection were 22.95 and 0.98 μA respectively. Constant potential amperometry was also used to evaluate stability, repeatability and interference from other compounds. Wintergreen oil was used for real sample study to establish the application of the bi-enzymatic biosensor for selective detection of plant pathogen infections.

Keywords: Agricultural biosensor, Bi-enzymatic electrode, Methyl salicylate, Alcohol oxidase, Horseradish peroxidase.

4.1 INTRODUCTION OF METHYL SALICYLATE AND ITS DETECTION

4.1.1 Methyl salicylate in plant metabolism and communication

As introduced in Chapter 1, an infected plant would produce various volatile organic compounds (VOCs) in different amount as opposed to a healthy plant. The VOCs in infected plants are produced through various metabolic pathways, such as octadecanoid pathway for fatty-acid derived green leaf volatiles (GLVs), monoterpenes, diterpenes, sesquiterpenes, isothiocyanates and a large diversity of aromatic metabolites. Among the various compounds in the volatile signature of plants, methyl salicylate (MeSA) plays an important role during pathogenic infections and infestations because it is released in large quantity for self-defense and communication. Therefore, MeSA is a suitable target compound (marker) for detecting biotic stresses of plants. MeSA is produced through Shikimate biosynthesis pathway, during a biotic stress event such as the pathogenic infection and herbivorous infestation (Kessler and Baldwin 2001, Loake and Grant 2007). For instance, the generation of MeSA as a VOC has been observed from *Tetranychus urticae* infested lima beans (De Boer and Dicke 2004, De Boer, Posthumus et al. 2004, James and Price 2004, Pickett, Bruce et al. 2006), and soybean aphid-infested soybeans (Zhu and Park 2005). In addition to infestation, production of MeSA is also reported upon infections by bacteria, fungi and viruses. For example, MeSA is detected when maize and pepper infected by *Fusarium* and *Phytophthora capsici* respectively (Buttery, Seifert et al. 1969, Piesik, Lemńczyk et al. 2011) and when tobacco plants are infected with *Tobacco mosaic virus* (TMV) (Seskar, Shulaev et al. 1998). Additionally, MeSA, is not only a signature VOC that produces in large quantity, also an allelochemical that released not just at the site of pathogen infection but throughout the plant through a systematic response. It is also one of the key markers for volatile-based detection of fungal diseases such as fruit blight, leaf blight, crown

rot *etc.*, which primarily affect cucurbit crops. Therefore, it is regarded as a suitable target analyte for phytodisease detection in crops.

4.1.2 Current method of detecting methyl salicylate

Although MeSA is crucial in plant disease detection, like many other VOCs introduced before, gas chromatography – mass spectrometry (GC-MS) is still the most commonly used technique. However, this technique requires the sample to be collected in the field and analyzed elsewhere in a laboratory. Moreover, the high cost of the instrument and complexity of the analysis prohibit it from being used for on-field detection. Given to the advantages provided by electrochemical biosensor introduced above, a type of bi-enzymatic biosensor was successfully developed and reported in this chapter.

4.1.3 Application of enzymes

Although being an ester, MeSA is relatively stable and not electroactive on the electrode, which renders difficulties in the direct measurement of MeSA electrochemically on the electrode. However, the products after the hydrolysis (either chemically or enzymatically, which will be introduced in Chapter 6) of MeSA can be detected on enzyme-immobilized biosensors. Therefore, a type of bi-enzymatic biosensor was developed by using alcohol oxidase (AOD) and horseradish peroxidase (HRP) for MeSA detection after hydrolysis.

The hydrolysis products from MeSA consist of both methanol and salicylate (SA). Therefore, the amount of the MeSA of interest is proportional to the amount of methanol or SA that present in the system after hydrolysis. The first pathway to detect the concentration of MeSA is to measure the concentration of methanol after hydrolysis. In order to fulfill this objective, the biorecognition elements consisting of two enzymes namely alcohol oxidase (AOD) and

horseradish peroxidase (HRP) were immobilized on a matrix of multiwalled carbon nanotubes (CNTs). The immobilization was achieved through an in-house established molecular tethering approach developed and evaluated through the previous experiments that introduced in Chapter 3. The mechanism of the detection can be illustrated in Figure 4.1.

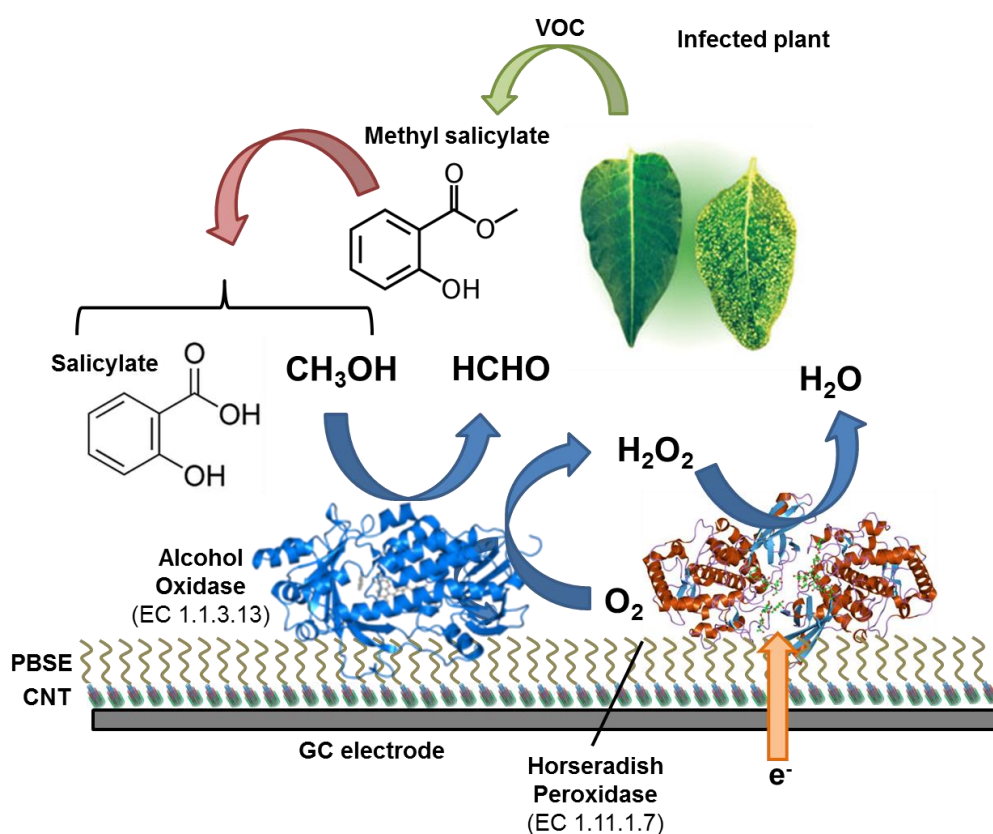


Figure 4.1: Schematic illustration of MeSA detection by AOD/HRP-immobilized electrode. Not drawn to scale. The process begins with hydrolysis of MeSA to form methanol and SA, oxidation of methanol and production of hydrogen peroxide, and direct electron transfer from electrode to hydrogen peroxide by HRP.

The detection was carried out in three steps. First, MeSA was hydrolyzed in potassium hydroxide (KOH) to generate SA and methanol (MeOH). The pH was adjusted to 7.6 by adding phosphoric acid. Secondly, the enzyme AOD converts methanol into formaldehyde via its native biochemical reaction, during which a simultaneous reaction that reducing oxygen to hydrogen

peroxide takes place (Patel, Hou et al. 1981, Ozimek, Veenhuis et al. 2005). The last step involves in the enzymatic reduction of hydrogen peroxide to H₂O in present of HRP, which results in an amperometric signal collected from the electrode through direct electron transfer (DET) (Akkara, Senecal et al. 1991, Ghindilis, Atanasov et al. 1997, Veitch 2004). Therefore, the amperometric signal is proportional to the concentration of the hydrolyzed MeSA.

4.2 MATERIALS AND METHODS

4.2.1 Materials

Alcohol oxidase (E.C. 1.1.3.13) from *Pichia pastoris* was purchased from Sigma Aldrich and used as received. Horseradish peroxidase (specific activity 281 units/mg solid) was purchased from Calbiochem Inc. Multiwalled carbon nanotubes (CNTs) were obtained from DropSens Inc (Spain). 1-Pyrenebutanoic acid succinimidyl ester (PBSE) was purchased from Ana Spec Inc. (Fremont, California, US) as cross-linker. Dimethylformamide (DMF) and sodium salicylate were purchased from Acros Organics Inc. (New Jersey, US). Chemicals for the interference study, such as *cis*-3-hexenol, hexyl acetate and *cis*-hexenyl acetate, are obtained from TCI America (Portland, Oregon, US) and used as received. Wintergreen oil purchased from Piping Rock Health Products was used for real-sample study. Methyl salicylate was used as received from Sigma-Aldrich Inc. (St. Louis, MO, US). All other chemicals used in this project were of the analytical grade. 0.1 mM potassium phosphate buffer (PB), pH 7.6 was used as the electrolyte for all the experiments. All aqueous solutions were prepared in 18.2 MΩ nano-pure de-ionized (DI) water. Electrolyte solutions were oxygenated by purging oxygen for 15 min prior to each set of experiments.

4.2.2 Apparatus

Cyclic voltammetry (CV) and constant potential amperometry (CPA) were performed using CHI 920 c potentiostat. A conventional three-electrode system consisting a platinum wire as counter electrode and 3 M Ag/AgCl as the reference electrode were used for electrochemical measurements. Both glassy-carbon (GC) electrode and glassy-carbon rotating disc electrode (RDE) from Pine Instrument Inc. were used as working electrode for different purposes. All experiments were carried out at 25 ± 2 °C.

4.2.3 Electrode preparation and electrochemical measurement

Both GC and RDE electrodes were surface polished on a polishing pad with 0.05 μm alumina polishing powder for 5 min before each use. The electrodes were then cleaned with ultrasonic cleanser and rinsed with DI water to remove the adhered polishing powder that attached to the electrodes. The CNT suspension was prepared by ultrasonication of 1 mg of multiwalled CNTs in 1 mL DMF for 1 h and the following electrode modification steps are shown in Figure 3.2. The CNT modified electrodes were prepared by drop casting 8 μL (in 8 steps of 1 μL) for GC and 12 μL (in 3 steps of 4 μL) for RDE followed by drying at 70 °C. CNT modified electrodes were placed on ice to cool down before applying 2 and 4 μL of 10 mM PBSE in DMF to allow non-covalent linkage between CNT and PBSE. The electrodes were incubated for 15 min and excessive PBSE was removed by rinsing with DMF and 20 mM potassium phosphate buffer, pH 7.6. HRP solution was prepared by dissolving 5 mg HRP lyophilized powder in 1 mL of 20 mM potassium phosphate buffer, pH 7.6. The bi-enzyme solution was prepared by mixing 5 μL of alcohol oxidase solution and 5 μL HRP solution. 10 μL of bi-enzyme solution was drop casted on the electrode surface and incubated on ice for 30 min to allow the immobilization of enzymes through covalent linkage. The electrodes were then rinsed with 20 mM potassium phosphate

buffer (PB), pH 7.6 to remove excessive enzyme. Potential range was set from 0.7 V to 0.2 V for CV measurements with a scan rate of 20 mV/s and sample interval of 0.001 V. The initial potential for CPA with RDE was 0.45 V with 0.1 s interval for signal collection.

4.2.4 Hydrolysis of methyl salicylate

MeSA is an ester that not electrochemically or enzymatically active, therefore, cannot be electrochemically or enzymatically detected easily. Thus, chemical hydrolysis of MeSA is required as the procedure shown in Figure 4.2.

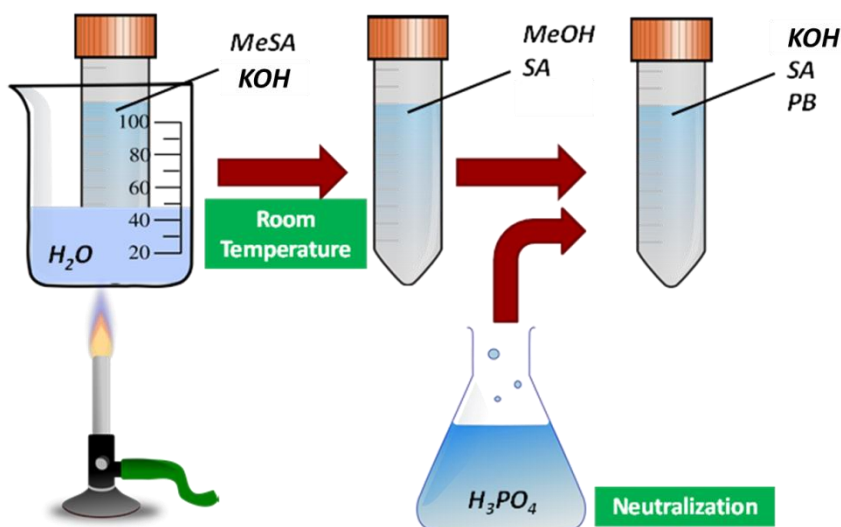


Figure 4.2: Schematic illustration of chemical hydrolysis of MeSA in KOH and pH adjustment with phosphoric acid.

MeSA was mixed with 0.19 M KOH in 15 mL falcon tube to balance the ionic strength of the buffer for hydrolysis. The falcon tube was sealed and placed in the boiling water bath for 30 min to allow hydrolysis. The solution was cooled to room temperature and pH was adjusted to 7.6 by addition of phosphoric acid.

4.3 RESULTS AND DISCUSSION

4.3.1 Cyclic voltammetry responses of AOD/HRP-immobilized electrode

As the mechanism of MeSA detection was based on the alcohol sensor in this project, the biosensor was evaluated first for methanol detection using 3 mM methanol in the electrolyte. For comparison, a CNT modified GC electrode immobilized with only one enzyme (either AOD or HRP) as bio-recognition element was also evaluated as control experiments. As shown in Figure 4.3, the amperometric signal indicated by the reduction wave starting from 0.6 V (with a reduction peak at 0.45 V) was observed only from the bi-enzyme immobilized biosensor. The cathodic wave corresponds to the reduction of hydrogen peroxide to water, which was the last step of cascadic reaction as described in Figure 4.1. No such reduction was observed in Figure 4.3 when any one of the two enzymes was absent on the electrode, indicating that the cascade reaction do not proceed if one of the enzymes was absent and that the hydrogen peroxide was formed as a result of cascade reactions. In addition, it also proved that none of oxidation and reduction of methanol can be observed on electrode at the range of 0.2 V to 0.7 V. Therefore, the amperometric signal could be solely attributed to the hydrogen peroxide reduction reaction by HRP.

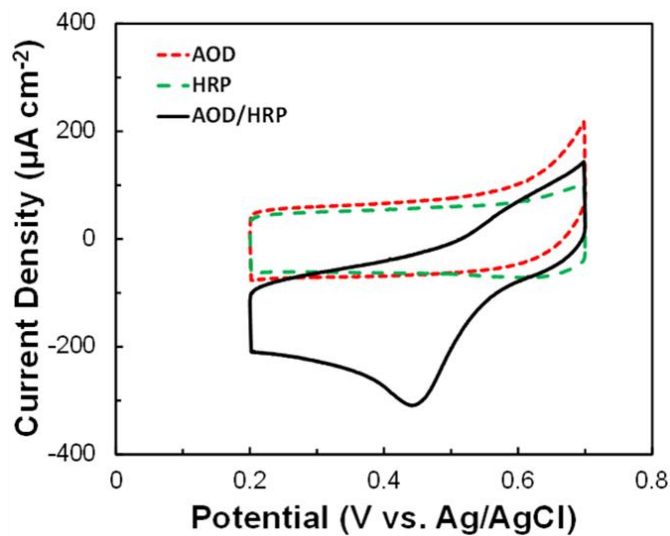


Figure 4.3: CV of 3 mM methanol on AOD, HRP and bi-enzyme immobilized electrodes.

The next step in the analysis was to evaluate if the intermediate compounds, *i.e.* salicylate (SA) and formaldehyde would contribute to the amperometric signal in the region of interest (0.6 V and below along the cathodic wave as it shown in Figure 4.4A. For this, the AOD and HRP immobilized electrodes were tested using CV in the same potential window using 5 mM SA and formaldehyde solutions respectively, and the corresponding results are displayed in Figure 4.4A. The results suggest that formaldehyde does not contribute to any visible electrochemical reaction due to lack of oxidation or reduction peaks in the potential window. On the other hand, however, SA exhibited a small redox peak around 0.5 V, but the signal was weak and much smaller compared to the electrochemical signal of hydrogen peroxide reduction. A large oxidation peak for SA oxidation above 0.65 V was also noticed in the voltammograms in Figure 4.4A. However, this oxidation did not interfere with the hydrogen peroxide reduction below 0.6 V. It can also be observed that SA did not interfere with current collected from the reduction of methanol that formed from the hydrolysis of MeSA as it shown in Figure 4.4B.

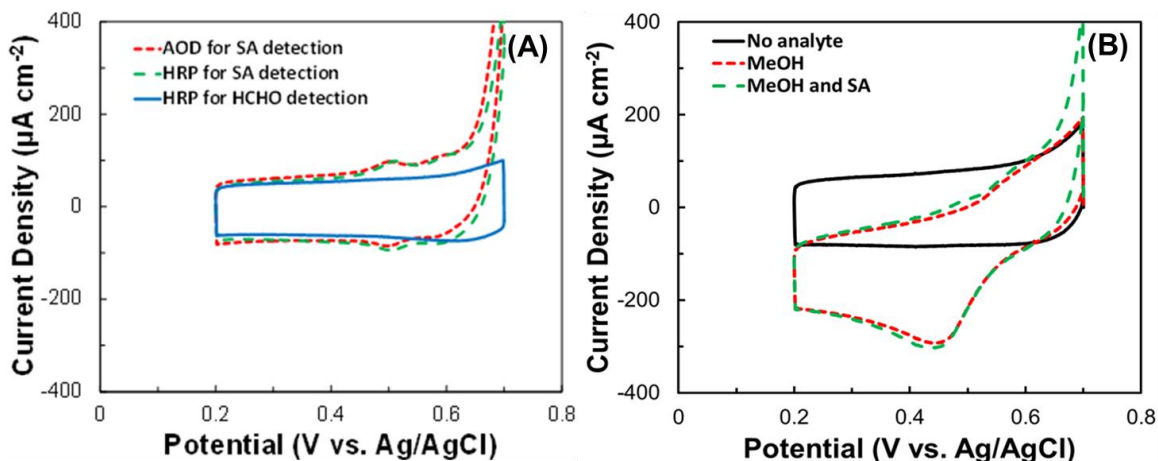


Figure 4.4: CV responses of 5mM formaldehyde and 5mM SA on mono-enzyme modified electrode (a). CV responses of 1.88 mM methanol and extra addition of 1.88 mM SA on bi-enzyme modified electrode (b) shows that SA does not offer significant interference.

All the previous results in Figure 4.3 and Figure 4.4 have indicated that methanol (from hydrolyzed MeSA) is the only compound responsible for the amperometric signal observed in the voltammogram. The next step in the analysis was to determine if MeSA can be detected amperometrically through the cascade reactions with no initial presence of methanol in the system. To carry this analysis out, 1.88 mM hydrolyzed MeSA (prepared as Figure 4.2 displays) was used as the analyte in the electrochemical cell and CV was performed in the same potential window. As shown in Figure 4.5, the voltammograms shows a similar electrochemical response for the bi-enzyme immobilized electrode for the hydrolyzed MeSA as it was for methanol, with the hydrogen peroxide reduction peak occurring at 0.45 V. Similarly, the electrode immobilized with only one enzyme (either AOD or HRP) and the electrode immobilized with no enzyme, exhibited no redox responses suggesting that the amperometric signal was generated only when both enzymes are present on the electrode to carry out the cascadic reaction.

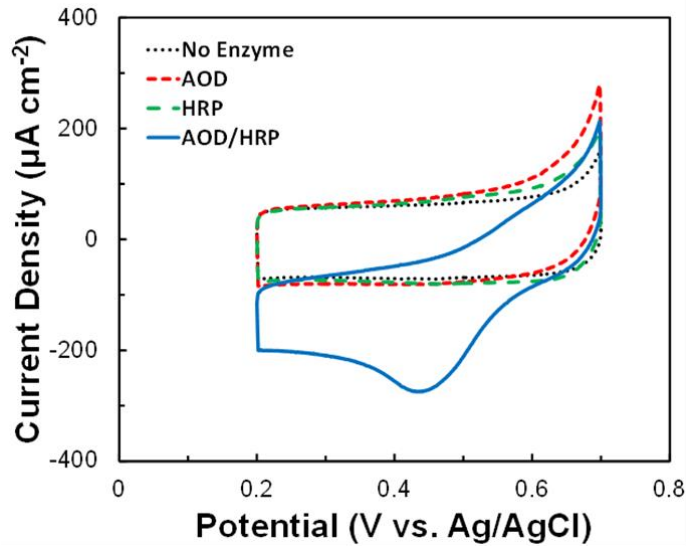


Figure 4.5: CV responses of 1.88mM hydrolyzed MeSA on bi-enzyme immobilized, AOD-immobilized, HRP-immobilized and no enzyme immobilized electrodes.

The results also confirmed that the electrochemical reduction of hydrogen peroxide requires presence of HRP, as no distinct signal for direct reduction of H_2O_2 was observed. Additionally, no electrochemical signal was generated for direct oxidation of either methanol or SA in the absence of enzyme. The results in Figure 4.5 demonstrate that only the bi-enzyme-immobilized biosensor can be effectively used for MeSA detection after hydrolysis.

Since bi-enzymatic system was used to carry out MeSA detection, the optimal loading of enzymes on the electrode was optimized by a series trial experiments with different mass ratios of both enzymes (2.8 U AOD / 14.0 U HRP, 5.5 U AOD / 7.0 U HRP and 11.0 U AOD / 3.5 U HRP), the results of which are giving in Figure 4.6.

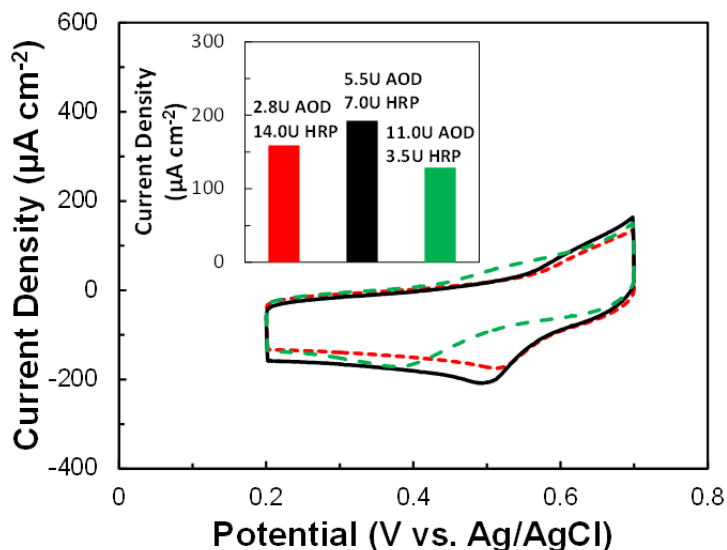


Figure 4.6: CV responses of 1.88 mM hydrolyzed MeSA on GC electrodes immobilized with different ratio of AOD and HRP.

Although all three ratio combinations display successful detection of hydrolyzed MeSA, the optimal mass ratio was determined to be 5.5 units of AOD and 7 units of HRP (1:1 mass ratio of AOD:HRP) on the CNT modified electrode due to the highest hydrogen peroxide reduction peak it displayed.

4.3.2 Electrochemical responses of the AOD/HRP-immobilized biosensor

The amperometric responses of the bi-enzyme immobilized electrode at different concentration of hydrolyzed MeSA were analyzed using both CV and CPA using RDE. The 11 different concentrations of the hydrolyzed MeSA from 1 μ M to 3 mM were studied by stepwise addition of hydrolyzed MeSA. The solution was mixed well and stabilized for 10 seconds before each measurement was made. The above concentration was chosen based on a series of experiments where the lowest limit was based on the noticeable increase in the reduction current upon an incremental addition of hydrolyzed MeSA into the electrolyte. Similarly, the upper concentration boundary limit was chosen based on the rate of decrease in oxidation current during subsequent

additions of hydrolyzed MeSA. Voltammograms shown in Figure 4.7 indicate that before the addition of hydrolyzed MeSA no reduction peak of methanol was observed. When the concentration of hydrolyzed MeSA in the electrolyte increased by stepwise addition of 10 μM and higher, noticeable hydrogen peroxide reduction waves were clearly observed starting from 0.6 V with a prominent peak appear around 0.45 V. It was also obvious that the peak increased as the increasing concentration of hydrolyzed MeSA in the electrolyte. Another oxidation peak around 0.5 V also appeared the concentration of hydrolyzed MeSA increased above 1 mM, which could be attributed to the oxidation of SA present in the hydrolyzed MeSA.

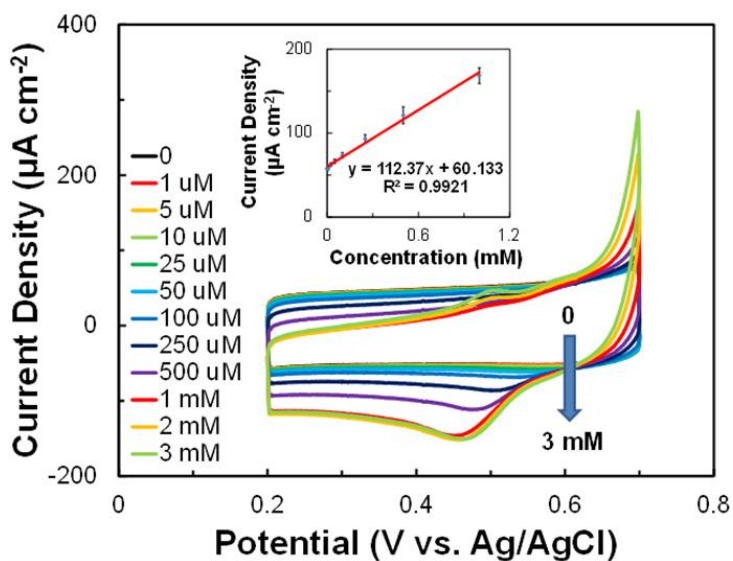


Figure 4.7: CV responses of hydrolyzed MeSA from 0, 1 μM to 3 mM on bi-enzyme modified GC electrode.

In order to quantitatively characterize the sensor behavior, amperometric sensor parameters such as sensitivity, limit of detection (LOD), and limit of quantification (LOQ) can be derived from the following equations.

$$\text{Sensitivity } (\mu\text{A} \cdot \text{M}^{-1} \cdot \text{cm}^{-2}) = \frac{\text{Slope of calibration curve } (\mu\text{A} \cdot \text{M}^{-1})}{\text{Area of electrode } (\text{cm}^2)}$$

$$\text{LOD (M)} = 3.3 \times \frac{\text{Standard deviation of peak current in the absence of analyte } (\mu\text{A})}{\text{Slope of linear calibration curve } (\mu\text{A} \cdot \text{M}^{-1})}$$

$$\text{LOQ (M)} = 10 \times \frac{\text{Standard deviation of peak current in the absence of analyte } (\mu\text{A})}{\text{Slope of linear calibration curve } (\mu\text{A} \cdot \text{M}^{-1})}$$

The calculated sensitivity, LOD, LOQ as well as linear range are tabulated in the Table 4.1 below.

Table 4.1: Electrochemical data for hydrolyzed MeSA from CV and CPA.

	Electrode	Sensitivity ($\mu\text{A} \cdot \text{cm}^{-2} \cdot \mu\text{M}^{-1}$)	LOD (μM)	LOQ (μM)	Linear range (mM)
CV	GC	0.11	22.95	69.55	10.0
CPA	RDE	0.28	0.98	2.97	0.5

According to Table 4.1, sensitivity of $0.11 \mu\text{A} \cdot \text{cm}^{-2} \cdot \mu\text{M}^{-1}$ can be achieved by GC electrode with CV while LOD and LOQ were determined to be $22.95 \mu\text{M}$ and $0.98 \mu\text{M}$ respectively. Since contributions of non-faradaic current are included in CV, it does not provide a steady state response of the amperometric sensor. Therefore, CPA was applied for MeSA detection. For this, a rotating disc glassy-carbon electrode (RDE) was used with the modification of bi-enzyme/CNT composite as the working electrode. The measurements were conducted at rotating speed of 1200 rpm to eliminate mass transfer limitation. The RDE was initially stabilized for 300 seconds before the addition of hydrolyzed MeSA from $0.1 \mu\text{M}$ to 1 mM in stepwise addition with an interval of 50 seconds. The first observable stepwise increase in reduction current appeared at the concentration of $0.5 \mu\text{M}$ as it shown in Figure 4.8.

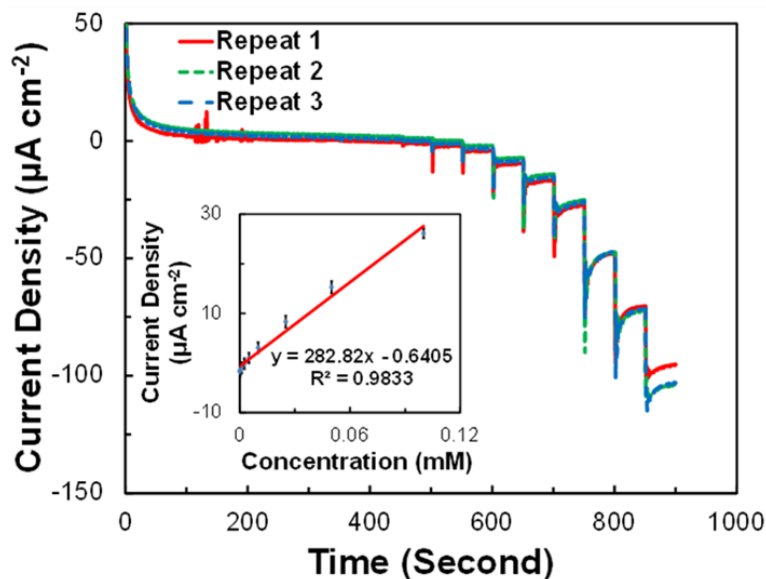


Figure 4.8: CPA responses of hydrolyzed MeSA from 0, 0.1 μM to 1 mM on bi-enzyme modified RDE electrode.

The corresponding electrochemical parameters such as sensitivity, LOD, LOQ and linear range can be found in Table 4.1. The results suggest a higher sensitivity can be achieved from CPA ($0.28 \mu\text{A}\cdot\text{cm}^{-2}\cdot\mu\text{M}^{-1}$) as opposed to that from CV ($0.11 \mu\text{A}\cdot\text{cm}^{-2}\cdot\mu\text{M}^{-1}$). In addition to the increase of sensitivity, both LOD and LOQ were improved to $0.98 \mu\text{M}$ and $2.97 \mu\text{M}$ respectively as opposed to $22.95 \mu\text{M}$ and $69.55 \mu\text{M}$ respectively from CV. To put the LOD into practical meaning, a typical MeSA release rate by plants is $283 \text{ ng}\cdot\text{h}^{-1}\cdot\text{plant}^{-1}$ (Shulaev, Silverman et al. 1997). At this typical rate, only 1.05 hours are needed to collect enough VOCs released by the diseased plants to reach $0.98 \mu\text{M}$ of MeSA in a 2 mL electrochemical cell for plant disease detection. Although the linear range of CPA was narrower than that of CV, it is still a preferable amperometric technique based on other estimated parameters.

4.3.3 Interference study of AOD/HRP-immobilized biosensor

MeSA is not the only VOC that released by the plants under biotic stresses. Other VOCs such as green leaf volatile volatiles (GLVs) that are non-specific to pathogen infection or pest infestations are also released at high concentrations, which could render interference during MeSA measurement. Therefore, a representative set of such VOCs including *cis*-3-hexenol, hexyl acetate and *cis*-3-hexen-1-yl acetate were used to determine the electrochemical effect of interference on the biosensor response using CPA. The bi-enzyme modified RDE was pre-conditioned with constant potential for 300 seconds until it stabilized. Then hydrolyzed MeSA was added in the electrochemical cell to maintain a working concentration of 50 μM , which is in the middle of linear range. The RDE was further stabilized for another 500 seconds before different concentrations of GLVs from 10 μM to 1 mM at a 50-second interval. This procedure was repeated for four times for all three GLVs as well the same volume of 0.1 M phosphate buffer (PB), pH 7.6 as the negative control. The interference data of current versus time is shown in Figure 4.9.

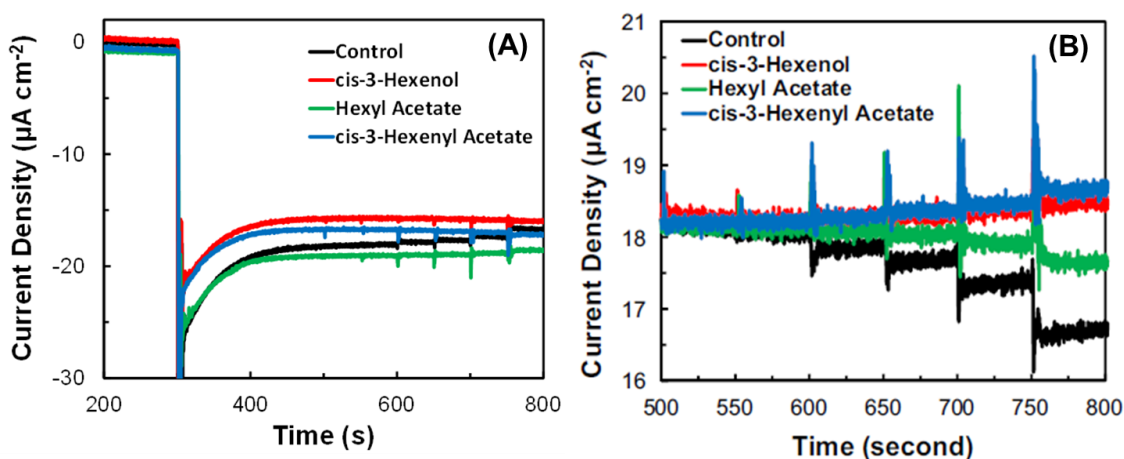


Figure 4.9: Interference of *cis*-3-hexenol, hexyl acetate and *cis*-3-hexyn-1-yl acetate by CPA (A) and its enlargement from 500 to 800 seconds (B). PB was used as the negative control.

While the typical GLV concentration is about 10 μM for *cis*-3-hexenol, 1 μM for hexyl acetate and 20 μM for *cis*-hexen-1-yl acetate (Umasankar, Rains et al. 2012), a wider concentration range for studying the GLVs (from 0 to 1 mM) interference was used to simulate the extreme case of GLV production (Danner, Boeckler et al. 2011). The original interference study information can be observed from Figure 4.9A, where the variation in amperometric current density of the biosensor was plotted against time during stepwise increase of the GLVs (*cis*-hexenol, hexyl acetate and *cis*-3-hexenyl acetate) concentration in presence of 50 μM of hydrolyzed MeSA. To account the decrease of current density due to the dilution of hydrolyzed MeSA during the addition of GLV solutions, a control interference study was also performed by addition of potassium phosphate buffer (PB), pH 7.6 to mimic the electrolyte volume change. As it shows in Figure 4.9B, the decrease in the current density values during the stepwise addition of PB in control experiment could be attributed to the dilution effects arising from the stepwise addition, as the buffer itself does not contribute to the interference study. On the other hand, CPA current density signals slightly increased in the presence of GLVs compare to the control experiment.

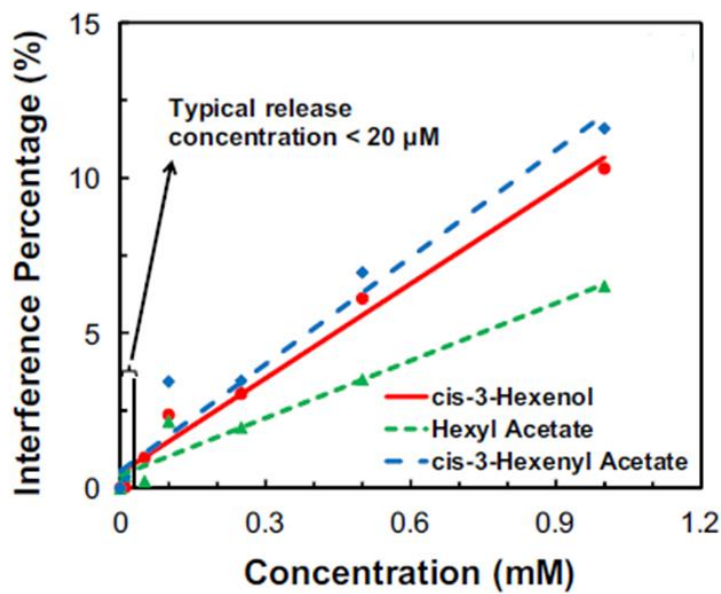


Figure 4.10: Percentage of current density interference caused by GLVs: *cis*-3-hexenol, hexyl acetate and *cis*-3-hexen-1-yl acetate at different concentrations.

Figure 4.10 shows the percentage rate of interference compounds at different testing concentrations, which range from 0 (for 0 μM of GLVs) to 2.36 %, 2.14% and 3.43 % respectively (for 100 μM of *cis*-3-hexenol, hexyl acetate and *cis*-3-hexen-1-yl acetate) as reported in Table 4.2.

Table 4.2: Current density interference of different concentration of GLVs in 50 μM in hydrolyzed MeSA.

Concentration of GLV (μM)	Current density interference percentage in 50 μM hydrolyzed MeSA (%)		
	<i>cis</i> -3-Hexenol	Hexyl Acetate	<i>cis</i> -3-Hexenyl Acetate
0	0	0	0
10	0.03	0.39	0.37
50	0.98	0.22	-0.03
100	2.36	2.14	3.43
250	3.04	1.94	3.46
500	6.11	3.49	6.95
1000	10.30	6.50	11.59

Since 100 μM of GLVs represent is about two orders of magnitude higher than typical concentrations of GLVs, we could conclude that none of the interference compound tested in this study has the significant impact on the hydrolyzed MeSA detection on the bi-enzymatic biosensor. Additionally, it is obvious that the interference behavior of *cis*-3-hexenol and *cis*-3-hexenyl acetate at high concentrations was similar, which can be explained by the generation of *cis*-3-hexenol after the hydrolysis of *cis*-3-hexenyl acetate. The interference of *cis*-3-hexenol and *cis*-3-hexenyl acetate was due to the enzymatic activity of alcohol oxidase towards the alcohol – *cis*-3-hexenol, although the activity of alcohol oxidase towards *cis*-3-hexenol is substantially lower compared to methanol due to its longer alkene chain.

In addition to the above-mentioned compounds, methanol, which produced by C3 plants, could also potentially interfere with MeSA detection, since the detection of MeSA by AOD/HRP sensor was based on the methanol that formed after hydrolysis. Therefore, the sensor was primarily developed for C4 plants, such as corns (Fall and Benson 1996). Previous research publications have indicated that significant amount of MeSA release by juvenile corn plant (*Zea mays*) was reported without methanol generation. In addition, the developed biosensor can also be used for crops, such as tobacco, as the methanol release level by tobacco crop is negligible compared to the quantity of MeSA (Shulaev, Silverman et al. 1997, Bernasconi, Turlings et al. 1998). Moreover, the biosensor can also be applied to methanol-releasing plants, if the volatile sample is pretreated to remove the contained methanol (Premkumar and Krishnamohan 2010).

4.3.4 Stability and repeatability of AOD/HRP-immobilized biosensor

Stability of the bi-enzymatic biosensor was evaluated for 11 days based on the appearance of significant amperometric current signal decrease over time. To fulfill this, the measurement was carried out with bi-enzyme modified RDE by using CPA and the current density from 50 μM

hydrolyzed MeSA, which is the concentration in the middle of the detection linear range, was collected before and after addition of the hydrolyzed MeSA. The RDE was then stored in 0.1 M PB, pH 7.6 at 4 °C and the stability evaluations were conducted on day 1, 2, 3, 4, 8, and 11 by following the same procedure. The original results of the stability evaluation are displayed in Figure 4.11.

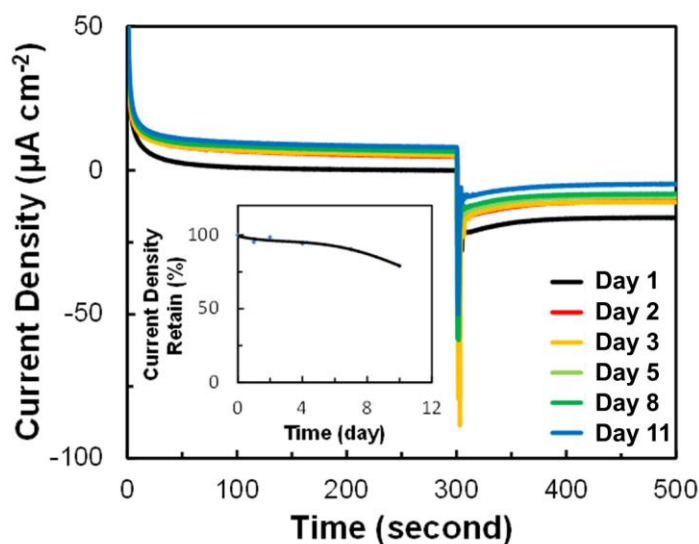


Figure 4.11: Stability of bi-enzyme modified electrode with 50 μM hydrolyzed MeSA from day 1 to day 11. The inset shows the retention of initial current density over time.

The results of the stability demonstrate that the current density from for H_2O_2 reduction decreased gradually over 10 days as the current density discrepancy before and after the addition of hydrolyzed MeSA decreased over time.

Table 4.3: Stability study of bi-enzyme modified electrode with 50 μM hydrolyzed MeSA.

Time (Day)	Current Density ($\mu\text{A cm}^{-2}$)	Current Density Retained (%)
1	16.42	100
2	15.64	95.27
3	16.17	98.52
5	15.47	94.27
8	14.85	90.44
11	12.99	79.13

Table 4.3 displays the net current density (the current density discrepancy before and after the addition of hydrolyzed MeSA) dropped from 100 % to 95.27 % within 1 day. However, the biosensor behaved relatively stable with very little current variations. The amperometric signal current was above 90 % of the initial value even after 7 days of storage. However, the current density sharply decreased to 79% after 10 days of storage, which could be attributed to the loss of enzyme activity. Since the biosensor was designed for one-time testing, the stability data here shows satisfactory retention of signal stability by the bi-enzyme biosensor for 7 days.

In addition to stability study, repeatability performance of the biosensor was also conducted. The experiments were carried out on the bi-enzyme modified RDE using 50 μM hydrolyzed MeSA was applied as the analyte. The measurements were repeated for 6 times in total with preparing the enzyme modified RDE for each time. The repeatability data shown in Figure 4.12 below display that the current density differed slightly between each measurements, which could be attributed to the systematic variances as well as the slight change in enzyme orientation on the electrode – the enzyme could orient itself in different ways upon immobilization on the electrode surface, and therefore, the active site of the enzyme could be either exposed to the electrolyte side or facing down the electrode.

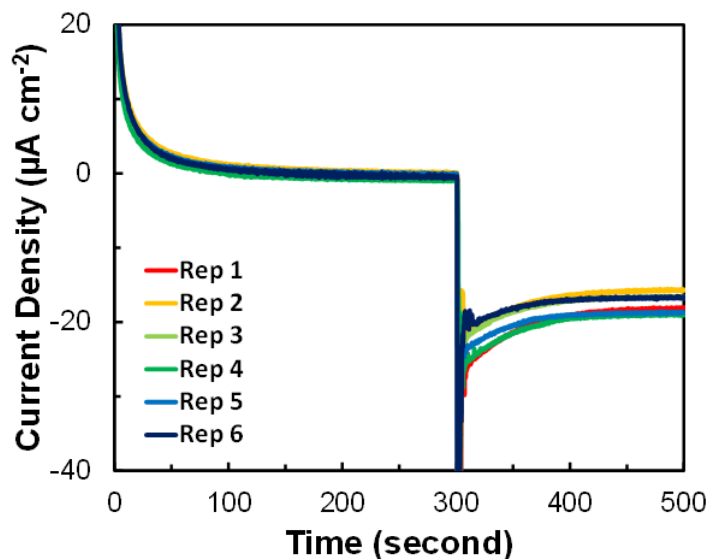


Figure 4.12: Repeatability of bi-enzyme modified electrode with 50 μM hydrolyzed MeSA. Six replicates have been tested for repeatability evaluation.

The variation of the enzyme orientation upon each modification could affect the substrate specific binding and reaction due to mass transfer limitation, thereby, causing small variances in the electrochemical performance of the biosensor in each set of experiments. Relative standard deviation (RSD) was calculated from the variances of the net current density (the current density difference before and after the addition of hydrolyzed methyl salicylate) in six replicates. The RSD for the repeatability experiments was 6.6 %, which is quite acceptable based on enzyme-based sensors.

4.3.5 Real sample study for methyl salicylate detection

Real sample study was conducted to evaluate reliability of the bi-enzyme biosensor on a native analyte containing MeSA. Wintergreen oil essentially contains 98 % of MeSA, which is produced by the enzymes of the wintergreen plant upon biotic and abiotic stresses. Wintergreen oil was hydrolyzed as stated before to generate enzymatic active SA and used as the analyte for

real-sample studies. However, MeSA is not naturally presented in the wintergreen plants, it can only be produced enzymatically from a glucoside within the leaves when macerated in warm water. Therefore, wintergreen oil was introduced to simulate the situation when plant produces MeSA due to plant infection. Different quantities of hydrolyzed wintergreen oil containing 98 % of MeSA was added stepwise to the electrochemical cell to maintain a final concentration of 0.1, 0.5, 1, 2.5, 5, 10, 25, 50 and 100 μM (*i.e.* the corresponding concentration of MeSA in the wintergreen oil is 0.098, 0.49, 0.98, 2.45, 4.9, 9.8, 24.5, 49 and 98 μM). The electrochemical signals were collected and the same experiment was repeated for three times. In addition, pure MeSA solution, after the hydrolysis using the same protocol, was added to maintain the same concentration of 0.1, 0.5, 1, 2.5, 5, 10, 25, 50 and 100 μM and the data was collected as standard working curve to determine the calculated concentration of MeSA from wintergreen oil. As it shows in Figure 4.13, three replicates of measurements obtained from hydrolyzed wintergreen oil display the same trend of that from the hydrolyzed pure MeSA.

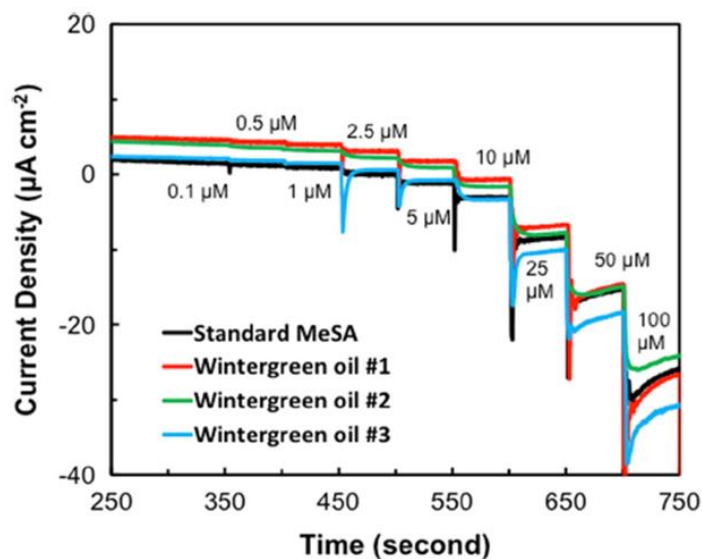


Figure 4.13: CPA of the RDE upon the stepwise addition of hydrolyzed wintergreen oil (3 replicates) resulting in concentrations of 0.1, 0.5, 1, 2.5, 5, 10, 25, 50 and 100 μM (98% MeSA) wintergreen oil. Control experiment / standard curve using pure MeSA at identical concentration gradients (black curve) is also displayed for comparison.

The standard concentration of from the wintergreen oil, the calculated concentration of MeSA, as well as the recovery are tabulated in Table 4.4.

Table 4.4: Standard concentration, calculated concentration, recovery, standard deviation (SD) and RSD of hydrolyzed wintergreen oil for real sample study.

Std. conc. (μM)	Cal. conc. (μM)	Recovery (%)	SD (μM)	RSD (%)
2.45	2.24	91	0.28	12.38
4.90	5.78	118	0.28	4.90
9.80	12.64	129	0.29	2.29
24.5	31.38	128	0.96	3.06
49.5	59.81	122	2.71	4.53

As seen in Table 4.4, the recovery obtained from the standard MeSA concentration and calculated MeSA concentration varies from 91 % to 122 %. The bias could be attributed to the

presence of other electrochemical active compounds in wintergreen oil such as α -pinene, myrcene, δ -3-carene, limonene, 3,7-guaiadine and δ -cadinene reacted directly on the electrode (Gurung 2007). Thus, the specificity of the electrode needs to be improved in the future work. From the RSD values in Table 4.4, it can be concluded that the current signals are highly repeatable when the concentration is around the middle point of the linear range (*e.g.* 49 μ M). It is also noteworthy that since the wintergreen oil is purified from the wintergreen oil leaf, it contains more compounds than the common VOCs that released to the air. Therefore, less false positive could be expected if VOC samples are used as analyte.

4.4 CONCLUSION

A bi-enzyme based amperometric electrochemical biosensor has been developed using AOD and HRP with established immobilization strategy. The biosensor demonstrated its capability of MeSA, a common VOC released by various plants under biotic stresses such as infestations and pathogen infections. The biosensor performance was characterized by both CV and CPA, among which, CPA demonstrated higher sensitivity and better LOD and LOQ, which allows for faster sample collection and detection of MeSA released from the stressed plants. The sensitivity and limit of detection successfully demonstrated the application potential for on-field MeSA detection. Wintergreen oil was applied for real-sample study, demonstrating the recovery of the MeSA detection varies from 91 % to 122 %, indicating that the specificity of the biosensor needs to be improved in the future work.

CHAPTER 5

DETECTION OF METHYL SALICYLATE USING SALICYLATE HYDROXYLASE / TYROSINASE – BASED BIOSENSOR

This chapter contains text modified from the following publications:

Yi Fang *et al.* 2016. *Biosensors and Bioelectronics* 85: 603-610.

Reprinted here with permission of the publisher.

Abstract

Volatile organic compounds have been recognized as important bio-marker chemicals to detect plant diseases caused by pathogens. Methyl salicylate has been identified as one of the most important volatile organic compounds released by plants during a biotic stress event such as fungal infection. Advanced detection of these marker chemicals could help in early identification of plant diseases and has huge significance for agricultural industry. This chapter describes the development of a novel bi-enzyme based electrochemical biosensor consisting salicylate hydroxylase and tyrosinase enzymes immobilized on carbon nanotube modified electrodes. The amperometric detection using the bi-enzyme platform was realized through a series of cascade reactions that terminate in an electrochemical reduction reaction. Electrochemical measurements revealed that the sensitivity of the bi-enzyme sensor was $30.6 \pm 2.7 \mu\text{A}\cdot\text{cm}^{-2}\cdot\mu\text{A}^{-1}$ and the limit of detection and limit of quantification were 13 nM and 39 nM respectively. Interference studies showed no significant interference from the other common plant volatile organic compounds. Synthetic analyte studies revealed that the bi-enzyme based biosensor can be used to reliably detect methyl salicylate released by unhealthy plants.

Keywords: Methyl salicylate, Biosensor, Salicylate hydroxylase, Tyrosinase, Volatile organic compound.

5.1 INTRODUCTION

5.1.1 Salicylate hydroxylase and tyrosinase as bi-enzyme system

Although the bi-enzymatic biosensor based on alcohol oxidase and horseradish peroxidase was successfully developed as discussed in Chapter 4, efforts to improve the sensitivity, limit of detection (LOD), limit of quantification (LOQ) and specificity, required better biosensor performance for methyl salicylate (MeSA) detection. In this chapter, a more selective enzyme combination for bi-enzymatic biosensor based on salicylate hydroxylase (SH) and tyrosinase (TYR) was used to improve the sensitivity and prevent unwanted cross-reaction that may result in the false positive signals. Salicylate (SA), a main compound formed after hydrolysis of MeSA, can be electrochemically detected using SH as the recognition element with high selectivity. The enzyme is immobilized through the methods described in the previous Chapter 4. SH is an FAD-dependent monooxygenase that converts SA to catechol in the presence of NADH and oxygen (Katagiri, Maeno et al. 1965, Yamamoto, Katagiri et al. 1965). Although SA acts as the natural substrate for SH, other pseudo-substrates such as benzoate derivatives can also be catalyzed by SH, thus generating false positive result. This issue can be addressed by introducing a second enzyme – TYR in the bio-recognition element, in order to build an enzyme cascade that provides highly selective MeSA detection. Additionally, as per the results discussed in Chapter 3, TYR not only could improve the specificity, but also increase the sensitivity for substrate detection. The stepwise reaction mechanism behind the MeSA is illustrated in Figure 5.1.

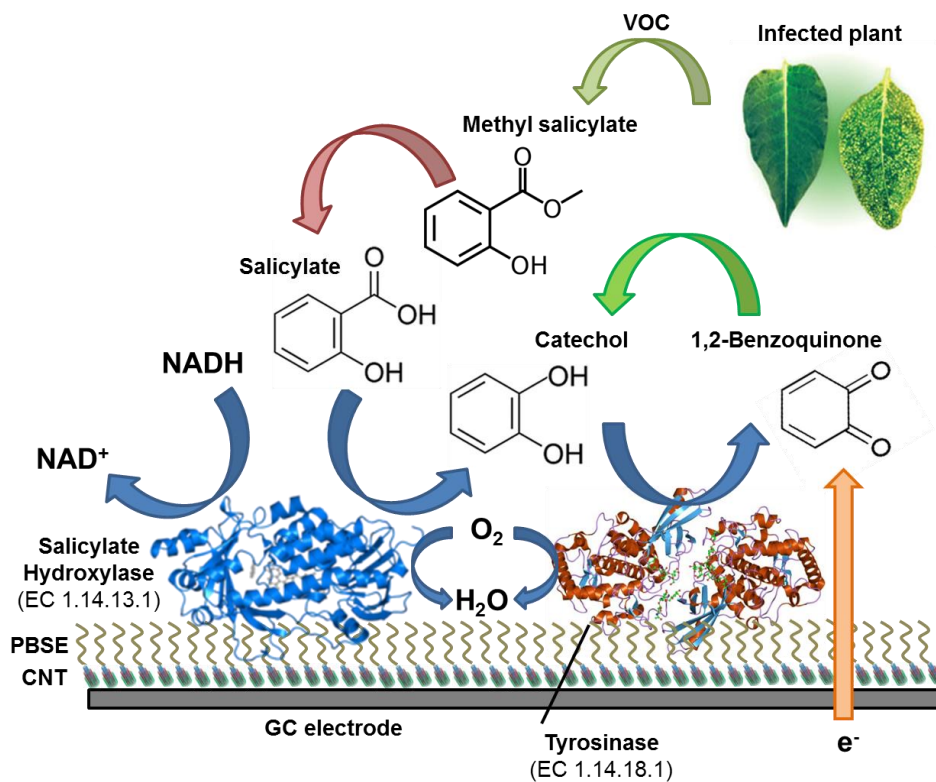


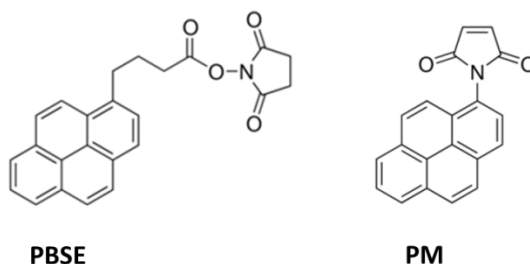
Figure 5.1: Schematic illustration of MeSA detection by SH/TYR-immobilized on carbon nanotube modified electrode. MeSA was hydrolyzed manually to generate methanol and SA. SA is catalyzed by SH to generate catechol in presence of NADH and oxygen. Catechol is further oxidized by TYR to form *o*-benzoquinone. The detection of MeSA is finally realized by measuring the reduction of *o*-benzoquinone on the electrode.

5.1.2 Exploration of other enzyme immobilization strategies

Although the enzyme immobilization strategy employing 1-pyrenebutanoic acid succinimidyl ester (PBSE) has been used as in the previous chapters, other cross-linking strategies were also evaluated in this study. The new immobilization methods used N-(1-Pyrenyl) maleimide (PM) and Poly-L-Lysine (PLL) as cross-linking agents to attach enzyme to carbon nanotube (CNT) modified electrodes.

5.1.2.1 1-pyrenebutanoic acid succinimidyl ester (PBSE) and N-(1-Pyrenyl) maleimide (PM)

Although the structure of both cross-linkers – PBSE and PM (as shown below) are similar in many aspects (*e.g.* the same pyrene group and the similar structure of succinimide and maleimide), the mechanisms of enzyme immobilization are quite different due to their chemical functionalities.



According to the structure of both cross-linkers – PBSE and PM, the binding of the pyrene group (from PBSE and PM) with CNT can be realized through the non-covalent bond π - π stacking. However, the cross-linking of PBSE and PM with enzyme is based on different mechanism – the succinimidyl group from PBSE can be replaced by the amine group from the enzyme (nucleophilic substitution reaction), while the alkene in maleimide from PM can be added by the thiol group from the enzyme (thiol-ene addition reaction). Therefore, both PBSE and PM are reported as hetero-bifunctional cross-linkers for enzyme immobilization.

5.1.2.2 Poly-L-Lysine (PLL)

In addition to the PBSE and PM, PLL, a polymer with a number of active primary amine groups, is also developed as the cross-linker for protein immobilization due to its good biocompatibility, flexible backbone and good water solubility. Some of the free amine groups on the PLL covalently cross-link with carboxyl-modified CNTs while the other free amine groups cross-link

with the carboxyl groups on the proteins to allow the immobilization of protein on the CNT-modified electrode. Accordingly, PLL becomes a homo-bifunctional cross-linking agent.

5.2 MATERIALS AND METHODS

5.2.1 Materials

Tyrosinase (E.C. 1.14.18.1) derived from mushroom (lyophilized powder, ≥ 1000 units / mg solid), methyl salicylate and farnescene were purchased from Sigma-Aldrich (St. Louis, MO, USA) and used directly as received. Humulene and tri-methylbenzene were obtained from Aldrich. Multiwalled carbon nanotubes (MWCNTs) and carboxyl modified single-walled carbon nanotubes (SWCNT-COOH) were purchased from DropSens Inc. (Spain) and used directly without further purification. Sodium salicylate, NADH and methylformamide (DMF) were obtained from Acros Organics (NJ, USA). FAD and dichlorobenzene were purchased from Alfa Aesar (Haverhill, MA, USA) and Eastman (Kingsport, TN, USA) respectively. 1-Pyrenebutanoic acid succinimidyl ester (PBSE) and N-(1-Pyrenyl) maleimide (PM) were obtained from AnaSpec Inc. (Fremont CA, USA). Poly-L-lysine (PLL), dicyclohexylcarbodiimide (DCC), and 1-(3-demethylaminopropyl)-3-ethylcarbodiimide hydrochloride (EDC) were purchased from Sigma, Aldrich and Alfa Aesar respectively for cross-linking evaluation. Methanol was obtained from Fisher Scientific (Waltham, MA, USA). All reagents used in the project were analytical grade unless other specification. 0.1 M potassium phosphate buffer (PB, pH 7.6) was used as the electrolyte for all experiments. All aqueous solutions were prepared in 18.2 M Ω nano-pure de-ionized (DI) water. Solutions were oxygenated by purging with oxygen for 15 min before experiments.

5.2.2 Apparatus

Cyclic voltammetry (CV) and constant potential amperometry (CPA) were performed using CHI 920 c model potentiostat. A glassy-carbon (GC) electrode purchased from Pine Instrument Company was used as working electrode for all experiments. Additionally, a 3 M Ag/AgCl electrode and a platinum wire were also used as reference and counter electrodes respectively to form a traditional three-electrode system together with working electrode for carrying out all electrochemical experiments in a conventional glass voltammetry cell. All experiments were conducted at 22 ± 2 °C.

5.2.3 Recombinant synthesis and purification of salicylate hydroxylase

SH has been discontinued from manufacturer and is not commercially available, therefore, synthesis and purification of SH with high activity with SA became the first task of the project. Gene *nahG* that codes for expression of SH was initially discovered in *Pseudomonas putida* (You, Ghosal et al. 1991). The *nahG* gene was codon optimized for expression in *Escherichia coli* and the gene sequence was sent to and synthesized by GenScript (Appendix A). Different cloning strategies were carried out with different primer designs to ensure that the failure of enzyme expression or activity could be dealt with.

5.2.2.1 Primer design for polymerase chain reaction (PCR)

Although the *nahG* gene was synthesized by GenScript in pUC57 plasmid, it does not contain any bio-affinity tag which renders difficulties for the future purification from the crude extract of the *E.coli*, therefore, cannot be directly used for transformation. Polyhistidine-tag (His-tag) is an amino acid motif that consists of at least six histidine (His) residues. It is commonly constructed in protein at either the N- or C-terminus of the protein. The His-tag on the recombinant protein

binds with affinity resin containing bound divalent nickel ions in the purification column while other expressed proteins that do not bind with the resin due to the lack of His-tag were removed by phosphate buffer with 5 mM of imidazole. The bound recombinant protein can be eluted by phosphate buffer (PB) with high concentration of imidazole (500 mM), which can compete with the His-tag to bind with the resin. The DNA primers were designed with 6 × histidine tag (His-tag) before the PCR amplification to allow the future purification from other proteins / enzymes that expressed by the *E.coli*. The His-tag was added on either C-terminus or N-terminus of the protein (Appendix B).

5.2.2.2 Construction of recombinant plasmid pTrc99a-*nahG*

The pUC57-*nahG* synthesized by GenScript was used as the template for PCR amplification, and both sets of primers (one set with His-tag on C-terminus and the other set with His-tag on N-terminus) were used (Appendix C). The PCR product was examined by the agarose gel and *nahG* gene was harvested before restriction enzymes – BamHI and HindIII were applied to clone the gene into the restriction enzyme-treated plasmid pTrc99A (Appendices C and D). The recombinant plasmid pTrc99A-*nahG* was constructed by cloning the *nahG* gene into pTrc99A that harbors ampicillin resistance gene (amp^{R}) as an antibiotic selection marker. The recombinant plasmid containing gene *nahG*-histidine tag was then transformed into *E. coli* XL 1-blue through electroporation at the potential of 1800 V. The resultant *E.coli* suspension was plated on the ampicillin-containing (100 $\mu\text{g}/\text{mL}$) agar LB plate for transformant selection for future enzyme expression purposes. The resultant transformants of *E. coli* XL 1-blue were inoculated in test tubes, where each contains 3 mL LB media with ampicillin concentration of 100 $\mu\text{g}/\text{mL}$. The strains were cultured overnight aerobically at 37 °C and each overnight culture was further inoculated into 250 mL fresh LB media with 100 $\mu\text{g}/\text{mL}$ of ampicillin and left to grow at the

temperature of 37 °C until the optical density at the wavelength of 600 nm (OD_{600}) reached 0.6, at which the *E. coli* reached log phase. The expression of *nahG* gene to synthesize SH was under the control of P_{lac} promoter and was induced by addition of isopropyl β -D-1-thiogalactopyranoside (IPTG). 1 mM of IPTG was added to initiate the expression of salicylate hydroxylase at 20 °C for 8 h Figure 5.2 shows the schematic illustration of the procedures involved in cloning and expression of *nahG* in *E. coli*.

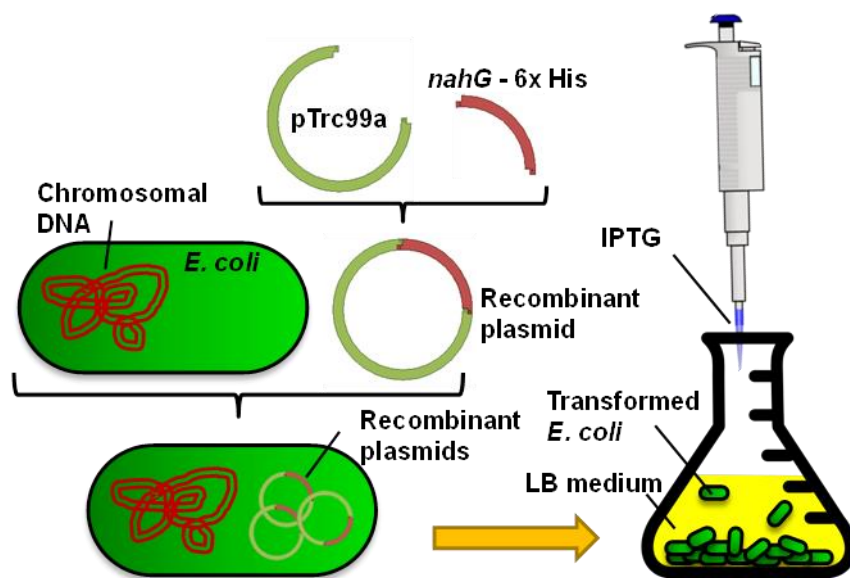


Figure 5.2: Schematic illustration of procedures involved in cloning and expression of recombinant *nahG* in *E. coli*: construction of recombinant plasmid using pTrc99A vector and *nahG* with 6 × histidine tag, transformation and expression of SH via IPTG induction. Not drawn to scale.

Cell pellets were harvested by centrifugation at 6000 rpm for 10 min. The cell pellets were resuspended and rinsed with 20 mM potassium phosphate buffer (PB), pH 7.6 twice to remove excess media before being lysed through the French Press. The lysed *E. coli* suspension was further centrifuged at 8000 rpm for 15 min and the supernatant was collected as the crude extract of SH. The crude extract was purified through fast-protein chromatography (FPLC) with

HisTrapTM HP column. The elution procedure was carried out with 20 mM PB, pH 7.6 with 5 mM imidazole as binding buffer (Buffer A) which allows the nickel-histidine binding on the HisTrapTM HP column. The volume ratio of the elution buffer (Buffer B) , which is 20 mM PB, pH 7.6 with 500 mM was gradually increase to elute SH from the HisTrapTM HP column due to higher affinity of nickel ion on the column with imidazole rather than histidine tag on the column. Different eluent fractions were collected in the fraction tubes and enzymatic activity was reassured by a traditional enzyme assay with addition of FAD as cofactor (Appendix E) (Yamamoto, Katagiri et al. 1965, White-Stevens and Kamin 1972). The fraction with highest enzyme activity was added with glycerol to final concentration of 20 % and the enzyme stock was frozen and stored at -80 °C (You, Murray et al. 1990) for all future experiments.

5.2.4. Electrode preparation for SH/TYR immobilization

GC electrode was first polished on a polishing pad with 0.05 µm alumina polishing powder for 5 min before each experiment. The electrode was then cleaned by ultrasonic cleaner for 5 min to remove the polishing powder adhered to the surface of electrode. The electrode was then rinsed with de-ionized (DI) water before further electrode modifications were carried out.

5.2.4.1 Immobilization with 1-pyrenebutanoic acid succinimidyl ester (PBSE)

Multi-walled carbon nanotube (MWCNT) was prepared by ultrasonicated 1 mg of MWCNT in 1 mL DMF for an hour. The electrode was then modified with CNT by drop casting 16 µL (in 8 steps of 2 µL) followed by drying in oven after each addition. The electrode was allowed to cool down on ice before 2 µL 10 mM PBSE in DMF was applied on the surface electrode for 15 min to allow the non-covalent binding between PBSE and CNTs. DMF and 0.1 M PB, pH 7.6 were consecutively used to remove the unattached PBSE from the electrode surface. A solution of

TYR was prepared by dissolving 5 mg TYR in 1 mL 20 mM PB, pH 6.6 and bi-enzyme solution mixture was prepared by mixing 5 μ L of previous prepared salicylate hydroxylase and 5 μ L of TYR solution. Bi-enzyme immobilized biosensor was fabricated by drop-casting 10 μ L of bi-enzyme solution on the electrode surface, and the electrode was incubated on the electrode for 30 min to allow covalent binding of PBSE and both enzymes. CV was performed after each step of modification and immobilization and the capacitance displayed was used to illustrate the modification procedures. For control study, mono-enzyme modified electrodes were prepared by drop casting 5 μ L of salicylate hydroxylase prepared previously instead of the enzyme mixture.

5.2.4.2 Immobilization with N-(1-Pyrenyl) maleimide (PM)

Similar to the immobilization protocol using PBSE, procedure of SH/TYR immobilization was also carried out and evaluated using cross-linker PM instead of using PBSE. The electrode cleaning protocol and CNT preparation method were exactly the same as introduced above in Section 5.2.4.1 and 2 μ L of 10 mM PM solution in DMF was used as the cross-linker instead of PBSE.

5.2.4.3 Immobilization with poly-l-lysine (PLL)

The GC electrode was polished and cleaned as above mentioned in Section 5.2.4.1. Single-walled carbon nanotubes modified with carboxyl group (SWCNT-COOH) were prepared by ultrasonically 1 mg of SWCNT-COOH in 1 mL DMF for an hour. 50 μ L of the 1 mg/mL SWCNT-COOH solution was modified with PLL by adding 0.5 μ L of 200 mg/mL PLL solution and 1.5 μ L of 200 mg/mL DCC (in DMF) and incubated in oven at 50 $^{\circ}$ C overnight. Three parallel incubations were also made and incubated overnight with only addition of PLL, only addition of DCC and no addition of DCC or PLL, respectively as negative control to evaluate the

effect of PLL immobilization. The incubated solution was drop casted on the electrode for a total loading of 16 μL (in 8 steps of 2 μL) followed by drying in oven at 50 $^{\circ}\text{C}$ after each addition. The electrodes were rinsed with DMF to remove DCC and unimmobilized PLL. 5 μL SH, 5 μL TYR and 5 μL of 60 mM EDC was mixed and drop casted on the electrode and the electrodes were kept at 4 $^{\circ}\text{C}$ for enzyme immobilization for 48 h. The electrodes were then rinsed by PB to remove the unimmobilized enzyme. The immobilization of enzymes with PLL can be illustrated briefly as Figure 5.3:

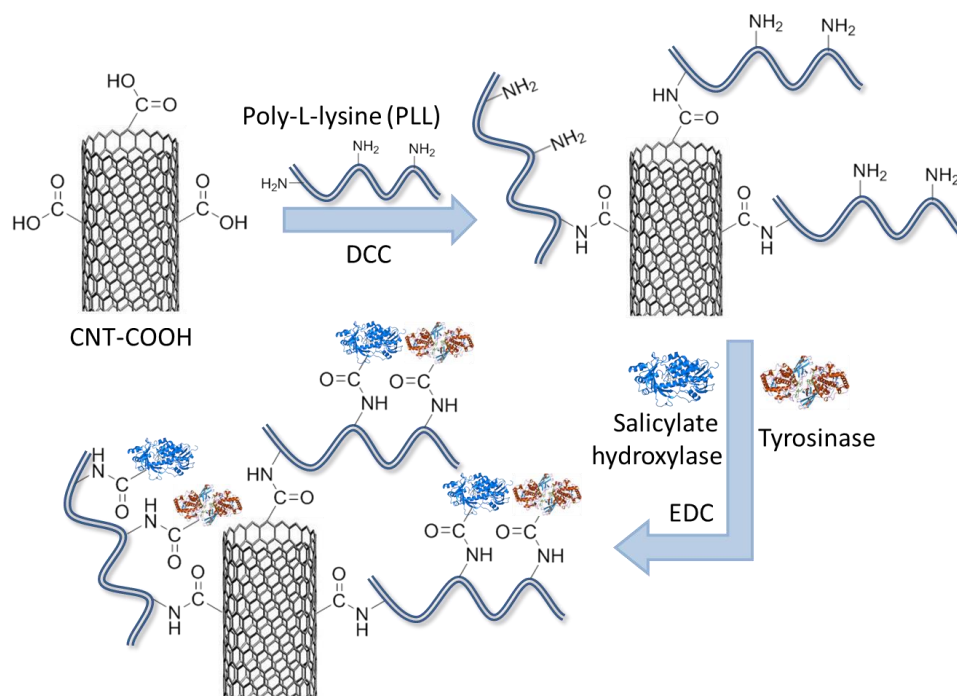


Figure 5.3: Schematic illustration of enzyme (SH and TYR) immobilization on CNT modified GC electrode with PLL.

5.2.5 Electrochemical measurements

A CHI 920 c potentiostat was used for all the experiments. For CV measurements, the potential was scanned from 0.4 V to -0.2 V to monitor the reduction current for bi-enzyme immobilized electrode and from -0.2 V to 0.4 V to monitor the oxidation current for mono-enzyme

immobilized electrode. Sampling interval of 1 mV and scan rate of 20 mV/s were used for all CV experiments. The initial potential for CPA was set to 0.025 V with 0.1 s interval for current collection.

5.3 RESULTS AND DISCUSSION

5.3.1 Expression and purification of salicylate hydroxylase

Crude extract of SH synthesized from *E. coli* XL 1-blue cells was collected from the French Press after homogenization and centrifugation as introduced previously. The crude extract was first evaluated by traditional SH enzyme assay with addition of FAD as cofactor (Yamamoto, Katagiri et al. 1965, White-Stevens and Kamin 1972) to calculate the enzyme activity and specific activity. In addition, the protein concentration of SH was determined by Bradford Assay to be ~ 35 mg of total protein in 4 mL (Kruger 1994, Kruger 2009). Catalytic assay revealed that the total and specific activity of SH were ~ 23 units and 0.67 unit / mg of protein. After the purification by fast-protein liquid chromatography (FPLC) with HisTrapTM column, 0.73 mg of protein with the total activity of 8.96 units was obtained. Although the purification yield was only 39 %, the specific activity of SH increased approximately 19 fold to ~ 12.3 units/mg as it shows in Table 5.1.

Table 5.1: Purification table of SH from *E. coli* XL 1-blue.

Step	Vol (mL)	Total protein (mg)	Total activity (unit)	Specific activity (unit/mg)	Purification fold	Yield (%)
Crude extract	4	34.8	23.3	0.67	(1)	(100)
HisTrap TM HP	2	0.73	8.96	12.34	19	39

The purification of SH from the crude extract of *E.coli* can be observed from the SDS-PAGE gel in Figure 5.4. Large amount of proteins have been expressed in the crude extract with the overexpression of SH between the marker 55 kDa and 36 kDa, which corresponds to the molecular weight of SH of 43 kDa to 47 kDa depends on different biological sources. After the purification, most of the unwanted proteins / enzymes were removed by the FPLC elution and only SH was retained.

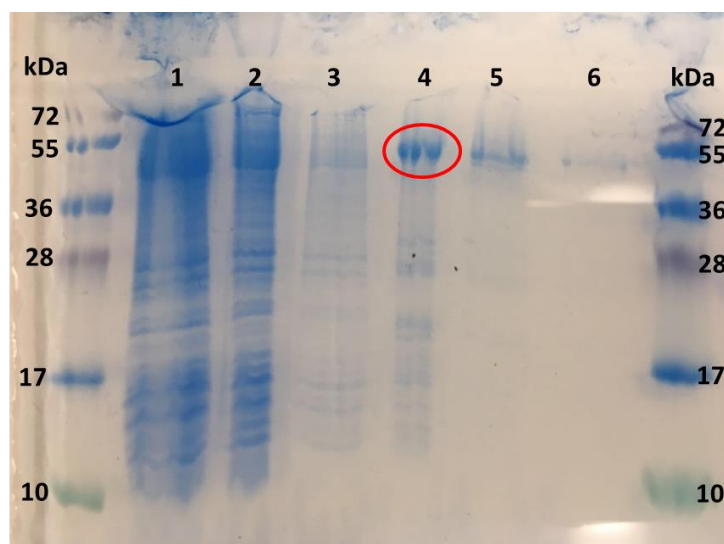


Figure 5.4: SDS-PAGE Gel image of crude extract in dilution factors of 10 (Lane 1), 20 (Lane 2) and 50 (Lane 3) and purified SH in original concentration (Lane 4), dilution factor of 5 (Lane 5) and 10 (Lane 6). The expression of SH is observed in Lane 4 as presented in the red circle between protein markers of 36 kDa and 55 kDa.

5.3.2 Cyclic voltammetry of bi-enzymatic biosensor with PBSE as cross-linker

The step-by-step electrode modification and immobilization (modification of CNT, PBSE and immobilization of bi-enzyme) can be demonstrated by the increase in capacitance captured by CV throughout the modification in Figure 5.5.

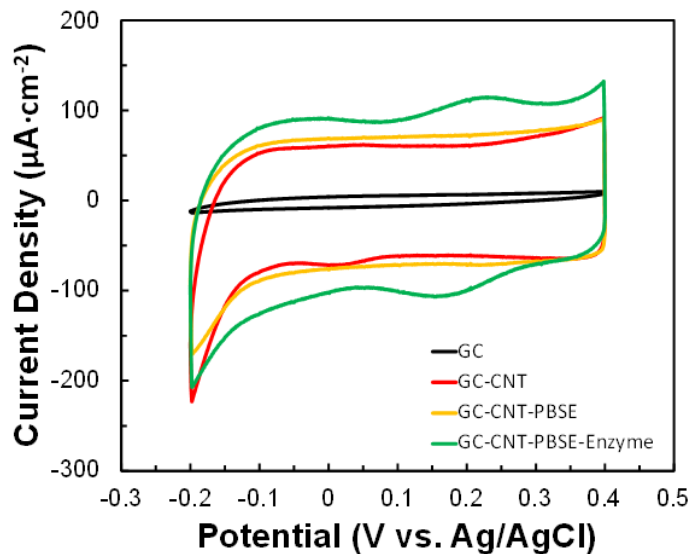


Figure 5.5: CV responses of bare GC electrode (black), the same electrode modified with CNT (red), with CNT and PBSE (orange) and with CNT, PBSE and the two enzymes SH/TYR (green).

In addition, two prominent peaks appeared at 0.23 V as oxidation peak and 0.15 V as reduction peak can be attributed to the electrochemical reaction of the copper center within TYR molecule. This result confirms the immobilization of TYR on the electrode surface.

Control experiments were first conducted using the mono-enzymatic biosensor consisting of only SH immobilized on CNT electrodes. The study was carried out by sequentially adding FAD, NADH and SA, which acted as analyte, followed by CV measurement after each addition of SA. 100 µL of 0.1 mM FAD was first added due to the requirement of FAD as the cofactor for the SH reaction. The CV result for this experiment can be found in Figure 5.6, which demonstrates that FAD does not show any electrochemical activity within the range from -0.2 V to 0.4 V and confirmed that any peak appeared in the subsequent experiments were not from the redox reactions of FAD.

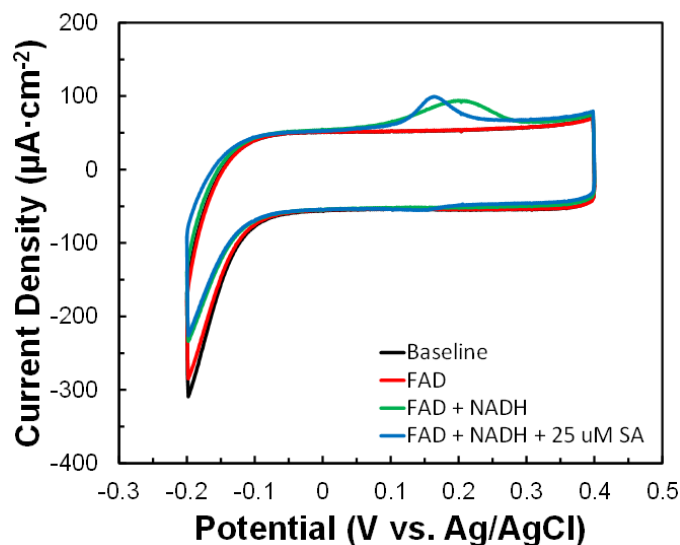
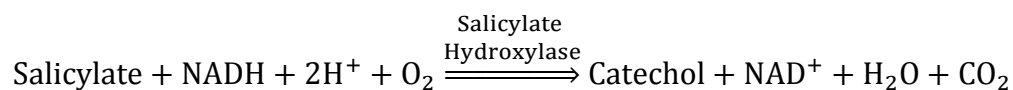


Figure 5.6: CV after sequential addition of 100 μL of 0.1 mM FAD (Red), 50 μL of 10 mM NADH (Green) and 25 μM salicylate (Blue) on SH-immobilized mono-enzyme CNT electrode consisting of SH.

Then 50 μL of 10 mM of NADH solution was added as the second cofactor for SH and the electrochemical redox activity of NADH was observed using CV between the same potential window. A small oxidation peak can be found around 0.2 V in Figure 5.6 due to the direct oxidation of NADH to NAD^+ , which corresponds with early publications of direction electrochemistry of NADH (Li, Wen et al. 2012, Li, Worley et al. 2012). In the next step, SA was added to the electrolyte to maintain the final SA concentration of 25 μM and another CV was performed to observe the electrochemical reaction. Under aerobic condition, SA would be enzymatically reduced by SH to catechol while NADH would be oxidized to NAD^+ simultaneously as per the reaction below.



The resulting CV response is displayed in Figure 5.6, where an oxidation peak at 0.15 V was observed upon addition of 25 μM , which can be attributed to the peaks overlap from both electrochemical oxidation of NADH and catechol on the electrode surface. Catechol is electrochemically oxidized to 1,2-benzoquinone as per the following reaction at 0.15 V (Enache and Oliveira-Brett 2011, Umasankar and Ramasamy 2013, Umasankar and Ramasamy 2014).



For all the experiments, the reduction wave below -0.1 V could be attributed to the reduction of dissolved oxygen present in the system.

Similar to the mono-enzymatic biosensor study discussed above, similar set of experiments was also performed using the bi-enzymatic biosensor composed of both SH and TYR as recognition elements. The study was carried out by sequential addition of FAD, NADH and SA followed by CV measurement after each addition.

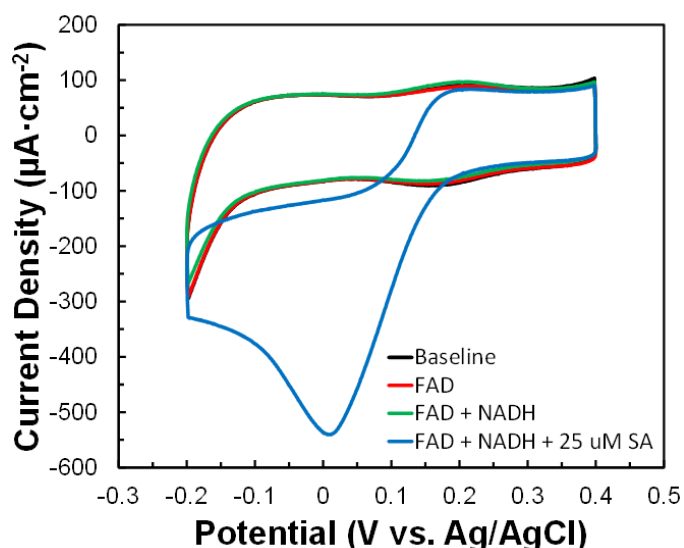
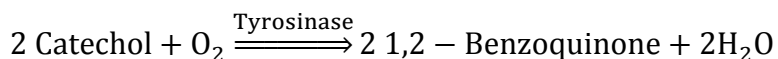


Figure 5.7: CV after sequential addition of 100 μL of 0.1 mM FAD (Red), 50 μL of 10 mM NADH (Green) and 25 μM SA (Blue) on SH/TYR-immobilized bi-enzyme CNT electrode using PBSE as cross-linker.

In Figure 5.7, similarly to the mono-enzymatic biosensor, no significant oxidation / reduction peak can be observed after adding FAD. The mild hump noticed at 0.2 V in all the voltammograms in Figure 5.7 is the characteristic redox peaks of the blue copper protein such as TYR as found in previous research work (Ramasamy, Luckarift et al. 2010, Umasankar and Ramasamy 2013, Umasankar and Ramasamy 2013). However, unlike the mono-enzymatic biosensor, the oxidation peak upon addition of NADH was not observed on bi-enzyme immobilized electrode. This could be due to the reduced transport of additional protein in the CNT matrix on the modified electrode. However, with addition of 25 μ M SA, a prominent reduction peak appeared below 0.025 V as shown in Figure 5.7 compared to the mild oxidation peak from the mono-enzymatic biosensor. This distinctive peak appears only when both SH and TYR were present in the electrochemical system and thus can be attributed to the electrochemical reduction of 1,2-benzoquinone that formed from the biocatalytic oxidation of catechol by TYR as per the following reaction.



Unlike the mono-enzymatic biosensor, the bi-enzyme electrode did not exhibit a direct electrochemical oxidation of the catechol in the 0.015 V region as it appeared in the mono-enzymatic biosensor. This suggests that the biocatalytic oxidation of catechol by TYR proceeds at the high rate that it depletes its surface concentration rapidly.

A further set of control experiments were performed with both unimmobilized electrode and TYR-immobilized mono-enzyme electrodes, both in presence and absence of catechol, to observe the electrochemical role of TYR on the electrode. The results of this experiment are shown in Figure 5.8, which clearly display the redox couple peaks at \sim 0.15 V in the absence of

TYR on the non-immobilized electrode. On the other hand, a much stronger reduction peak was observed at ~ 0.05 V from the same concentration of catechol, which can be attributed to the reduction of 1,2-benzoquinone to 1,2-hydroquinone on the electrode surface. Due to the proximity of the TYR, 1,2-benzoquinone generated from the TYR can be rapidly accumulated to the electrode surface and renders high reduction current density.

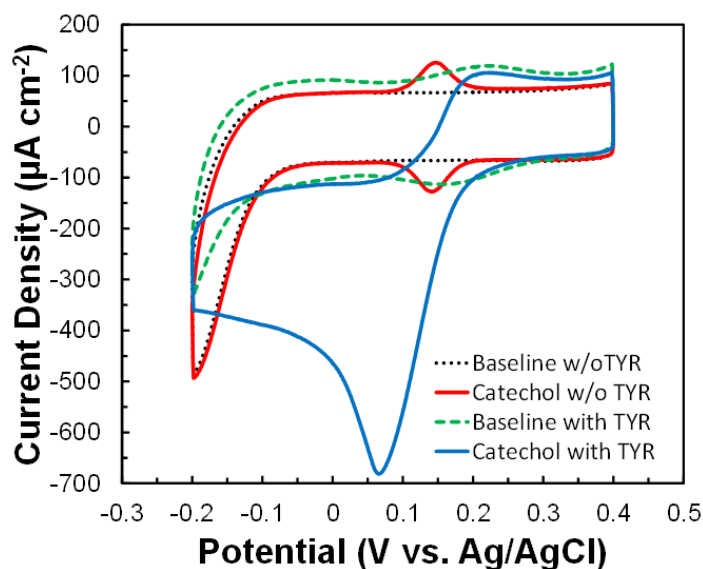


Figure 5.8: CV responses of unimmobilized and TYR-immobilized mono-enzyme CNT electrodes in the presence and absence of catechol.

Another set of control experiments was performed on both unimmobilized and TYR-immobilized nano-enzyme electrodes, both in the presence and absence of SA. The results of which are shown in Figure 5.S1. None of the voltammograms shown in Figure 5.S1 showed a direct electrochemical reduction peak for 1,2-benzoquinone as observed in Figure 5.8. This indicates that the 1,2-benzoquinone could only be produced in the enzymatic system through the cascadic reactions (Steps 1-4), when both SH and TYR are present. The results provide conclusive evidence that the bi-enzyme biosensor consisting both SH and TYR immobilized on the CNT modified electrode provides a reliable detection of salicylate at potentials below 0.15 V.

5.3.3 Cyclic voltammetry of bi-enzymatic biosensor with PM and PLL as cross-linkers

In addition to PBSE, PM was evaluated as the cross-linker for enzyme immobilization. After 100 μL of 0.1 mM FAD, 50 μL of 10 mM NADH and SA were consecutively added to maintain a concentration of 25 μM , a reduction peak for 1,2-benzoquinone appeared similar to that of the bi-enzymatic electrode immobilized by PBSE, demonstrating the applicability of PM as a cross-linker for enzyme immobilization. However the current density achieved using PM was not significantly higher compared to that of PBSE (Figure 5.S2). The immobilization mechanism can be explained by the thiol-ene reaction occurred between maleimide group of PM and the thiol-group of cysteine from both SH (Appendix A) and TYR.

The same experiments were conducted for evaluating the immobilization efficiency of the cross-linker PLL. As introduced in Section 5.2.4.3, four electrodes were prepared with PLL as the cross-linker and DCC as the reaction agent, PLL only, DCC only and free of PLL and DCC as controls. The 1,2-benzoquinone reduction peak obtained from the DCC/PLL cross-linker demonstrate that PLL can also be used as cross-linker for enzyme immobilization (Figure 5.S3A and Figure 5.S3B). It was also proved that DCC can be used to increase the combination of PLL on the CNT due to the higher reduction peak obtained from DCC/PLL (Figure 5.S3A) than that of PLL-only case (Figure 5.S3B). The results further indicated that no reduction peak was observed in the two control groups without PLL (Figure 5.S3C and Figure 5.S3D). The immobilization function of PLL can be explained by the condensation reaction occurred between amine group of PLL and the carboxyl group of acidic amino acid residues such as aspartic acid and glutamic acid from both salicylate hydroxylase (Appendix A) and tyrosinase.

Although the use of PM and PLL as cross-linkers for enzyme immobilization were successfully demonstrated, no significant increase of the reduction current density was obtained, therefore, the following experiments would follow the traditional PBSE cross-linking strategy.

5.3.4 Determining optimal enzyme ratio of SH and TYR on electrode surface

The loading of either enzymes (SH and TYR) as well as the ratio of their loadings on the CNT electrode surface would have a significant impact on the electrochemical detection and the resulting sensor performance. Therefore, the difference in catalytic parameters (such as K_m and k_{cat}) between the two enzymes and differences in mass transport coefficients of the reactants and products must be optimized in order for the cascadic reaction to proceed efficiently (Steps 1-4). To be specific, if the loading of SH on the electrode is insufficient compared to TYR, the cascadic reactions would be limited by the catechol generation reaction, resulting in low 1,2-benzoquinone generation and hence low currents on the electrode, thereby directly impacting the sensitivity of SA detection. On the other hand, the cascade reactions will also be limited by the step that converts catechol to 1,2-benzoquinone (Step 3), if the loading of TYR is insufficient compare to SH, which can also impact the sensitivity of detection. Therefore, it is essential to optimize the kinetics and transport inside the enzyme-CNT matrix of the bi-enzyme sensor to ensure optimal conditions for reliable detection of SA. However, precise optimization and control could only be achieved by theoretical treatment of the sensor surface, which is a separate task and project all by itself. Therefore, a simpler experimental design approach for fabricating bi-enzyme sensor with different loadings of the two enzymes was attempted in this work. For this purpose, five different volume ratio combination of SH and TYR enzymes were used for the immobilization on CNT modified electrodes. The loading of SH and TYR used respectively in each set were: 1 μ L and 9 μ L, 3 μ L and 7 μ L, 5 μ L and 5 μ L, 7 μ L and 3 μ L and 9 μ L and 1 μ L

on the electrode surface. The other steps of modifications remained the same as introduced previously. CV was performed on all the five bi-enzyme electrodes in the presence of the same concentration of FAD, NADH and SA and the results are displayed in Figure 5.9.

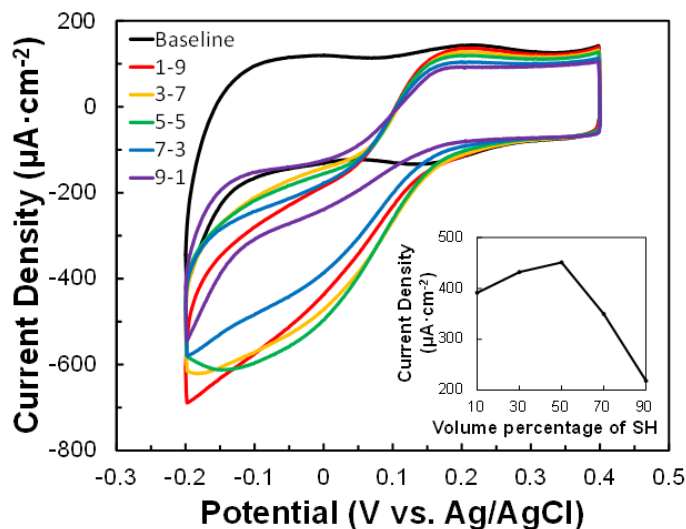


Figure 5.9: CV responses of the bi-enzyme biosensor containing immobilized SH and TYR. The 2 mL electrolyte consists of 27.8 µM SA with FAD (4.7 µM) and NADH (0.23 mM). The ratio of SH:TYR loadings by volume on the electrode respectively are 1:9 (red), 3:7 (orange), 5:5 (green), 7:3 (blue) and 9:1 (purple). The inset shows the current density of the sensor measured at 0.025 V for different enzyme loading ratios showing the maximum sensitivity was obtained when the enzyme volume ratio was 1:1.

The results show that the rate of 1,2-benzoquinone reduction (as determined by the slope of the reduction wave below 0.15 V) differed significantly as the enzyme ratio of SH and TYR changed. The inset of Figure 5.9 demonstrated the current density observed at 0.1 V as a function of volume percentage of SH in the mixture, *i.e.* 50 % refers to 1:1 volume loading ratio of SH:TYR used for immobilization. The potential of 0.1 V was an ideal reference point to measure the electrochemical rate because it was outside both kinetic and mass transport limited regions. Additionally, it is noteworthy that the current for 1:9 SH:TYR ratio was higher than that for 9:1 SH:TYR ratio. The trend of the inset of Figure 5.9 also indicates that the cascading reactions were

more limited by the reaction catalyzed by TYR (Step 3) than by SH (Step 2). The highest sensitivity (current density) was observed for a SH:TYR volume ratio 1:1. This corresponds to 0.022 unit of SH and 67.175 units of TYR in the bi-enzyme mixture. Consequently, the mixture of 5 μL SH and 5 μL TYR (5 mg/mL) was used in all the following experiments to investigate the biosensor performance such as sensitivity and limit of detection/quantification.

5.3.5 Electrochemical responses of the bi-enzymatic biosensor

Transient performance of the biosensor was measured using CV to determine electrochemical parameters such as sensitivity, LOD and LOQ and reliable linear range for the SA detection. Since no electrochemical redox peaks can be observed from FAD and NADH from Figure 5.7, baseline was collected by CV after addition of 100 μL 0.1 mM FAD and 50 μL 10 mM NADH. Then SA solution was added in steps to a concentration gradient from 2.3 μM , 4.6 μM , 9.3 μM , 18.6 μM , 27.8 μM and 46.3 μM . CV was then performed after each addition of SA. The resulting voltammograms displayed in Figure 5.10 indicated that the 1,2-benzoquinone reduction increased progressively (below 0.15 V) with the SA concentration in the electrolyte.

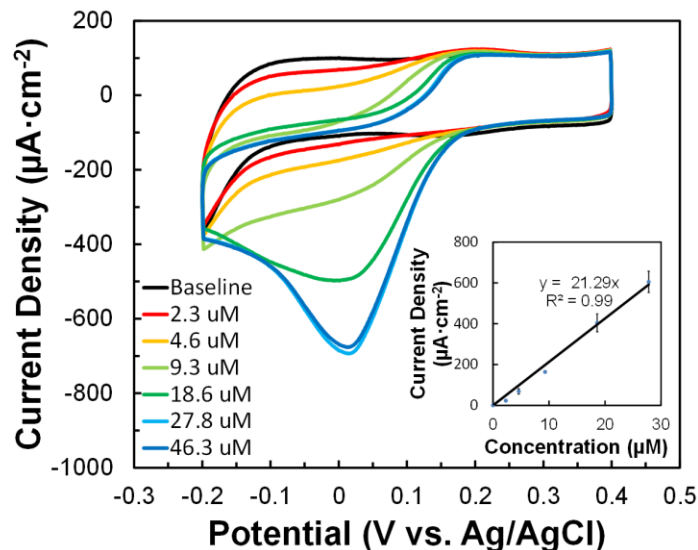


Figure 5.10: CV responses of SA with presence of FAD and NADH, and sensitivity, linear range and R^2 value (Inset).

The reduction currents increased up to 27.8 μM of SA beyond which the enzyme exhibited substrate saturation. The effect of substrate limitation on the enzyme kinetics can be explained by the Michaelis-Menten equation below:

$$V = V_{\max}[S]/(K_m + [S])$$

As the concentration of substrate $[S]$ increased, the enzymatic reaction rate eventually reached saturation and be equal to V_{\max} . The biosensor parameters were calculated from the CV data at 0.025 V where current peak was. The inset in Figure 5.10 shows the current density at 0.025 V at different concentrations within the linear range of detection. The values were average of 3 replicates. From the CV data, the sensitivity was calculated to be $21.3 \pm 1.9 \mu\text{A}\cdot\text{cm}^{-2}\cdot\mu\text{M}^{-1}$ and the LOD and LOQ were determined to be $0.14 \pm 0.02 \mu\text{M}$ and $0.42 \pm 0.04 \mu\text{M}$, respectively. The linear range of SA detection using CV is 0 – 27.8 μM ($R^2 = 0.99$) as listed in Table 5.2.

Table 5.2: Sensor performance metrics for SA detection using CV and CPA techniques.

Method	Linear range (μM)	R^2	Sensitivity ($\mu\text{A}\cdot\text{cm}^{-2}\cdot\mu\text{M}^{-1}$)	LOD (μM)	LOQ (μM)
CV	0 – 27.8	0.99	21.3 ± 1.9	0.14 ± 0.01	0.42 ± 0.04
CPA	0 – 27.8	0.99	30.6 ± 2.7	0.013 ± 0.005	0.039 ± 0.015

Since CV is a transient technique, it is usually used to obtain a firsthand understanding of the sensor, but is generally not used as a quantitative measurement tool in real biosensor fabrication situation. A more reliable and steady state measurement can be achieved by CPA. For the CPA, the initial potential was set at 0.025 V and biosensor was stabilized for 2 min before 100 μL of 0.1 mM FAD and 50 μL of 10 mM NADH was consecutively added at 1-min interval. After 1 min of pre-conditioning, SA solution was introduced stepwise into the electrochemical cell in different quantities to maintain a final concentration of 2.3 μM , 4.6 μM , 9.3 μM , 18.6 μM , 27.8 μM and 46.3 μM . The reduction current was continuously monitored by CPA for 1 min after each addition. For each addition of SA, the reduction current reached steady value within short time and at high concentrations began to fade within 10 seconds due to the mass transfer limitations as it shown in Figure 5.11.

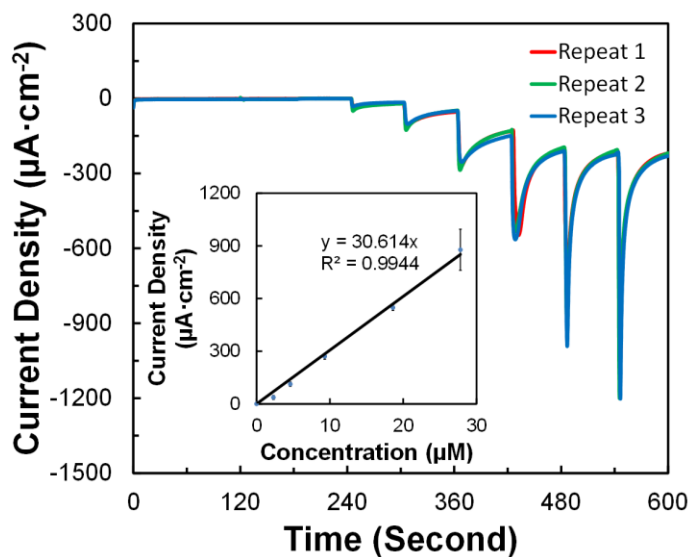


Figure 5.11: CPA responses of SA with presence of FAD and NADH and sensitivity, linear range and R^2 value (Inset).

Therefore, the highest current measured at each concentration was used for calculating the sensor parameters, which are also reported in Table 5.2. Compared to the CV, the bi-enzyme biosensor exhibited higher sensitivity ($30.6 \pm 2.7 \mu\text{A}\cdot\text{cm}^{-2}\cdot\mu\text{M}^{-1}$), lower LOD ($0.013 \pm 0.005 \mu\text{M}$) and lower LOQ ($0.039 \pm 0.015 \mu\text{M}$) in the CPA measurements with the same linear range of salicylate detection $0 - 27.8 \mu\text{M}$ ($R^2 = 0.99$) as it shows in Table 5.2. Compared to the previously developed bi-enzymatic biosensor based on alcohol oxidase and horseradish peroxidase for MeSA detection (Chapter 4), we successfully increased the sensitivity by over 110 fold from $0.28 \mu\text{A}\cdot\text{cm}^{-2}\cdot\mu\text{M}^{-1}$ to $30.6 \mu\text{A}\cdot\text{cm}^{-2}\cdot\mu\text{M}^{-1}$ and lowered the limit of detection from $0.98 \mu\text{M}$ to 13 nM . The above parameters allowed us to realize the quantification of MeSA released by plants in less than 3 min under the assumptions that the produced MeSA is captured in 2 mL electrochemical cell for detection based on the MeSA production rate of 283 ng/plant/h (Shulaev, Silverman et al. 1997).

5.3.6 Evaluation of the reusability of the SH/TYR biosensor

Enzyme based biosensors are not meant for extended period of storage or repeated use as the enzymes in the biorecognition element deteriorate over time. However, the biosensor needs to be tested to perform repeatedly during multiple usages within a short period of time, to justify its adoption to a commercial product over other competitive technologies. To this end, reusability of the bi-enzyme biosensor was evaluated for 10 repetitions of SA detection and the results are shown in Figure 5.12.

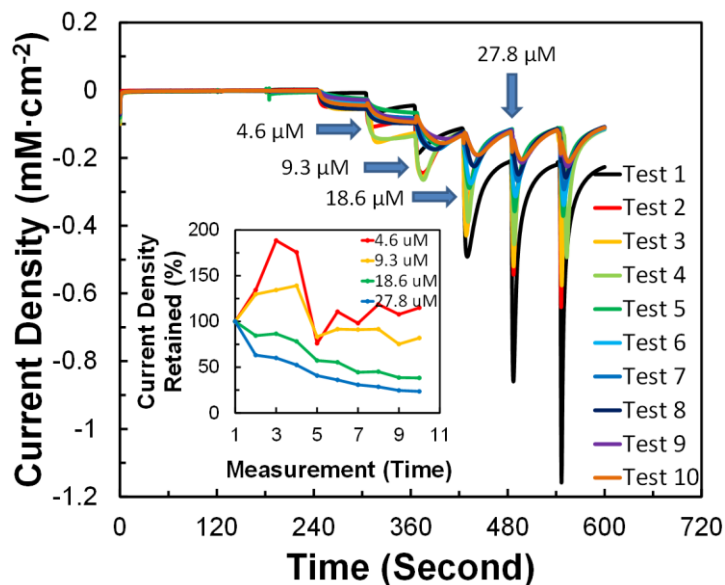


Figure 5.12: Reusability of bi-enzymatic biosensor for SA from 2.3 μM to 46.3 μM . Current density retention over number of measurements in reusability is displayed in insets with two low concentrations (4.6 μM and 9.3 μM) and two high concentrations (18.6 μM and 27.8 μM).

Similar to the sensitivity and LOD determination, SA solution was added stepwise in the electrochemical cell in the presence of FAD and NADH followed by CPA measurements after each addition. The experiment was carried out for 10 times using the same fabricated biosensor, and after each measurement the electrode was rinsed to remove any residual catechol or 1,2-benzoquinone on the electrode surface. Four SA concentrations within the linear range – two low

concentrations (4.6 μM and 9.3 μM) and two high concentrations (18.6 μM and 27.8 μM) were analyzed. For low SA concentrations of 4.6 and 9.3 μM , the current density increased during the first few repetitions (the inset of Figure 5.12). This could be caused by the residues of 1,2-benzoquinone remained on the electrode surface from the previous repetition that was not removed completely during the rinsing. For low concentrations of 4.6 and 9.3 μM , the current density remained constant around 100 % of its original value, throughout the 10 repetitions with no obvious loss in the sensitivity. On the other hand, a continuous loss in sensitivity was observed during the 10 repetitions at high concentrations of salicylate at 18.6 and 27.8 μM , suggested that the bi-enzyme biosensor in its current form could not be used to reliably detect high concentrations of SA beyond 10 μM without suitable calibration. The reason for the sensitivity loss during repeatable measurements at high SA concentrations could be attributed to the imbalance in the kinetics and mass transport at the sensor-electrolyte interface. It is also important to note that detection of SA concentrations above 10 μM are generally not necessary due to the low release rate of MeSA by typical plants.

5.3.7 Stability of the bi-enzyme biosensor

In addition to reusability, the stability of the biosensor was also evaluated using CPA technique. The bi-enzyme biosensor was fabricated on day 1 and used to measure different concentrations of SA (4.6, 9.3, 18.6 and 27.8 μM) on the same day, using the previously described experimental procedure. After the experiments were conducted on day 1, the electrode was rinsed by 0.1 M phosphate buffer and stored in 0.1 M PB with 10 % glycerol at 4 °C. The same sets of experiments were repeated on days 2, 4, 6 and 8 and the current density for SA detection was monitored over time. The results of the stability studies are displayed in Figure 5.13.

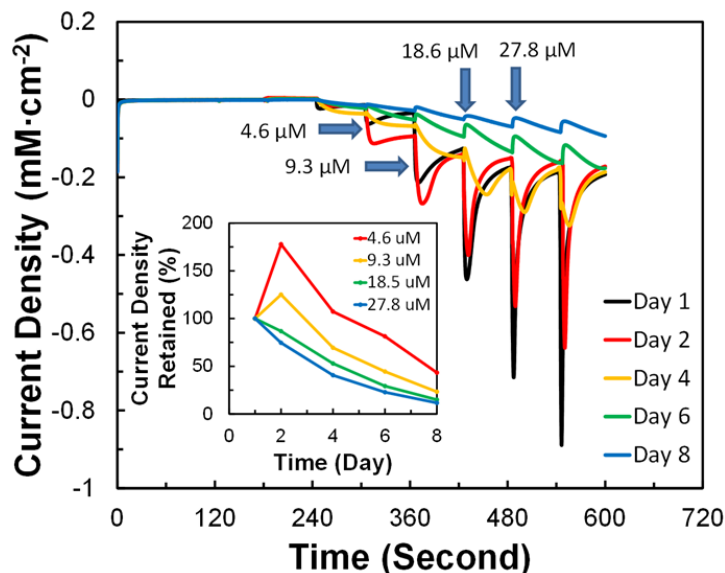


Figure 5.13: Stability of bi-enzyme biosensor for SA from 2.3 μM to 46.3 μM . Current density retention over time is displayed in insets with two low concentrations (4.6 μM and 9.3 μM) and high concentrations (18.6 μM and 27.8 μM).

Similar to the results obtained from during reusability evaluation, the currents at low SA concentrations (4.6 and 9.3 μM) increased during the second measurement on day 2, likely due to the residual catechol or 1,2-benzoquinone present on the electrode that could not be removed during rinsing. The current density for all other SA concentrations decreased gradually after day 2 due to the deterioration of enzymes on the sensor surface. In addition, the currents took longer time (10 – 60 seconds) to reach steady values unlike that on day 1, where it reached steady state within 2 seconds. The results suggest that the biosensor could not be stored for long-term and a suitable stabilization method must be developed before it can be employed for a practical application. While this could be a goal of the future project, the results also indicate that bi-enzyme sensor provides superior detection capabilities on the first day.

5.3.8 Effect of interference on the bi-enzyme biosensor

In addition to MeSA, other volatile organic compounds (VOCs) can also be released by both healthy and stressed plants. For instance, dichlorobenzene (DCB) and 1,2,3-trimethylbenzene (TMB) are among the most common expressed VOCs released by healthy uninfected soybean (Zhu and Park 2005). On the other hand, farnesene (FAR) and humulene (HUM) are reported to be VOCs that released by soybean aphid-infected soybean plant in addition to methyl salicylate (Zhu and Park 2005). Therefore, the interference caused by FAR, HUM, DCB and TMB on amperometric detection of MeSA using bi-enzyme sensor were evaluated. Since the eventual quantitative detection of MeSA was realized after the hydrolysis, one potential interfering compound that is produced during the hydrolysis, *i.e.* methanol (MeOH), was also evaluated. In order to maintain the same ionic strength with 0.1 M phosphate buffer, pH 7.6, 0.19 M KOH was used to hydrolyze the above-mentioned interfering VOCs for 2 h in 90 °C water bath as it shown in Figure 4.2. Interfering VOC samples were prepared by adding phosphoric acid to adjust pH to 7.6 before the evaluation experiments were carried out. CPA was used for interference evaluation in the presence of 100 μ L of 0.1 mM FAD and 50 μ L of 10 mM NADH. Very high concentrations ranging from 9.3 μ M to 1.9 mM of MeOH, FAR, HUM, DCB and TMB were used for the interference study. The upper range of 1.9 mM is significantly higher than the typical VOCs concentration released by pathogen-infected plants. The reason for using such high concentrations of interfering compound is to ensure the conservative estimate of interference under extreme (unfavorable) conditions. The experiments of interference study carried out were similar to that of earlier CPA measurements to determine sensitivity and LOD. The results of these measurements are shown in Figure 5.14.

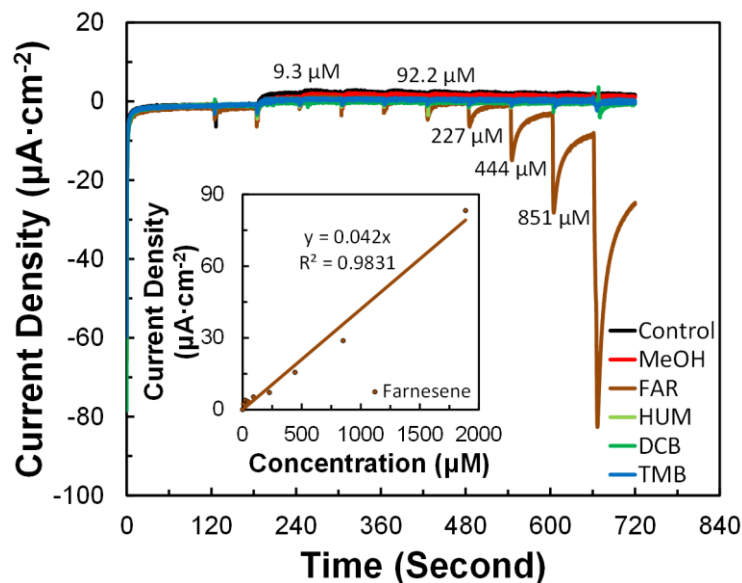


Figure 5.14: CPA responses of interference compounds – methanol (MeOH), farnesene (FAR), humulene (HUM), dichlorobenzene (DCB), 1,2,3-trichlorobenzene (TCB) and control (PB).

In order to consider the volume change as interference solution was added stepwise in the electrochemical cell, PB with same volume was stepwise added as the control to compare with the experimental interference compounds. The results indicate that MeOH, HUM, DCB and TMB did not contribute to significant interference with the SA detection current at the CPA operation potential of 0.025 V as shown in Figure 5.14. Although FAR exhibits a noticeable interference (sensitivity of $0.04 \mu\text{A}\cdot\text{cm}^{-2}\cdot\mu\text{M}^{-1}$) as shown in inset of Figure 5.14, the current is negligible compared to that of the salicylate detection without interfering compounds ($30.61 \mu\text{A}\cdot\text{cm}^{-2}\cdot\mu\text{M}^{-1}$). It can be concluded that none of the most common interference compounds identified above cause significant interference to the bi-enzyme sensor towards the detection of SA of MeSA.

5.3.9 Evaluation of bi-enzyme biosensor using synthetic analyte

Previous reports provide detailed information about the types of volatile signatures including the compositions and relative molarity of the compounds that are released by uninfected and aphid-infected soybean plants (Zhu and Park 2005). Based on this information, the cocktails of the VOC mixtures simulating both the healthy and infected soybean VOCs were prepared and used as synthetic analyte to evaluate the performance of the bi-enzyme sensor at near-practical conditions. The compositions of these synthetic analytes are given in Table 5.3.

Table 5.3: Compositions of synthetic analyte simulating the VOC signature of uninfected and soybean-aphid infected soybean plants

Uninfected synthetic analyte		Soybean aphid-infected synthetic analyte	
VOC	Concentration (mM)	VOC	Concentration (mM)
Dichlorobenzene	10	Methyl salicylate	10
1,2,3-trimethylbenzene	7	Farnesene	15
		Humulene	10

The synthetic analytes were prepared in 0.19 M KOH solution and hydrolyzed at 90 °C water bath for 2 h followed by pH neutralization by addition of phosphoric acid to 7.6, before CPA measurement was carried out with the synthetic analyte samples. For the CPA measurement, the pH adjusted synthetic analyte sample was gradually added to the electrolyte containing 100 μ L 0.1 mM of FAD and 50 μ L of 10 mM NADH. The results of the measurements shown in Figure 5.15 indicate that the uninfected synthetic analyte did not exhibit any noticeable reduction current even at high concentrations of the synthetic analyte.

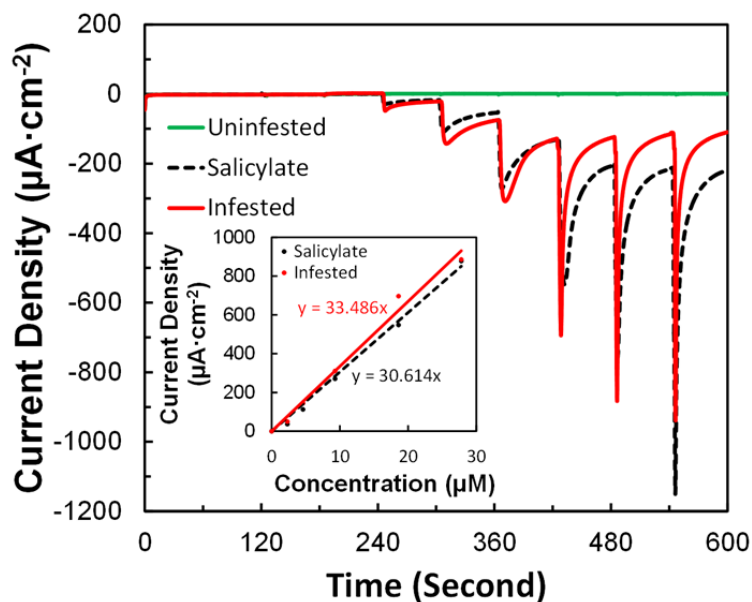


Figure 5.15: Uninfested synthetic analyte, infested synthetic analyte and SA as control in simulated sample study. The inset shows the sensitivity of the infested synthetic analyte and pure SA.

On the other hand, for the infested synthetic analyte, a stepwise increase in reduction currents with concentration was observed. From the previous data, we can conclude the reduction current increase is due to the concentration of SA produced after hydrolysis of MeSA in the analyte sample. The qualitative and quantitative trend of aphid-infested analyte was nearly identical to that of the responses from pure SA as analyte. The measured concentration of MeSA in the synthetic analyte was calculated based on the current versus concentration data given in Figure 5.11 and the results are tabulated in Table 5.4.

Table 5.4: Simulated sample study with measuring simulated samples for uninfested, infested and SA.

Concentration Added (μM)	Concentration Measured (μM)	Recovery (%)
4.6	4.73	102.77
9.3	10.15	109.11
18.6	22.76	122.34
27.8	28.93	104.06

The ratio of the measurement concentration to the original concentration added was used to determine the recovery. As shown in Table 5.4, most concentrations within the linear range of detection exhibit satisfactory recovery (~ 100 %), demonstrating reasonable sensor accuracy for real sample measurement and quantification. The bi-enzyme biosensor exhibited a sensitivity of $33.49 \mu\text{A}\cdot\text{cm}^{-2}\cdot\mu\text{M}^{-1}$ for the infected analyte, which was not significant different from that of the sensitivity obtained for pure SA ($30.61 \pm 2.68 \mu\text{A}\cdot\text{cm}^{-2}\cdot\mu\text{M}^{-1}$) as analyte (RSD = 8.8 %). The minor sensitivity difference between the simulated infected sample and upper limit of the pure SA can be explained by the cross-reaction resulting from the interference compounds especially farnescene. These results strongly suggest that the bi-enzyme biosensor can be used for reliable detection of the analyte (MeSA) released by infected crops as discussed in the introduction.

5.4 CONCLUSION

A bi-enzymatic electrochemical biosensing platform consisting SH and TYR as recognition elements immobilized on CNT modified electrode surface was constructed in this work. The detection of SA – after hydrolysis of MeSA – was based on the cascade of four reaction steps that culminate in the electrochemical reduction of 1,2-benzoquinone on the electrode. The fabricated biosensor was evaluated for the selective detection of SA, a derivative compound of MeSA present in the volatile organic signature of infected crops. The bi-enzyme biosensor displayed high sensitivity and nano molar range for LOD, which is a significant improvement over the previously demonstrated bi-enzymatic biosensor consisting alcohol oxidase and horseradish peroxidase discussed in the earlier chapter. The detection suffered very little interference from other common VOCs released by both uninfected healthy plant and soybean-aphid-infected plants. Synthetic analyte studies confirmed that the sensor can be used for reliable detection of analytes indicative of crop infection with high selectivity.

5.5 SUPPLEMENTARY DATA

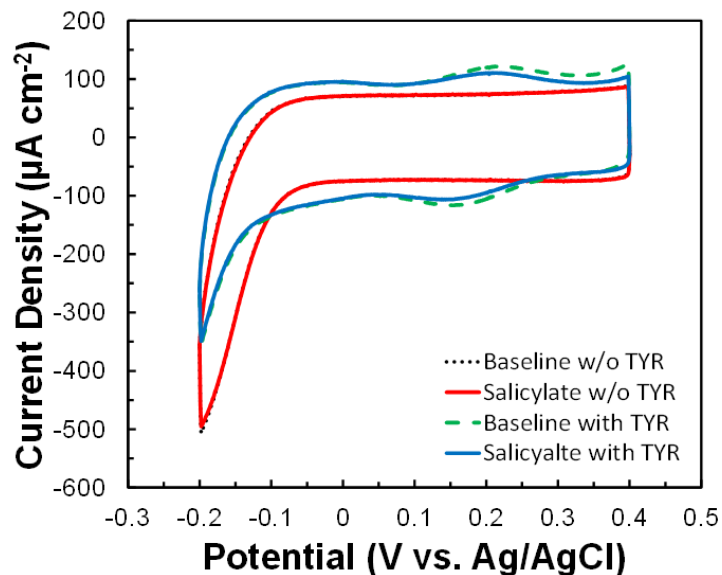


Figure 5.S1: CV responses of unimmobilized and TYR-immobilized mono-enzyme CNT electrodes in the presence and absence of SA.

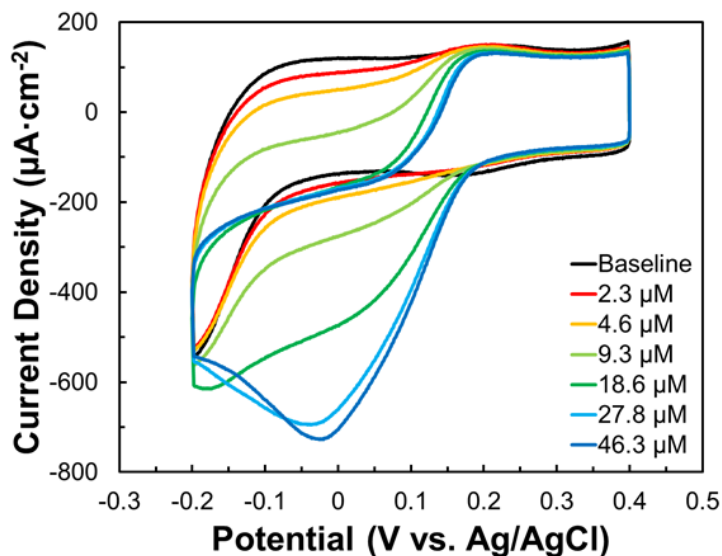


Figure 5.S2: CV of SA concentration effect on SH/TYR-immobilized GC electrode using PM as cross-linker.

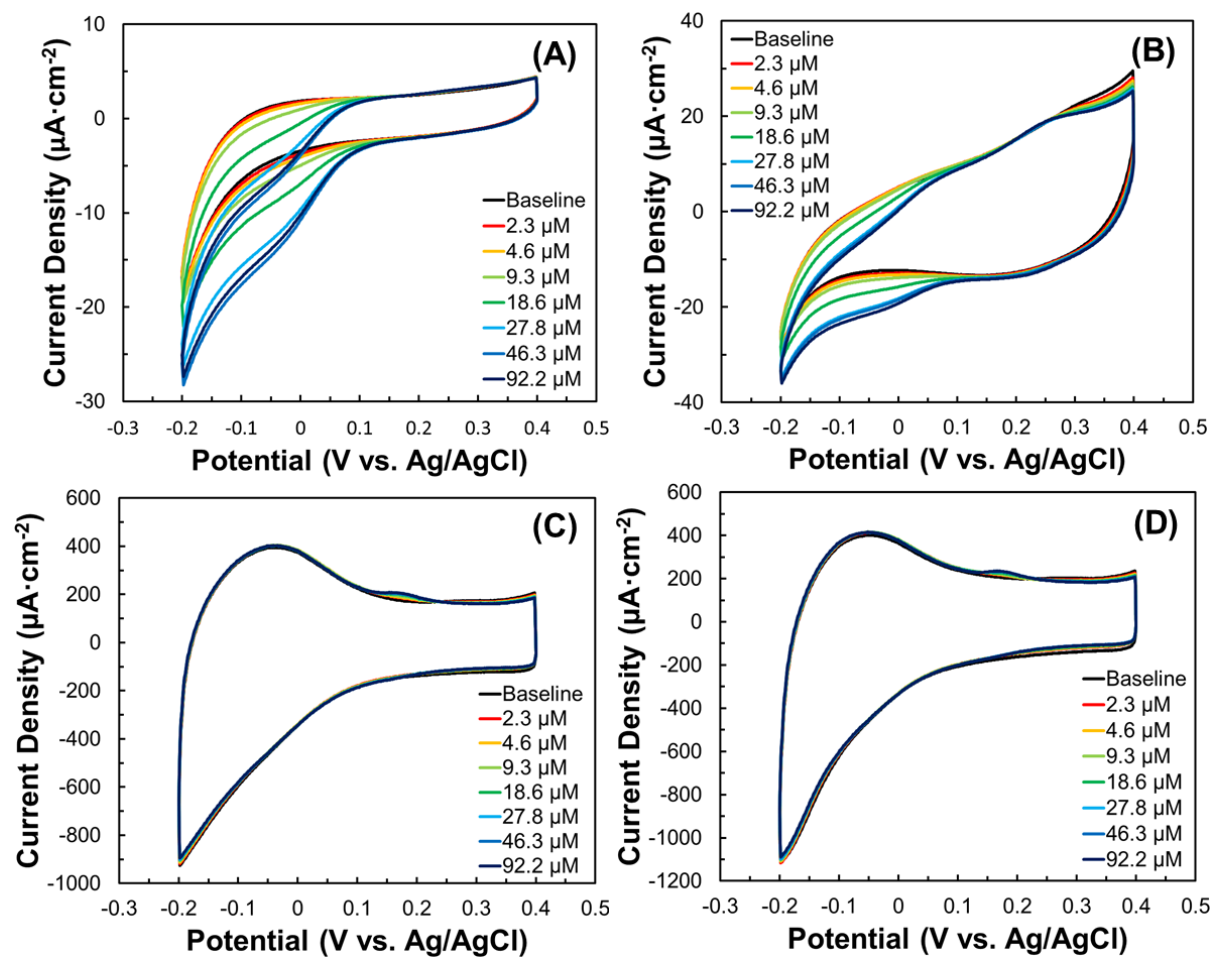


Figure 5.S3: CV of SA concentration effect on SH/TYR-immobilized GC electrode using PLL as cross-linker with both PLL and DCC as reaction agent (A), only PLL as cross-linker (B), only DCC as reaction agent (C) and no cross-linker or reaction agent (D).

CHAPTER 6

DIRECT DETECTION OF METHYL SALICYLATE USING ESTERASE / SALICYLATE HYDROXYLASE / TYROSINASE – BASED TRIENZYMATIC BIOSENSOR

To be submitted to Biosensors and Bioelectronics.

6.1 INTRODUCTION

6.1.1 Current limitations of the chemical hydrolysis of methyl salicylate

In the previous chapters, the developments of two types of bi-enzymatic biosensors consisting of alcohol oxidase / horseradish peroxidase and salicylate hydroxylase (SH) / tyrosinase (TYR) have been successfully demonstrated for the detection of methyl salicylate (MeSA). Although the electrochemical parameters such as sensitivity, limit of detection (LOD) and limit of quantification (LOQ) satisfy the requirement for the detection, pretreatment of MeSA (*i.e.* chemical hydrolysis of MeSA to form methanol and salicylate (SA)) prior to detection is necessary. The chemical hydrolysis of MeSA consists of KOH hydrolysis of the sample followed by phosphoric acid neutralization. These additional pre-treatment requirements impact the biosensor performance and device miniaturization as the pre-treatment requires hot water bath for hydrolysis and pH meter for pH adjustment after the hydrolysis. This step greatly limits the applicability of the biosensor for widespread commercial use by unskilled users. Therefore, a more effective and easy-to-handle method for MeSA hydrolysis is necessary and proposed in this chapter.

6.1.2 Application of esterase for hydrolysis

In this work, the hydrolysis step was carried out by an enzymatic reaction in an effort to avoid pretreatment of the sample. Esterase (ES) (E.C. 3.1.1.1), also called carboxyl esterase or carboxylic-ester hydrolase, is an enzyme which catalyzes a chemical reaction of the form as below:



To carry out the hydrolysis of MeSA, ES was used to catalyze the reaction as shown below to generate SA that can be used for detection using SH and TYR.



A tri-enzymatic biosensor consisting ES, SH and TYR can be employed for the detection of MeSA without additional pre-treatment requirements for MeSA hydrolysis. In order to hydrolyze MeSA, ES was mixed with SH and TYR to prepare a tri-enzyme mixture for immobilization on the electrode. The entire detection mechanism is illustrated by the scheme in Figure 6.1:

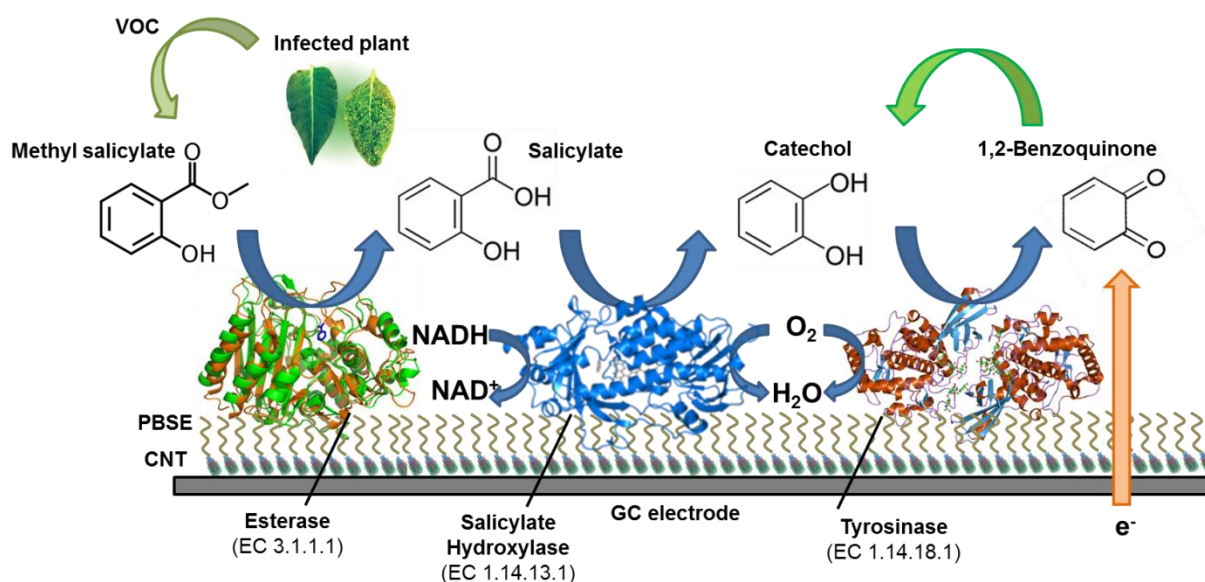


Figure 6.1: Schematic illustration of tri-enzyme with all three enzymes – ES, SH and TYR immobilized on the electrode. Not drawn to scale.

As shown in the Figure 6.1, MeSA diffused to the electrode surface to form methanol and SA by the enzyme ES immobilized on the electrode. SA can then be decarboxylated by SH to form catechol, which will further be oxidized by TYR to form 1,2-benzoquinone. The direct detection of MeSA will eventually be realized through reduction of 1,2-benzoquinone to 1,2-hydroquinone as introduced in Chapter 5.

An alternative option to immobilize all three enzymes on the electrode is to maintain ES in the bulk electrolyte potassium phosphate buffer (PB, pH 7.6) to enable bulk hydrolysis of MeSA to form SA, before SA is measured in the cascade reactions catalyzed by SH/TYR bi-enzymatic recognition element as introduced in Chapter 5, which is shown in Figure 6.2.

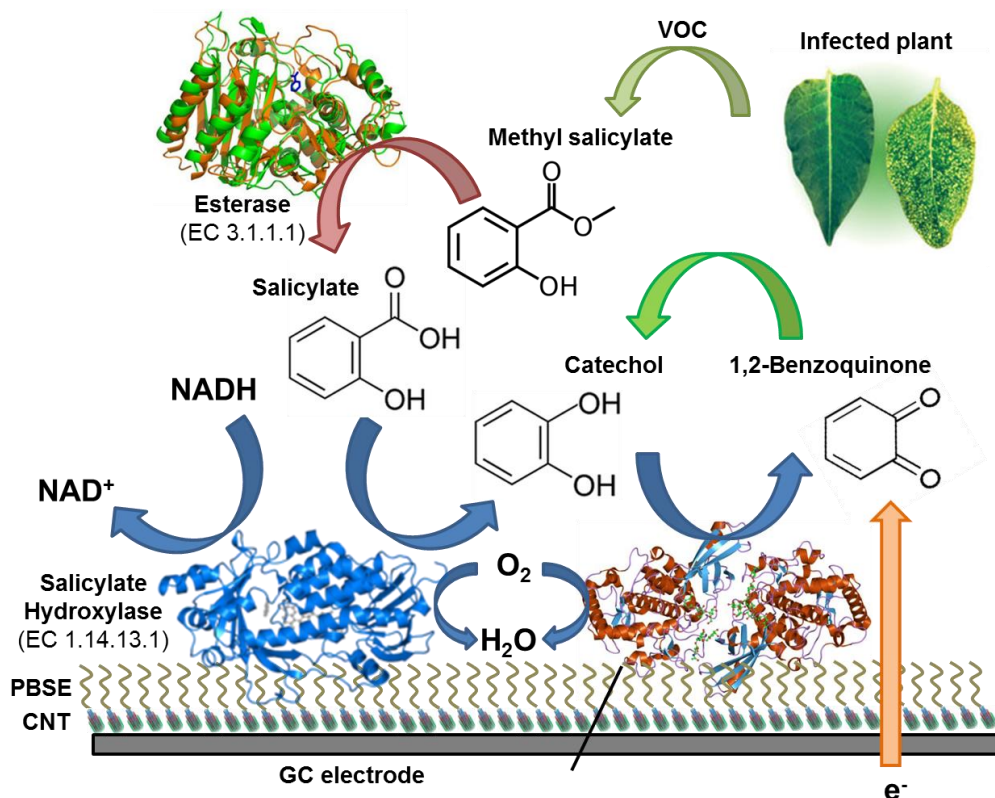


Figure 6.2: Schematic illustration of tri-enzyme with two enzymes (*i.e.* SH and TYR) immobilized on the electrode and esterase added in the solution. Not drawn to scale.

As shown in Figure 6.2, this approach for MeSA detection involves 2 steps. First, MeSA produced by diseased plants can be collected and pre-concentrated in the electrolyte. During the collection and pre-concentration, ES present in the electrolyte would simultaneously hydrolyze the MeSA to generate SA and methanol. The resulting solution containing SA can be used for MeSA detection (through SA) in the second step.

6.1.3 Gaseous methyl salicylate collection and pre-concentration system

Since either the bi-enzyme or tri-enzyme biosensor requires an aqueous solution, a collection and pre-concentration of gaseous MeSA step is necessary to enable detection. Thus, a purge-and-trap device will be designed for VOC collection. As introduced above, ES can also be added in the electrolyte so the MeSA collected from the VOCs released by the diseased plant can be hydrolyzed before the real detection and proceed simultaneously during detection. In order to maintain favorable operating condition for ES to hydrolyze MeSA in bulk electrolyte, a PB at pH 7.6 will be used for the collection and pre-concentration of MeSA released by the plants. The proposed collection and pre-concentration system is illustrated in Figure 6.3.

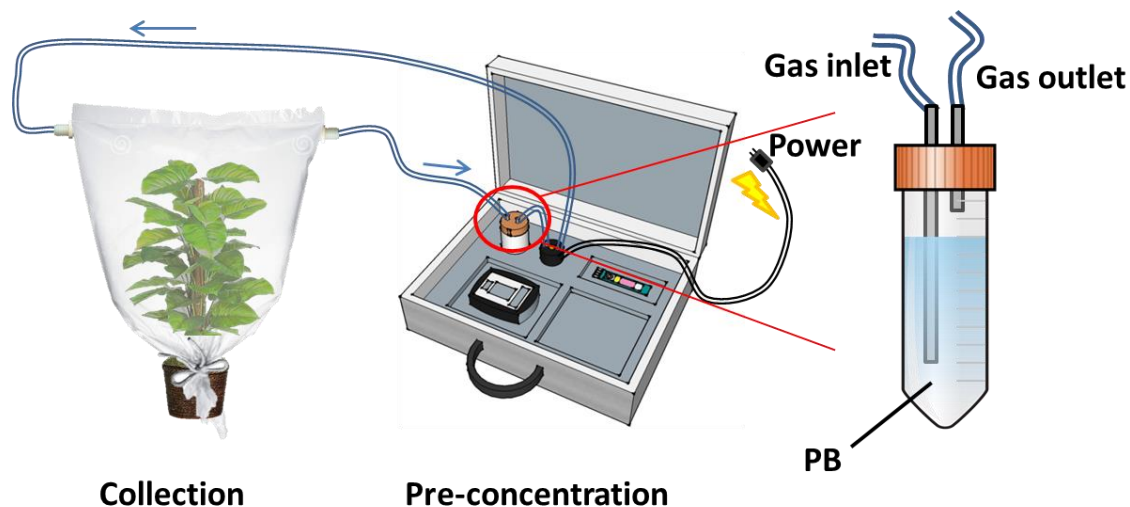


Figure 6.3: Schematic of proposed collection and pre-concentration system for MeSA generated by stressed plants. Computer control system not shown. Not drawn to scale.

In the collection / pre-concentration system, the VOCs including MeSA are collected in the plastic bag, and the ambient air is purged by a micro air pump through the connected hose to the PB electrolyte in the pre-concentration reservoir. The gaseous MeSA is pre-concentrated in the reservoir and hydrolyzed by esterase in the reservoir.

Although the procedure of collection and pre-concentration can be manually carried out, a computer controlled automation platform could be used to start and stop the purge-and-trap. The temperature measurement program can be controlled by computer to measure the ambient temperature for compensation of enzyme activity instead of conducting temperature measurement using a thermometer by the end-users. In this project, a platform that realizes the automatic collection and ambient temperature measurement is proposed.

6.2 MATERIALS AND METHODS

6.2.1 Materials

Salicylate hydroxylase (E.C. 1.14.13.1) was expressed and purified from *E.coli* XL-1 blue transformed with pTrc99A-*nahG*-His tag as introduced in Chapter 5. Esterase from porcine liver (lyophilized powder, ≥ 15 units / mg solid), tyrosinase (E.C. 1.14.18.1) derived from mushroom (lyophilized powder, ≥ 1000 units / mg solid) and methyl salicylate were purchased from Sigma-Aldrich (St. Louis, MO, USA) and used directly as received. Multiwalled carbon nanotubes (MWCNTs) were purchased from DropSens Inc. (Spain) and used directly without further purification. Sodium salicylate, NADH and methylformamide (DMF) were obtained from Acros Organics (NJ, USA). Dimethyl sulfoxide (DMSO), FAD and 1-pyrenebutanoic acid succinimidyl ester (PBSE) were purchased from VWR, Alfa Aesar (Haverhill, MA, USA) and AnaSpec Inc. (Fremont CA, USA) respectively. All reagents used in the project were analytical grade. Potassium phosphate buffer (PB, 0.1 M, pH 7.6) was used as the electrolyte for all experiments. All aqueous solutions were prepared in 18.2 M Ω nano-pure de-ionized (DI) water. Solutions were oxygenated by purging with oxygen for 15 min before experiments.

6.2.2 Methods

6.2.2.1 GC and SP Electrode preparation

Multi-walled carbon nanotube (MWCNT) was prepared by ultrasonically dispersing each 1 mg of MWCNT in 1 mL DMF for glassy-carbon (GC) electrode and 1 mL DMSO for screen-printed (SP) electrode for an hour for electrode modification. Both GC and SP electrodes were then modified with CNT by drop casting 16 μL (in 8 steps of 2 μL) followed by drying in oven after each addition. The electrodes were allowed to cool on ice before 2 μL of 10 mM PBSE (prepared in DMF and DMSO for GC and SP, respectively) was applied on the surface electrode for 15 min to allow the non-covalent binding between PBSE and CNTs. DMF and DMSO were respectively used to rinse the GC and SP to remove unattached PBSE before 0.1 M potassium phosphate buffer (PB, pH 7.6) was consecutively used to remove the solvents from the electrode surface. Solutions of TYR and ES were prepared by dissolving 5 mg TYR and ES in 1 mL of 20 mM PB, pH 7. Bi-enzyme and tri-enzyme solutions were prepared by mixing SH/TYR solution and ES/SH/TYR solution for enzyme immobilization on both GC and SP electrodes. The enzyme-immobilized biosensors were fabricated by drop-casting 10 μL of bi-enzyme solution or 15 μL of tri-enzyme on the electrode surface, and the electrode was incubated on the electrode for 30 min to allow covalent binding of PBSE and the enzymes.

6.2.2.2 Electrochemical experiments

In CV experiments, the potential was scanned from 0.4 V to -0.2 V by CHI 920 c potentiostat to monitor the reduction current for both bi-enzyme and tri-enzyme immobilized electrode.

6.3 RESULTS AND DISCUSSION

6.3.1 Concentration effect of tri-enzyme immobilized on GC electrode

Three enzymes – ES, SH and TYR were immobilized on the GC electrode in the construction of the tri-enzyme biosensor, and the biosensor performance was evaluated. For this purpose, the enzyme ratio of three enzymes needs to be optimized to achieve the best biosensor performance. First, bi-enzyme ratio – the ratio of SH and TYR was optimized with different volumes (SH and TYR: 1 μ L and 9 μ L, 3 μ L and 7 μ L, 5 μ L and 5 μ L, 7 μ L and 3 μ L and 9 μ L and 1 μ L) on the GC electrode. The results proved that bi-enzymatic biosensor achieve best sensitivity when the ratio of SH and TRY of 3 μ L and 7 μ L as used (Figure 6.S1), the difference of this and the optimal enzyme ratio in Chapter 5 (which is SH/TYR: 5 μ L / 5 μ L) can be explained by the usage of new batches of enzymes. Therefore, the enzyme volume ratio of SH and TYR was fixed to 3:7 for the tri-enzyme ratio optimization. Different tri-enzyme mixtures with different volumes of ES, SH and TYR (ES/SH/TYR: 1 μ L / 4.2 μ L / 9.8 μ L, 3 μ L / 3.6 μ L / 8.4 μ L, 5 μ L / 3 μ L / 7 μ L, 7 μ L / 2.4 μ L / 5.6 μ L, 9 μ L / 1.8 μ L / 4.2 μ L, 11 μ L / 1.2 μ L / 2.8 and 13 μ L / 0.6 μ L / 1.4 μ L) were prepared and immobilized on the GC electrode and tested using 46.3 μ M of MeSA with FAD and NADH by cyclic voltammetry (CV). The peak current of 1,2-benzoquinone reduction versus esterase volume percentage are shown in Figure 6.4.

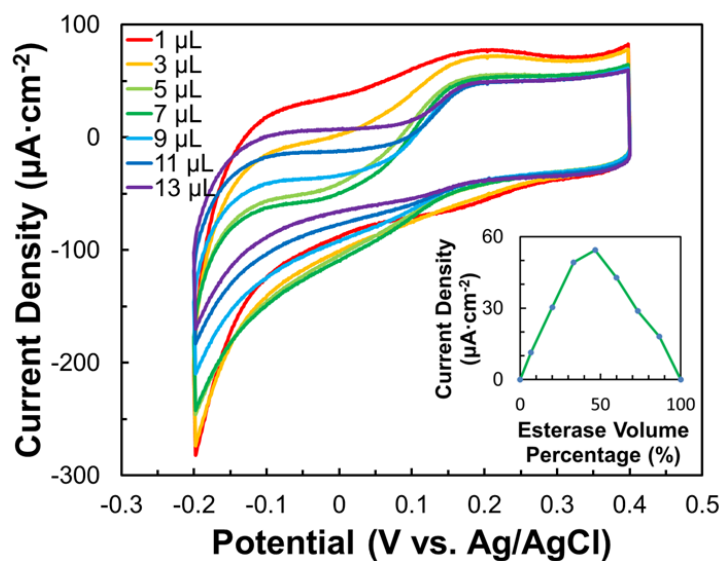


Figure 6.4: CV responses of the tri-enzyme GC electrode containing immobilized ES, SH and TYR. The 2 mL electrolyte consists of 46.3 μM MeSA with FAD (4.7 μM) and NADH (0.23 mM). The ratio of ES:SH:TYR loadings by volume on the electrode, respectively, are 1:4.2:9.8 (red), 3:3.6:8.4 (orange), 5:3:7 (light green), 7:2.4:5.6 (green), 9:1.8:4.2 (light blue), 11:1.2:2.8 (blue) and 13:0.6:1.4 (purple).

The results (Figure 6.4) indicated that current density increased as the volume percentage of esterase increased and reached its maximum when the enzyme loadings of ES/SH/TYR: 7 μL / 2.4 μL / 5.6 μL was applied for GC electrode immobilization. However, the current density decreased when the volume percentage of ES was beyond 47 % (corresponds to 7 μL of ES among 15 μL of enzyme mixture) due to insufficient immobilization of SH/TYR, which limits the conversion of salicylate to catechol and further to 1,2-benzoquinone for electrochemical reduction. Therefore, the enzyme loading of ES/SH/TYR: 7 μL / 2.4 μL / 5.6 μL (corresponding to 0.595 unit / 0.011 unit / 75.236 units) was used for the sensitivity, LOD and LOQ determination.

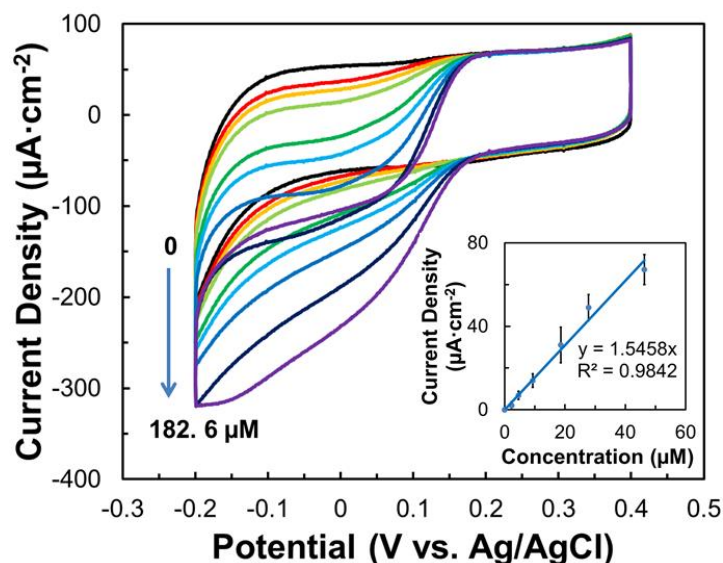


Figure 6.5: Concentration effect of MeSA (2.3, 4.6, 9.3, 18.6, 27.8, 46.3, 92.2 and 182.6 μM) on tri-enzyme (ES/SH/TYR: 7 μL / 2.4 μL / 5.6 μL) immobilized GC electrode.

Different volumes of 10 mM MeSA stock solution were then added to 2 mL PB electrolyte supplemented with 100 μL 0.1 mM FAD and 50 μL 10 mM NADH to maintain concentrations of MeSA of 2.3, 4.6, 9.3, 18.6, 27.8, 46.3, 92.2 and 182.6 μM . CV was applied to measure each of concentration of MeSA, and the data were shown in Figure 6.5. The current density at 0.025 V was used to plot against the concentration which shown as the inset of Figure 6.5. A sensitivity of $1.55 \mu\text{A}\cdot\text{cm}^{-2}\cdot\mu\text{M}^{-1}$ was found, which was significantly lower than the bi-enzyme GC electrode in Chapter 5 (which is $21.3 \mu\text{A}\cdot\text{cm}^{-2}\cdot\mu\text{M}^{-1}$), although the LOD and LOQ (which are 0.70 and 2.13 μM) were similar to that of bi-enzyme sensor (Table 6.1). The decrease of the sensitivity of tri-enzyme compare to bi-enzyme GC electrode can be explained by the low reaction rate of esterase, *i.e.* it takes longer time for the electrode to accumulate enough SA for the next reaction to take place.

Table 6.1: Sensitivity, linear range, LOD and LOQ of MeSA detection with the tri-enzyme modified GC electrode, tri-enzyme modified SP electrode, SH/TYR modified SP as WE with ES in solution and SH/TYR modified SP as chip with ES in solution.

Electrode	Sensitivity ($\mu\text{A}\cdot\text{cm}^{-2}\cdot\mu\text{M}^{-1}$)	Linear range (μM)	LOD (μM)	LOQ (μM)
GC-tri-enzyme	1.55 ± 0.24	0 – 46.3 (0.9842)	0.7 ± 0.3	2.1 ± 0.8
SP-tri-enzyme	0.01 ± 0.24	0 – 693 (0.9911)	208 ± 66	605 ± 200
SP(W)-bi-enzyme-ES in solution	2.63 ± 0.04	0 – 18.6 (0.9825)	1.0 ± 0.1	3.0 ± 0.2
SP(chip)-bi-enzyme-ES in solution	3.10 ± 0.19	0 – 18.6 (0.9732)	0.8 ± 0.2	2.3 ± 0.6

6.3.2 Concentration effect of tri-enzyme immobilized on SP electrode

Although the GC electrode displayed satisfactory LOD and LOQ after tri-enzyme immobilization, SP electrode was used as the substrate for the immobilization to make the biosensor strip disposable and easier to use. Similar bi-enzyme ratio (the ratio of SH and TYR) was firstly carried out to determine the optimal SH and TYR ratio and the results (Figure 6.S2) indicated that the SH/TYR of 5 μL / 5 μL generated the highest current density, and was used for tri-enzyme ratio optimization. Similar to the tri-enzyme ratio carried out for GC electrode, the SH and TYR was fixed to 1:1 while different volumes of ES were used to make a ES volumes gradients (ES/SH/TYR: 1 μL / 7 μL / 7 μL , 3 μL / 6 μL / 6 μL , 5 μL / 5 μL / 5 μL , 7 4 μL / 4 μL , 9 μL / 3 μL / 3 μL , 11 μL / 2 μL / 2 μL and 13 μL / 1 μL / 1 μL) for CV measurements, and the results are displayed in Figure 6.6 below.

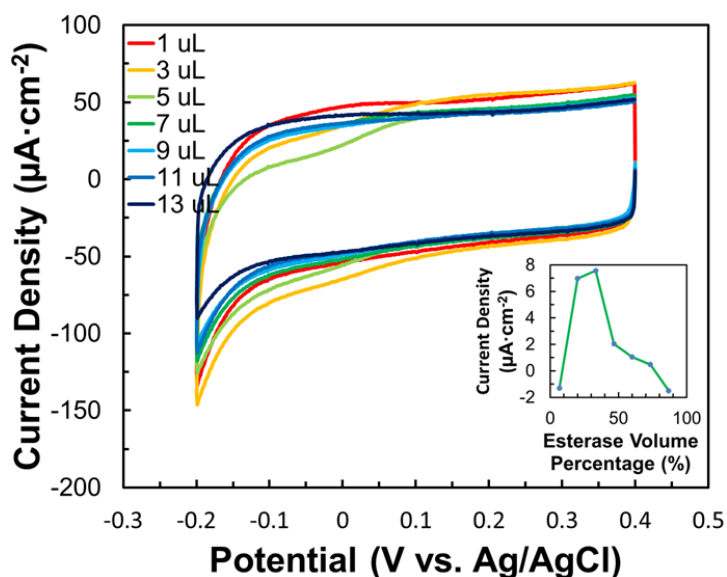


Figure 6.6: CV responses of the tri-enzyme GC electrode containing immobilized ES, SH and TYR. The 2 mL electrolyte consists of 183 μM MeSA electrode respectively are 1:7:7 (red), 3:6:6 (orange), 5:5:5 (light green), 7:4:4 (green), 9:3:3 (light blue), 11:2:2 (blue) and 13:1:1 (purple).

Similar to the tri-enzyme immobilized GC electrode, the current density of 1,2-benzoquinone reduction from MeSA conversion through SA and catechol increased as more ES was present in the tri-enzyme mixture. The highest current density was observed when tri-enzyme ratio of ES/SH/TYR: 5 μL / 5 μL / 5 μL was used. However, further increase of ES resulted in sharp decrease of current density. Therefore, tri-enzyme combination of ES/SH/TYR of 5 μL / 5 μL / 5 μL was used for determination of sensitivity, LOD and LOQ.

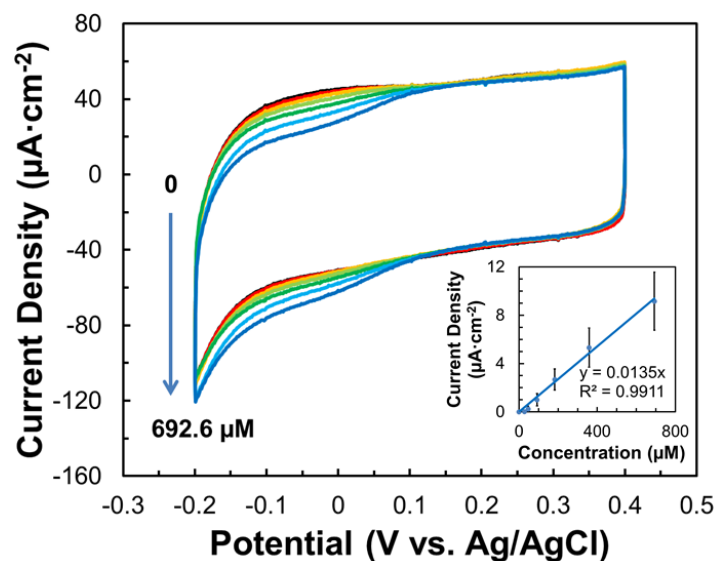


Figure 6.7: Concentration effect of MeSA (28, 46, 92, 183, 359 and 693 μM) on tri-enzyme (ES/SH/TYR: 5 μL / 5 μL / 5 μL) immobilized SP electrode.

Different concentrations of MeSA (28, 46, 92, 183, 359 and 693 μM) were used to evaluate the tri-enzyme immobilized SP electrode in presence of FAD and NADH. CV results were shown in Figure 6.7, and the current density versus concentration was shown in the inset. Although the reduction current density of 1,2-benzoquinone increased as higher concentrations of MeSA were added in the electrolyte, the reduction peaks were not prominent as they were on tri-enzyme immobilized GC electrode. Data in Table 6.1 further indicate that the sensitivity was significantly compromised ($0.01 \mu\text{A}\cdot\text{cm}^{-2}\cdot\mu\text{M}^{-1}$) compared to that of tri-enzyme immobilized GC electrode and SH/TYR-bi-enzyme immobilized SP (Figure 6.S2), which could be attributed to the poor immobilization of ES. LOD and LOQ are determined to be 208 μM and 605 μM respectively, which are much higher than expected. Therefore, the strategy of tri-enzyme immobilization on SP electrode needs to be reconsidered for practical development of MeSA biosensor.

6.3.3 SH/TYR-immobilized biosensor as working electrode for ES-treated MeSA

Since the tri-enzyme immobilized biosensor did not provide the desired sensitivity and LOD for MeSA detection, a second strategy which includes pre-treatment of MeSA in the electrolyte by ES and detection of SA with a SH/TYR-immobilized biosensor. To investigate this strategy, a SH/TYR mixture with 5 μL SH and 5 μL TYR were prepared and immobilized on the electrodes as introduced above. Since ES would be added in the electrolyte to hydrolyze MeSA before SH/TYR-immobilized biosensor was used for measurement, the time required by ES to hydrolyze MeSA must be determined. MeSA, 27.8 μM , was prepared in 2 mL PB, pH 7.6, containing 100 μL of 0.1 mM FAD, 50 μL of 10 mM NADH and 5 μL of ES. CV measurements were performed after 0 min, 30 min, 1 h, 2 h and 4 h of reaction and cyclic voltammograms were displayed in Figure 6.8, and the peak current density versus reaction time is also plotted as inset.

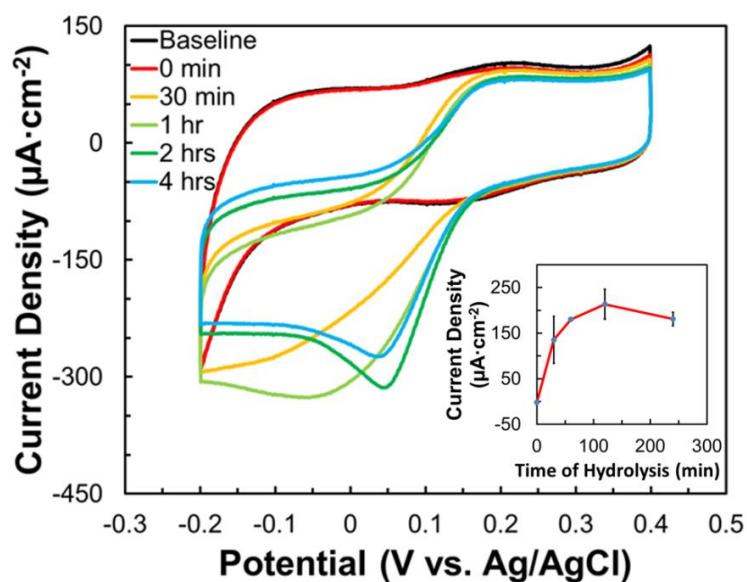


Figure 6.8: CV responses of 27.8 μM MeSA on a SH/TYR-immobilized GC electrode after 0 min, 30 min, 1 h, 2 h and 4 h treatment with esterase.

From the data displayed in Figure 6.8, no electrochemical reduction peak was observed immediately after the addition of MeSA into the electrolyte containing ES, which can be explained by the inactivity of MeSA and slow conversion of MeSA. However, the reduction peak quickly appeared after 30 min and further increased in the measurements conducted after 1 h and 2 h, which can be attributed to the hydrolysis of MeSA to SA in the electrolyte. Finally, the hydrolysis procedure reached a maximum after 2 h. Since the MeSA concentration of 27.8 μM is high in the detection range, the actual hydrolysis time required will be shorter, and, 2 h would be sufficient for the hydrolysis in practical applications.

Six different concentrations of MeSA – 2.3, 4.6, 9.3, 18.6, 27.8 and 46.3 μM were prepared in mL PB, pH 7.6 containing 100 μL 0.1 mM FAD, 50 μL 10 mM NADH and 5 μL ES. After 2 h, CV measurement was performed for each concentration. The cyclic voltammograms and the reduction peak current density are plotted in Figure 6.9.

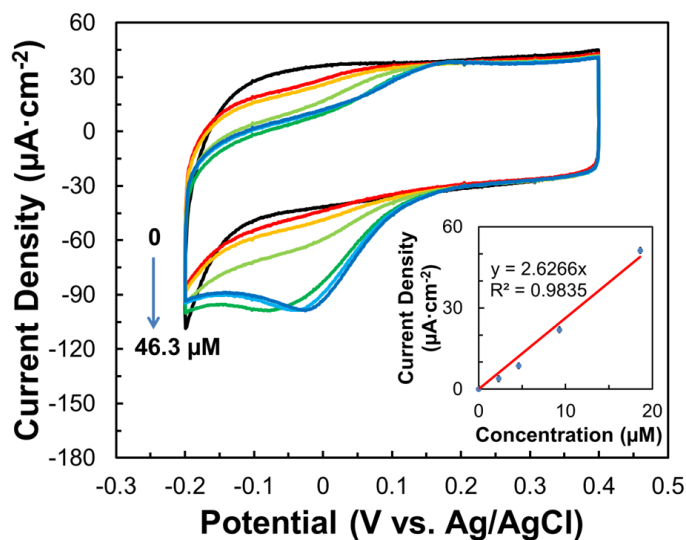


Figure 6.9: Concentration effect of MeSA (2.3, 4.6, 9.3, 18.6, 27.8 and 46.3 μM) with 2 h hydrolysis of ES on SH/TYR-immobilized (SH/TYR: 5 μL / 5 μL) SP electrode.

The results in Figure 6.9 indicated the increase of current density with the increase of MeSA concentration and the quantitative parameter can be found in Table 6.1. The results demonstrate better sensitivity ($2.63 \mu\text{A}\cdot\text{cm}^{-2}\cdot\mu\text{M}^{-1}$) and lower LOD ($1.0 \mu\text{M}$) and LOQ ($3.0 \mu\text{M}$) which is competitive compared to tri-enzyme immobilized GC electrode. Therefore, the strategy of measuring MeSA through pre-hydrolyzed MeSA by SH/TYR-immobilized biosensor has been successfully developed.

6.3.4 SH/TYR-immobilized biosensor as sensor chip for ES-treated MeSA

Although the SH/TYR-immobilized SP electrode has proved successful as a working electrode in pre-hydrolyzed MeSA detection, an extra of Pt wire as the counter electrode and 3 M Ag/AgCl reference electrode are required to perform the detection together with the SP working electrode. However, the Ag/AgCl electrode, although it provides an accurate reference potential, contains 3 M KCl solution, which limits its application as a reference electrode for the development of a lab-on-chip device, where all three electrodes (*i.e.* working, counter and reference electrodes) are required to be non-aqueous. Because of the difficulty in finding a reference electrode for a non-aqueous solvent that does not contaminate the test solution with undesirable species, a quasi-reference electrode (QRE) is often employed. This is usually just a metal wire, Ag or Pt, used with the expectation that no change occurs in the bulk solution during the measurement (Bard, Faulkner et al. 1980). Since Ag/Ag Cl electrode was used for all previous experiments, SP electrodes configured with Ag wire as QRE and printed carbon as CE were used to carry out the MeSA detection (Figure 6.10).

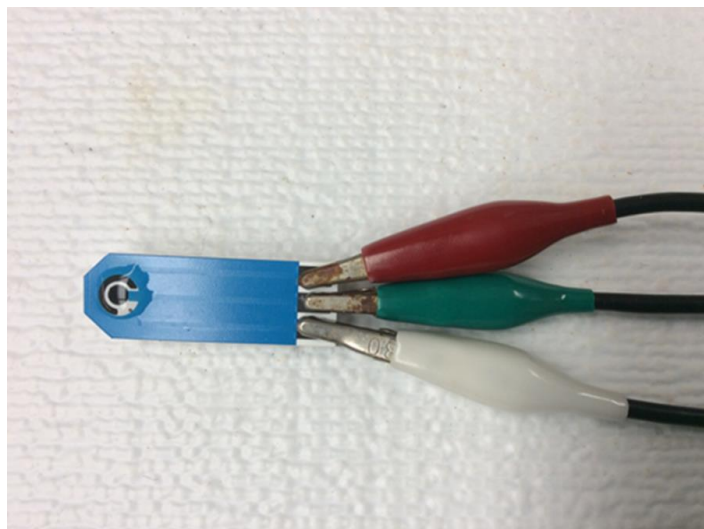


Figure 6.10: Setup of SH/TYR immobilized SP electrode using the configured SP carbon and Pt wire as counter electrode and quasi-reference electrode.

The working electrode of SP was immobilized with SH/TYR mixture as introduced above and the concentration gradients of MeSA from 2.3, 4.6, 9.3, 18.6, 27.8 to 46.3 μM was prepared in presence of FAD, NADH and ES as introduced above. After 2 h hydrolysis, CV measurement was carried out at all concentrations, and cyclic voltammograms and the concentration effect are shown in Figure 6.11.

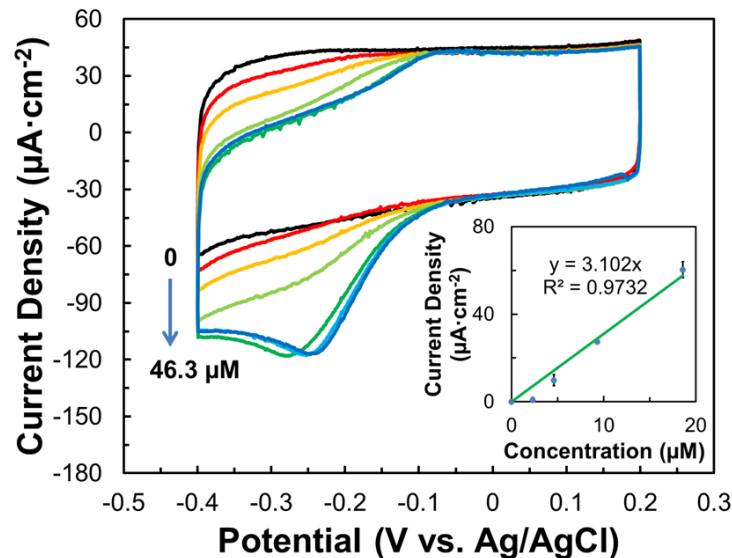


Figure 6.11: Concentration effect of MeSA (2.3, 4.6, 9.3, 18.6, 27.8 and 46.3 μM) with 2 h hydrolysis of ES on SH/TYR-immobilized (SH/TYR: 5 μL / 5 μL) SP electrode with configured SP carbon as counter electrode and Ag wire as quasi-reference electrode.

In Figure 6.11, similar increase trend of reduction peak can be observed as the concentration of MeSA increased from 2.3 μM to 18.6 μM and reached saturation beyond 27.8 μM . However, a significant peak potential shift was also observed from -0.05 V (when only WE of SP electrode was used) to -0.28 V, which can be explained by the application of the quasi-reference electrode. Table 6.1 tabulates the estimated sensitivity, LOD and LOQ to be 3.10 $\mu\text{A}\cdot\text{cm}^{-2}\cdot\mu\text{M}^{-1}$, 0.75 μM and 2.27 μM , respectively. Although the sensitivity is not as high as previously reported, LOD and LOQ are still satisfactory based on the practical MeSA release rate, which allows the farmer to collect VOCs for less than 1 h before the detection can be carried out.

6.3.5 Computer controlling system design with MOSFET and Arduino Uno

A 9 V air pump was used for VOCs collection from the plant in this project. The pump was controlled by the computer via a USB port on the computer. However, the USB port provides only 5 V potential (less than 9 V), and therefore a MOSFET (metal-oxide-semiconductor field-

effect transistor) field-effect transistor was used for amplifying or switching electronic signals to control the air pump which requires 9 V. A IRF520N type MOSFET was purchased and used (Figure 6.S3). In order to facilitate communication between the computer and the air pump through MOSFET, computer hardware Arduino (Figure 6.S4) was purchased to design the microcontroller for controlling the air pump. In addition, because the enzymatic biosensor will be affected by temperature, it is necessary to measure the ambient temperature prior to the detection of MeSA after the collection of VOC. Thus, a precision temperature sensor TMP36 was used for ambient temperature detection.

After connection of all major parts and two LED lights (red for purge-and-trap on and yellow for purge-and-trap off and temperature measurement) on the Arduino Uno as displayed in Figure 6.12, a code was executed to allow 2 h of collection of VOCs by switching on the air pump and red LED (Appendix F). And the entire set up of the VOC collection platform was displayed in Figure 6.S5.

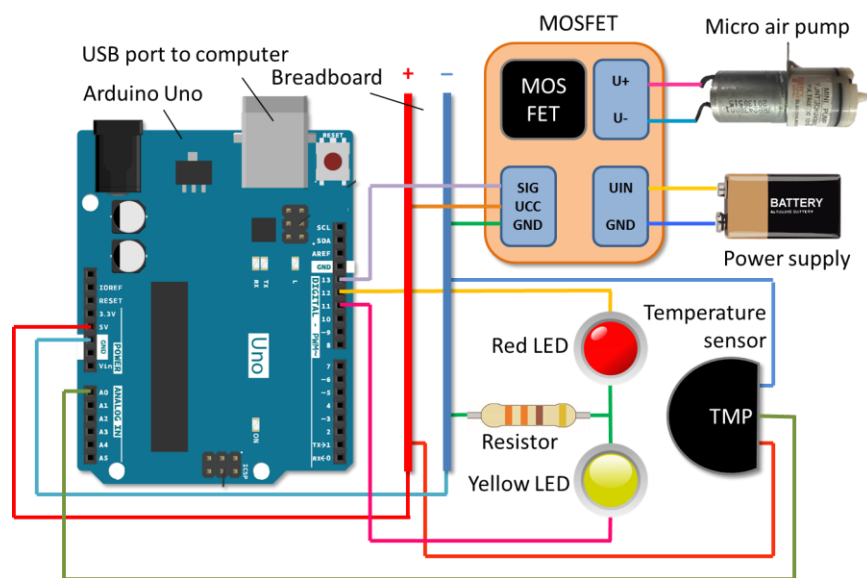


Figure 6.12: The circuit diagram of the platform for automatic VOC collection and temperature measurement.

After 2 h of collection, the computer automatically switched off the air pump and turned on the temperature sensor for temperature detection and temperature compensation when SH/TYR-immobilized biosensor is used for MeSA detection.

6.4 CONCLUSION

In addition to SH and TYR that were used for development of bi-enzymatic biosensor for MeSA detection, this project successfully employed ES as another bio-recognition element for tri-enzymatic biosensor fabrication that allows the direct detection of MeSA without chemical hydrolysis of MeSA. However, ES/SH/TYR-immobilized GC electrode displayed significant lower sensitivity ($1.54 \mu\text{A}\cdot\text{cm}^{-2}\cdot\mu\text{M}^{-1}$) compared to the bi-enzymatic biosensor developed in Chapter 5 ($21.3 \mu\text{A}\cdot\text{cm}^{-2}\cdot\mu\text{M}^{-1}$). Lower sensitivity was obtained when SP electrode was used for tri-enzyme immobilization. Thus, ES was applied in the electrolyte for MeSA hydrolysis during the VOC collection rather than being immobilized on the electrode. The experiment indicated that 2 h is sufficient for hydrolysis of a high concentration of MeSA. The whole SP electrode was used as the detection chip, which does not require extra counter and reference electrodes. The enzymatic SP chip rendered sensitivity of $3.1 \mu\text{A}\cdot\text{cm}^{-2}\cdot\mu\text{M}^{-1}$ for MeSA detection. In addition to the detection chip, automation of the VOC collection system was designed using a micro air pump, Arduino Uno as controlling system, and MOSFET as an electronic switch. The automation system allows the end-user to use a computer for operating and monitoring such as switching on/off micro air pump for VOC collection and temperature measurement.

6.5 SUPPLEMENTARY DATA

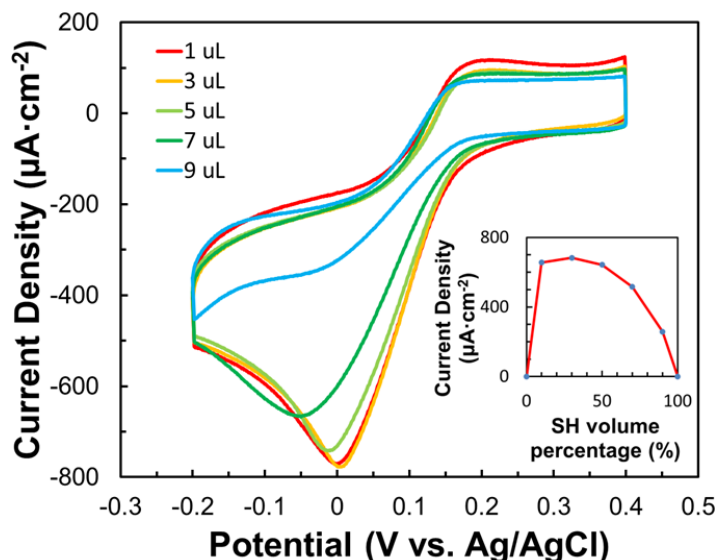


Figure 6.S1: CV responses of the bi-enzyme GC electrode containing immobilized SH and TYR. The 2 mL electrolyte consists of 27.8 μM SA with FAD (4.7 μM) and NADH (0.23 mM). The ratio of SH:TYR loadings by volume on the electrode respectively are 1:9 (red), 3:7 (orange), 5:5 (light green), 7:3 (green) and 9:1 (light blue).

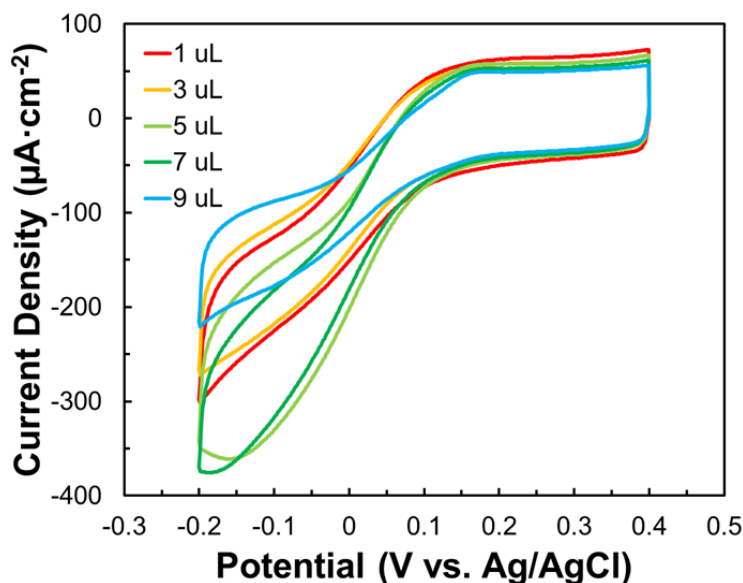


Figure 6.S2: CV responses of the bi-enzyme SP electrode containing immobilized SH and TYR. The 2 mL electrolyte consists of 27.8 μM SA with FAD (4.7 μM) and NADH (0.23 mM). The ratio of SH:TYR loadings by volume on the electrode respectively are 1:9 (red), 3:7 (orange), 5:5 (light green), 7:3 (green) and 9:1 (light blue).

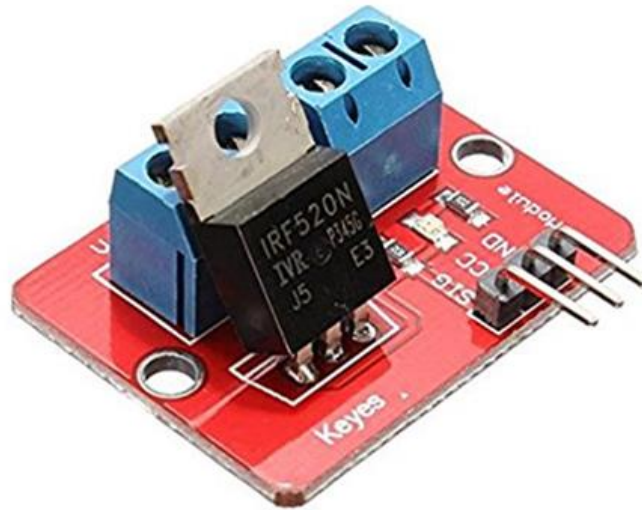


Figure 6.S3: The IRF520N MOSFET used to control the purge-and-trap.

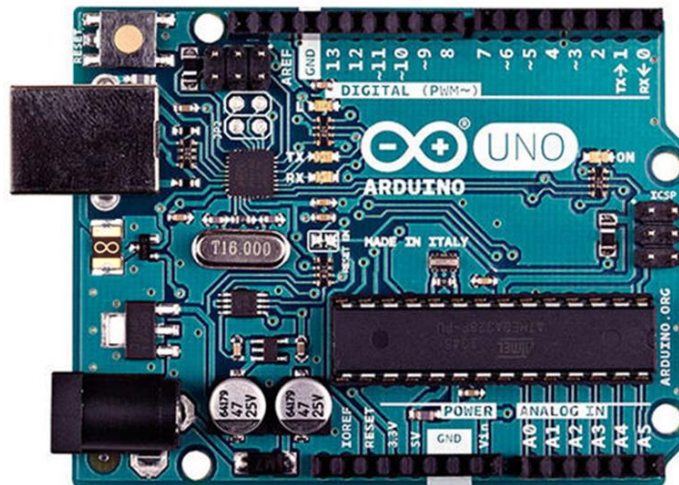


Figure 6.S4: The Arduino Uno used for computer to interact with MOSFET/Air pump and temperature sensor.

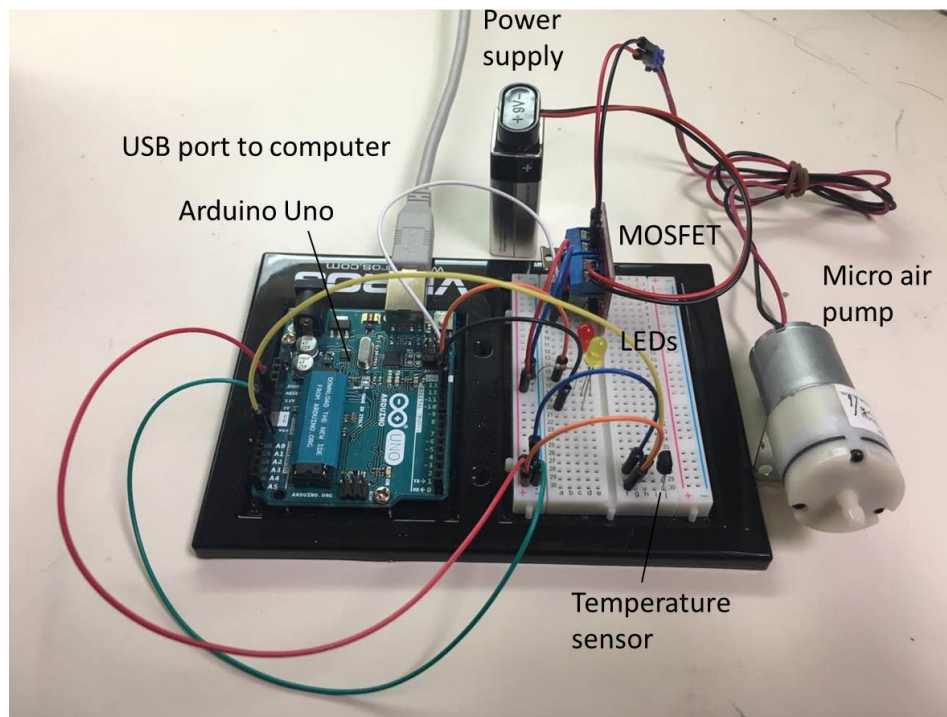


Figure 6.S5: The setup of the platform for automatic VOC collection and temperature measurement.

CHAPTER 7

COMPUTATIONAL MODELING OF BIENZYMATIC BIOSENSOR

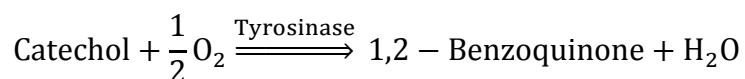
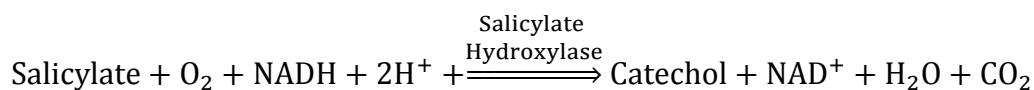
To be submitted to Journal of Electrochemical Society.

7.1 INTRODUCTION

The platform of bi-enzymatic electrochemical biosensor consisting salicylate hydroxylase (SH) and tyrosinase (TYR) for methyl salicylate (MeSA) detection has been successfully established as introduced in the previous chapters. Although the obtained biosensor parameters such as sensitivity, limit of detection (LOD) and limit of quantification (LOQ) satisfy the requirements of MeSA detection for plant disease prediction, the improvement of the biosensor performance is always desired. In order to improve the performance of the biosensor, it is important to understand the mechanism of both enzyme kinetics and electrochemical kinetics. However, the current research is primarily based on the experiments to determine the biosensor performance (*e.g.* determination of enzyme ratio), rather than from the study of the underlying theory and mechanisms. Therefore, the theory of operation the biosensor including the study of enzyme kinetics and the methodology of electrochemical kinetics that enable the design of better biosensors are discussed in this chapter.

7.1.1 Enzyme kinetics

As introduced in the previous chapters, the detection of MeSA can be realized through either bi-enzymatic approach using SH and TYR, or the tri-enzymatic approach that additionally uses esterase (ES) for hydrolysis before bi-enzymatic detection. Therefore, the key reaction in the cascade is the conversion of salicylate to catechol, and then to electroactive 1,2-benzoquinone, which is described as following kinetic equations:



In addition, the experiments performed in Chapter 6 suggested that ES could be added directly into the electrolyte for MeSA hydrolysis instead of immobilizing on the electrode surface. Therefore, only SH and TYR for the theoretical treatment is discussed in this chapter. The kinetic mechanism of SH and TYR will be examined by initial rate measurements by Ultraviolet–visible spectrometry using the corresponding enzyme assays and the corresponding kinetic parameters such as Michaelis-Menten constants will be calculated in the experiments for the electrochemistry modeling.

7.1.2 Electrochemical Modeling

In addition to the enzyme kinetics, the study of electrochemical theory that directly determines the signal obtained from the reduction of 1,2-benzoquinone is necessary for understanding the mechanism of the bi-enzyme biosensor. The computational modeling has been widely applied to various scientific researches including the application of mathematical modelling to investigate the biosensor behavior (Mell and Maloy 1975, Schulmeister 1990). The computational modeling can be widely used for understanding the kinetics of the biosensor through which physical experiments required for biosensor fabrication and improvement could be designed. Governing equations, initial conditions and boundary conditions are derived from first principles for the computational modeling in this work. However, solving the mathematical model has not been attempted as it is beyond the scope of the work.

7.2 MATERIALS AND METHODS

7.2.1 Materials

Salicylate hydroxylase (E.C. 1.14.13.1) was expressed and purified from pTrc99a-*nahG* transformed *E.coli* XL-1 blue as introduced in Chapter 5. Tyrosinase (E.C. 1.14.18.1) derived

from mushroom (lyophilized powder, ≥ 1000 units / mg solid) was purchased from Sigma-Aldrich (St. Louis, MO, USA) and used directly. Sodium salicylate, catechol and NADH were obtained from Acros Organics (NJ, USA) and FAD was purchased from Alfa Aesar (Haverhill, MA, USA). All reagents used in the project were analytical grade. 0.1 M potassium phosphate buffer (PB, pH 7.6) was used to prepare the enzyme assay for both SH and TYR for all experiments. Manganese (II) chloride tetrahydrate, sodium iodide, sodium hydroxide, sulfuric acid, sodium thiosulfate and starch were obtained from Alfa Aesar (Haverhill, MA, USA), Carolina (Burlington, NC, USA), J.T. Baker (Phillipsburg, NJ, USA), Fisher Scientific (Fair Lawn, NJ, USA), Sigma (St. Louis, MO, USA) and J.T. Baker (Phillipsburg, NJ, USA), respectively for dissolved oxygen measurement. All aqueous solutions were prepared in 18.2 M Ω nano-pure de-ionized (DI) water.

7.2.2 Apparatus

The initial rate measurements were carried out using Genesys 10S UV-Vis from Thermo Scientific, and all experiments were conducted at 22 ± 2 °C.

7.2.3 Methods

7.2.3.1 Initial rate measurements

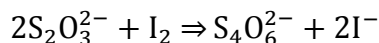
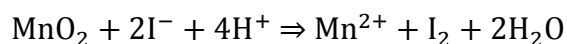
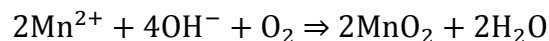
Since SH requires three substrates (*i.e.* salicylate (SA), NADH and oxygen), two sets of enzyme assays are required to calculate the enzymatic parameters. The enzyme assays using different combinations of SA concentration (10 μ M, 20 μ M and 50 μ M) and NADH concentrations (10 μ M, 20 μ M and 50 μ M) were performed (Appendix G) with air-saturated solution. In addition, the assay was also performed using different concentration of SA (10 μ M, 20 μ M and 50 μ M) at the NADH concentration of 100 μ M with nitrogen, air and oxygen saturated solutions

respectively. The measurements of initial reaction rate in each assay were realized through the UV measurement at the wavelength of 340 nm, which monitors the decrease of NADH during the enzymatic reaction. Due to the potential impurities present in the recombinant expressed enzyme (*e.g.* NADH dehydrogenase, which causes the consumption of NADH), the decrease of NADH absorption before and after addition of SA needs to be monitored to calculate the activity from SH. 0.1 M PB buffer at pH 7.6, water, FAD, NADH, SH were added in the cuvette and measured for 1 min to record the absorption decrease of NADH as control. Then SA was added and NADH absorption was measured for another minute as experimental groups. The difference in UV absorption change rate before and after addition of SA was recorded and used for the reaction rate calculation.

The TYR enzyme assay (Appendix G) using different concentrations of catechol (10 μ M, 20 μ M and 100 μ M) was based on the increase in optical density of 1,2-benzoquinone at the wavelength of 470 nm as experimental when catechol was incubated with TYR (Boscan, Powrie et al. 1962). The net initial rates were calculated from the UV absorption difference of the experimental and the control samples (performed in absence of TYR). In addition to the air-saturated experiments, the same experiments were also conducted in nitrogen and oxygen saturated electrolytes for obtaining the initial reaction rate at three different oxygen concentrations.

7.2.3.2 Dissolved oxygen measurement

Since SH and TYR depend on the concentration of dissolved oxygen in the electrolyte, it is necessary to study the oxygen concentration effect. In this project, the concentration of the oxygen in the assay purged with nitrogen, air and oxygen was measured by Winkler titration method (Carpenter 1965) (Appendix H) which can be explained by the following steps.



The Winkler reagent manganese (II) chloride was used to fix the oxygen in MnO_2 in the basic condition. Then MnO_2 was reduced back to Mn^{2+} under acidic condition while oxidizing I^- to I_2 , which can be correlated with the amount of sodium thiosulfate during the titration. The dissolved oxygen concentration can be calculated from the following equation:

$$C \text{ (mM)} = 0.18 V \text{ (mL)},$$

where C and V denotes the concentration of dissolved oxygen (mM) and volume of $\text{Na}_2\text{S}_2\text{O}_3$ used during the titration (mL).

7.3 RESULTS AND DISCUSSION

7.3.1 Enzymatic kinetics

7.3.1.1 Salicylate Hydroxylase

Wang *et al.* indicated that SA and NADH bind to the SH in random order resulting a ternary complex and release NAD^+ before further binds with O_2 (Wang and Tu 1984). Therefore, the reaction rate equation based on the three substrates can be simplified from the equation (Dalziel 1969):

$$\frac{e}{v} = \phi_0 + \frac{\phi_A}{[A]} + \frac{\phi_B}{[B]} + \frac{\phi_C}{[C]} + \frac{\phi_{AB}}{[A][B]} + \frac{\phi_{BC}}{[B][C]} + \frac{\phi_{AC}}{[A][C]} + \frac{\phi_{ABC}}{[A][B][C]}$$

to the following equation (Wang and Tu 1984):

$$\frac{e}{v} = \phi_0 + \frac{\phi_{\text{Sal}}}{[\text{Sal}]} + \frac{\phi_{\text{NADH}}}{[\text{NADH}]} + \frac{\phi_{\text{O}_2}}{[\text{O}_2]} + \frac{\phi_{\text{Sal}\cdot\text{NADH}}}{[\text{Sal}][\text{NADH}]}$$

where e is the concentration of active center (which is equivalent to the concentration of SH in this case), v is the observed initial rate and e/v is the reciprocal of the initial reaction rate. The concentrations of SA, NADH and oxygen are denoted as $[\text{Sal}]$, $[\text{NADH}]$ and $[\text{O}_2]$ respectively. The reciprocal of the maximum rate with unit enzyme concentration is shown as ϕ_0 , whereas ϕ_{Sal} , ϕ_{NADH} and ϕ_{O_2} are functions of rate and/or dissociation constants as defined by Dalziel (Dalziel 1969).

The reciprocal initial reaction rate of SH were examined at various concentrations of SA and NADH at a fixed oxygen concentration first. When concentrations of SA were varied at several concentrations of NADH and a constant oxygen concentration, double reciprocal plots of initial reaction rates yielded a set of lines that converged to a common point (Figure 7.1). Such double reciprocal plot clearly indicated that the SH is capable of forming ternary complex consisting SH, SA and NADH before other enzymatic reaction takes place.

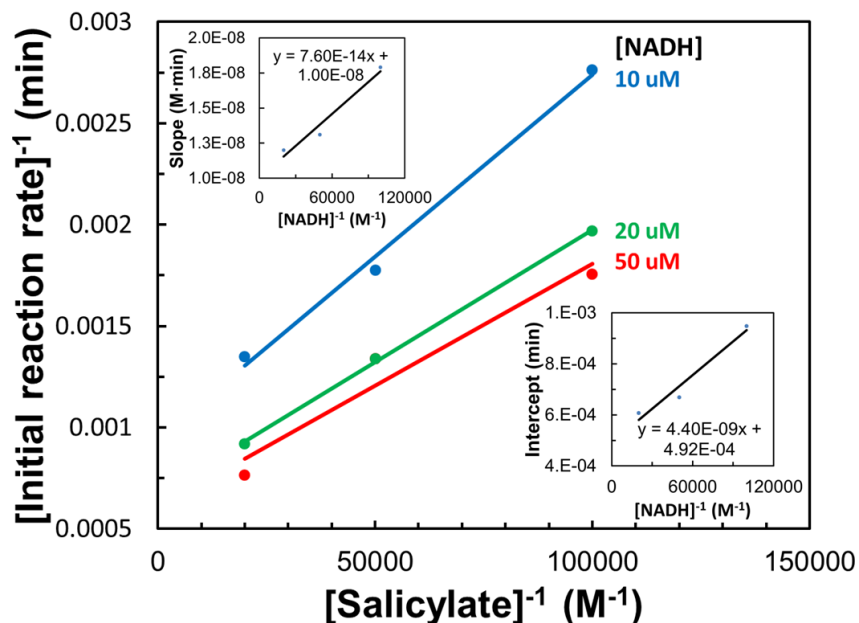


Figure 7.1: Lineweaver-Burk plots of SH activity versus salicylate concentration (10 μM , 20 μM and 50 μM) at several NADH concentrations of 10 μM , 20 μM and 50 μM and a fixed oxygen concentration of 0.28 mM. Insets show the secondary plots by plotting the slopes and intercepts from the primary plot against the reciprocal concentration of NADH.

The secondary plots can be derived by plotting the slopes and intercepts from the primary plot (Figure 7.1) against the reciprocal concentration of NADH (the insets of Figure 7.1) which yields the parameters – $\phi_{\text{Sal}\cdot\text{NADH}}$, ϕ_{Sal} and ϕ_{NADH} as it shown in Table 7.1.

Table 7.1: Biological meanings of the slopes and intercepts from the secondary plot for SH.

Secondary plot	Slope	Intercept
Slope $\sim 1/[\text{NADH}]$	$\phi_{\text{Sal}\cdot\text{NADH}}$	ϕ_{Sal}
Intercept $\sim 1/[\text{NADH}]$	ϕ_{NADH}	$\phi_0 + \phi_{\text{O}_2}/[\text{O}_2]$
Intercept $\sim 1/[\text{O}_2]$	ϕ_{O_2}	$\phi_0 + \phi_{\text{NADH}}/[\text{NADH}]$

Double reciprocal plot of initial rate versus reciprocal concentration of SA at several concentrations of dissolved oxygen and a fixed NADH concentration of 100 μM , however,

produced a set of parallel lines (Figure 7.2), indicating a ping-pong model of reaction; subsequent to the formation of ternary complex of SH, SA and NADH.

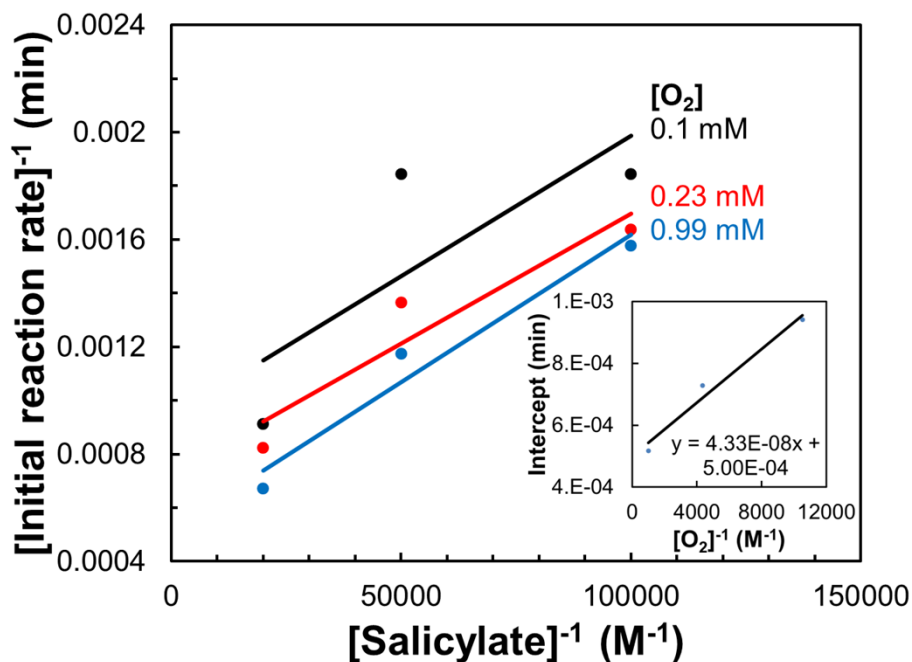


Figure 7.2: Lineweaver-Burk plots of SH activity versus salicylate concentration (10 μM , 20 μM and 50 μM) at several oxygen concentrations of 0.1 mM, 0.23 mM and 0.99 mM and a fixed NADH concentration of 100 μM . Insets show the secondary plots by plotting the intercepts from the primary plot against the reciprocal concentration of oxygen.

Since parallel lines were obtained from Figure 7.2, intercepts were used for the secondary plot against the reciprocal concentration of oxygen. Therefore, ϕ_{O_2} can be derived from the slope of the secondary plot and ϕ_0 can be calculated accordingly.

The reciprocal of the maximum rate with unit enzyme ϕ_0 was calculated and other parameters listed in Figure 7.1 were obtained directly from the slopes and intercepts, and are tabulated in Table 7.2 while $K_{\text{m, sal}}$, $K_{\text{m, NADH}}$ and $K_{\text{m, O}_2}$ are Michaelis-Menten constants for SA, NADH and oxygen respectively.

Table 7.2: Kinetic coefficients for SH.

Term	Value determined	Kinetic equivalent
\emptyset_0	3.97×10^{-4} min	-
\emptyset_{Sal}	1.00×10^{-8} M·min	$K_{m,\text{sal}} \cdot \emptyset_0$
\emptyset_{NADH}	4.40×10^{-9} M·min	$K_{m,\text{NADH}} \cdot \emptyset_0$
\emptyset_{O_2}	4.43×10^{-8} M·min	$K_{m,\text{O}_2} \cdot \emptyset_0$
$\emptyset_{\text{Sal}\cdot\text{NADH}}$	7.60×10^{-14} M ² ·min	-

Additionally, the Michaelis-Menten constants for SA, NADH and oxygen were calculated according to Table 7.2, and determined to be 25 μM , 11 μM and 0.11 mM respectively. It is noteworthy that $K_{m,\text{sal}}$ of 25 μM coincides with the linear range of SA detection in Chapter 5 and 6 (~ 27.8 μM), *i.e.* the linear range of the detection does not exceed the $K_{m,\text{sal}}$ due to the saturation of the enzyme by the substrate. The Michaelis-Menten constant of SH for NADH ($K_{m,\text{NADH}}$) further proved that the concentration of NADH in the electrochemical cell (0.23 mM) during the MeSA detection was significantly higher (more than 20 fold) than $K_{m,\text{NADH}}$, which is 11 μM . This indicated that the reaction rate was not limited by NADH concentration.

7.3.1.2 Tyrosinase

Similar to the tri-substrate enzymatic reaction, a similar equation can also be derived for TYR which catalyzes two substrates (*i.e.* catechol and oxygen) as it shown below:

$$\frac{e}{v} = \emptyset_0 + \frac{\emptyset_{\text{Cat}}}{[\text{Cat}]} + \frac{\emptyset_{\text{O}_2}}{[\text{O}_2]} + \frac{\emptyset_{\text{Cat}\cdot\text{O}_2}}{[\text{Cat}][\text{O}_2]}$$

where e is the concentration of active center (which is equivalent to the concentration of tyrosinase in this case), v is the observed initial rate and e/v is the reciprocal of the initial reaction

rate. The concentrations of catechol and oxygen are denoted as [Cat] and [O₂] respectively. The reciprocal of the maximum rate with unit enzyme concentration is shown as ϕ_0 , whereas ϕ_{Cat} and ϕ_{O_2} are functions of rate and/or dissociation constants as defined by Dalziel (Dalziel 1957).

The reciprocal of initial reaction rate was plotted against different catechol concentrations (10 μM , 20 μM and 100 μM) and oxygen concentrations prepared by purging nitrogen (0.1 mM), air (0.26 mM) and oxygen (0.94 mM). When the concentration of catechol varies at different oxygen concentration, the Lineweaver-Burk plot generated a set of linear lines converging to a common point (Figure 7.3). This plot indicated the ternary complex formation consisting TYR, catechol and oxygen (Siegbahn 2004).

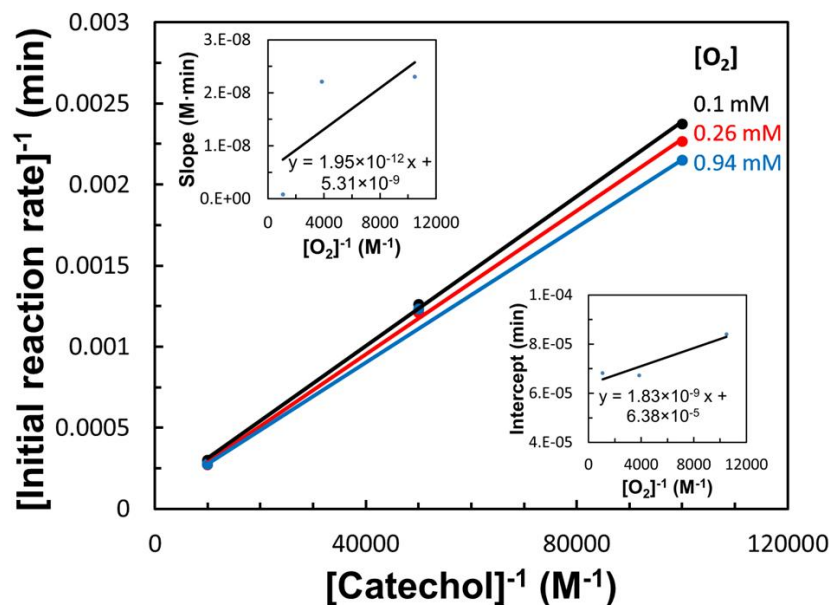


Figure 7.3: Lineweaver-Burk plots of TYR activity versus catechol concentration (10 μM , 20 μM and 100 μM) at several oxygen concentrations of 0.1 mM (purged with nitrogen), 0.26 mM (purged with air) and 0.94 mM (purged with oxygen). Insets show the secondary plots by plotting the slopes and intercepts from the primary plot against the reciprocal concentration of oxygen.

Secondary plots were generated by plotting the slopes and intercepts of the primary plot against the reciprocal of oxygen concentration. The parameters (*i.e.* ϕ_0 , ϕ_{Cat} , ϕ_{O_2} and $\phi_{\text{Cat-O}_2}$) can be derived from the Table 7.3 and the values are tabulated in Table 7.4.

Table 7.3: Biological meanings of the slopes and intercepts from the secondary plot for TYR.

Secondary plot	Slope	Intercept
Slope $\sim 1/[\text{O}_2]$	$\phi_{\text{Cat-O}_2}$	ϕ_{Cat}
Intercept $\sim 1/[\text{O}_2]$	ϕ_{O_2}	ϕ_0

Table 7.4: Kinetic coefficients for TYR.

Term	Value determined	Kinetic equivalent
ϕ_0	$6.38 \times 10^{-5} \text{ min}$	-
ϕ_{Cat}	$5.31 \times 10^{-9} \text{ M} \cdot \text{min}$	$K_{\text{m,Cat}} \cdot \phi_0$
ϕ_{O_2}	$1.83 \times 10^{-9} \text{ M} \cdot \text{min}$	$K_{\text{m,O}_2} \cdot \phi_0$
$\phi_{\text{Cat-O}_2}$	$1.95 \times 10^{-12} \text{ M}^2 \cdot \text{min}$	-

Additionally, K_{m} values for catechol and oxygen (*i.e.* $K_{\text{m,Cat}}$ and $K_{\text{m,O}_2}$) were calculated and determined to be 83 μM and 29 μM respectively.

7.3.2 Modeling

After understanding the mechanism of the enzymatic reaction and the derivation of kinetic parameters, a one-dimensional continuum mathematical model was developed to understand the electrochemical mechanisms involving three regions: the enzyme layer, diffusion layer, and bulk solution region as shown in Figure 7.4, where d and f represent thickness of the enzyme layer and diffusion layer respectively.

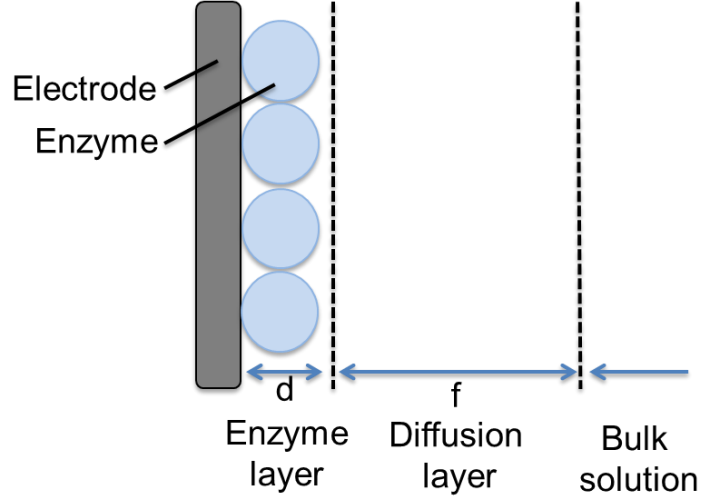


Figure 7.4: Schematic illustration of three regions: enzyme layer, diffusion layer and bulk solution region formed on the electrode surface.

7.3.2.1 Governing Equations

In the enzyme layer, enzymatic reactions of both enzymes play an important role on the electrode surface in addition to mass transfer, therefore, coupling the enzymatic reaction in the enzyme with the Fick's second law of diffusion is necessary to derive the governing equations ($0 < x < d$, $t > 0$):

$$\begin{aligned} \frac{\partial U_{1,e}}{\partial t} &= D_{1,e} \frac{\partial^2 U_{1,e}}{\partial x^2} - v_1 & \frac{\partial U_{2,e}}{\partial t} &= D_{2,e} \frac{\partial^2 U_{2,e}}{\partial x^2} - v_1 - \frac{v_2}{2} & \frac{\partial U_{3,e}}{\partial t} &= D_{3,e} \frac{\partial^2 U_{3,e}}{\partial x^2} - v_1 \\ \frac{\partial U_{4,e}}{\partial t} &= D_{4,e} \frac{\partial^2 U_{4,e}}{\partial x^2} - 2v_1 & \frac{\partial U_{5,e}}{\partial t} &= D_{5,e} \frac{\partial^2 U_{5,e}}{\partial x^2} + v_1 - v_2 & \frac{\partial U_{6,e}}{\partial t} &= D_{6,e} \frac{\partial^2 U_{4,e}}{\partial x^2} + v_2 \end{aligned}$$

where v_1 and v_2 refer to the enzymatic reaction of SH and TYR that discussed in Section 7.3.1, and x and t stand for space from the electrode and time respectively, $U_{1,e}$, $U_{2,e}$, $U_{3,e}$, $U_{4,e}$, $U_{5,e}$ and $U_{6,e}$ are molecular concentrations of the substrates (SA, oxygen, NADH, proton), intermediate (catechol) and product (1,2-benzoquinone) in enzyme layer of thickness d , respectively. And $D_{1,e}$,

$D_{2,e}$, $D_{3,e}$, $D_{4,e}$, $D_{5,e}$ and $D_{6,e}$ are the diffusion coefficients of the corresponding compounds in enzyme layer. And r_1 and r_2 refer to reaction rate of SH and TYR respectively.

In the diffusion layer ($d < x < d + f$, $t > 0$), only the mass transfer of all species take place due to lack of enzymatic reaction, therefore, second Fick's law can be applied directly as below:

$$\begin{aligned} \frac{\partial U_{1,d}}{\partial t} &= D_{1,d} \frac{\partial^2 U_{1,d}}{\partial x^2} & \frac{\partial U_{2,d}}{\partial t} &= D_{2,d} \frac{\partial^2 U_{2,d}}{\partial x^2} & \frac{\partial U_{3,d}}{\partial t} &= D_{3,d} \frac{\partial^2 U_{3,d}}{\partial x^2} \\ \frac{\partial U_{4,d}}{\partial t} &= D_{4,d} \frac{\partial^2 U_{4,d}}{\partial x^2} & \frac{\partial U_{5,d}}{\partial t} &= D_{5,d} \frac{\partial^2 U_{5,d}}{\partial x^2} & \frac{\partial U_{6,d}}{\partial t} &= D_{6,d} \frac{\partial^2 U_{4,d}}{\partial x^2} \end{aligned}$$

where $U_{1,d}$, $U_{2,d}$, $U_{3,d}$, $U_{4,d}$, $U_{5,d}$ and $U_{6,d}$ are molecular concentrations of the substrates (SA, oxygen, NADH, proton), intermediate (catechol) and product (1,2-benzoquinone) in diffusion layer of thickness f , respectively. And $D_{1,d}$, $D_{2,d}$, $D_{3,d}$, $D_{4,d}$, $D_{5,d}$ and $D_{6,d}$ are the diffusion coefficients of the corresponding compounds in diffusion layer.

7.3.2.2 Initial conditions

At the beginning of the biosensor operation ($t = 0$), oxygen, NADH and protons are already present in the electrolyte throughout enzyme layer and diffusion layer as the same concentration in the bulk solution.

$$U_2(x, 0) = U_2^* \quad U_3(x, 0) = U_3^* \quad U_4(x, 0) = U_4^* \quad (0 \leq x \leq d + f)$$

where U_2 , U_3 and U_4 represent the concentrations of oxygen, NADH and protons throughout the three regions while U_2^* , U_3^* and U_4^* represent the corresponding concentrations in the bulk solution.

Both catechol and 1,2-benzoquinone are not presented at the beginning of the reaction ($t = 0$), thus both concentrations are zero:

$$U_5(x, 0) = U_6(x, 0) = 0 \quad (0 \leq x \leq d + f)$$

where U_5 and U_6 represent the concentration of catechol and 1,2-benzoquinone throughout three regions.

SA is added into the electrochemical system at the beginning of the reaction ($t = 0$), therefore the concentration at the boundary of diffusion layer is the same as that in the bulk solution. However, the concentration of salicylate within both enzyme and diffusion layer are not affected:

$$U_1(d + f, 0) = U_1^*$$

$$U_1(x, 0) = 0 \quad (0 \leq x < d + f)$$

where U_1 and U_1^* represent the concentrations of SA throughout the three regions and the concentration of SA in the bulk solution.

7.3.2.3 Boundary conditions

Boundary conditions are examined at the boundaries between the electrode and enzyme layer ($x = 0$), between enzyme layer and diffusion layer ($x = d$) and between diffusion layer and bulk solution ($x = d + f$)

All the compounds in the cascadic reaction other than 1,2-benzoquinone (*i.e.* SA, oxygen, NADH, proton and catechol) are considered to be electrochemically inactive due to lack of redox peaks from abovementioned compounds, therefore the fluxes at the electrode surface ($x = 0$) are considered as 0:

$$D_{1,d} \frac{\partial U_{1,e}}{\partial x} = D_{2,d} \frac{\partial U_{2,e}}{\partial x} = D_{3,d} \frac{\partial U_{3,e}}{\partial x} = D_{4,d} \frac{\partial U_{4,e}}{\partial x} = D_{5,d} \frac{\partial U_{5,e}}{\partial x} = 0 \quad (x = 0)$$

During the measurement of MeSA, the electrode was polarized causing the consumption of 1,2-benzoquinone for detection, therefore, the biosensor was assumed to be non-Clark type and 1,2-benzoquinone is assumed to be constantly reduced to zero at the electrode surface.

$$U_{6,e} = 0 \quad (x = 0)$$

At the boundary of enzyme layer and diffusion layer ($x = d$), the entering and ongoing fluxes from all species at both sides of the boundary are considered to be equal. Additionally, the concentrations of all species are considered to be continuous, therefore, the concentrations of all species at both sides of the boundary are considered to be equal.

$$D_e \frac{\partial U_e}{\partial x} = D_d \frac{\partial U_d}{\partial x} \quad (x = d)$$

$$U_e(d, t) = U_d(d, t)$$

At the boundary between diffusion layer and bulk solution ($x = d + f$), the concentrations of all reactants – SA, oxygen, NADH and protons remain the same as those in bulk solution respectively, and the concentration of both intermediate – catechol and final enzymatic product – 1,2-benzouquinone remain 0.

$$U_{1,d}(d + f, t) = U_1^* \quad U_{2,d}(d + f, t) = U_2^* \quad U_{3,d}(d + f, t) = U_3^* \quad U_{4,d}(d + f, t) = U_4^*$$

$$U_{5,d}(d + f, t) = U_{6,d}(d + f, t) = 0$$

7.3.2.4 Biosensor response

Cathodic current collected from the reduction of 1,2-benzoquinone formed after enzymatic reaction is used as biosensor response. The current density can be determined by Faraday's Law and Fick's law:

$$i(t) = n_e F D_{6,e} \frac{\partial U_{6,e}}{\partial x} (x = 0)$$

7.4 CONCLUSION

Lineweaver-Burke plots were generated for SH and TYR by plotting the reciprocal of initial reaction rate against various reciprocal concentrations of reactants. The results indicated the SH firstly formed SH-SA-NADH ternary complex with substrates SA and NADH before releasing the product (NAD^+). After that, the SH reacts with oxygen and generates catechol, carbon dioxide and water as ping-pong type mechanism. The results also proved that ternary complex TYR-catechol- O_2 was formed during catalysis. Enzyme-kinetic parameters such as the reciprocal of the maximum rate with unit enzyme concentration (ϕ_0) and the functions of rate and/or dissociation constants defined by Delziel ($\phi_A, \phi_B, \text{etc.}$) were calculated from the secondary plots and Michaelis-Menten constant was calculated for computational modeling. The linear range of the MeSA detection ($0 - 27.8 \mu\text{M}$) could be explained by $K_{m,\text{Sal}}$ ($25 \mu\text{M}$), within which the reaction rate is proportional to the concentration of SA. Additionally, governing equations, initial conditions, boundary conditions and biosensor response equation was derived for computational modelling.

CHAPTER 8

COMMERCIALIZATION POTENTIAL FOR A PORTABLE PLANT DISEASE DETECTION SYSTEM

8.1 OVERVIEW AND MOTIVATION

8.1.1 The proposed early-detection device for plant disease detection

Economic losses in the agricultural field due to pathogen infection and pest-infestation have been introduced in Chapter 1 in detail. It has been estimated that over \$40 billion worth of economic loss could be attributed to pathogen infection and pest-infestation in the U.S. alone (Pimentel, Zuniga et al. 2005, Roberts, Schimmelpfennig et al. 2006). The narrow profit margins limit most of the producers' option from choosing highly effective controls for most pathogen/pest-induced diseases. Instead, the traditional preventive approaches such as large-scale-spraying of chemicals (*e.g.* fungicides or pesticides) on a pre-determined schedule is still the most widely adopted solution to control and/or prevent most plant diseases caused by pathogens and pests in the agricultural field during cultivation. This results in excessively unnecessary chemical sprayings that increase the production costs and impacts environment and food quality. However, when the chemical spraying is not properly timed or late, it proves ineffective and could result up to 90 % of grower losses (Granke, Quesada-Ocampo et al. 2012). Therefore, end-user operable diagnostic device for early detection of pathogen infection / pest infestation would help growers,

distributors and other food processors to monitor and contain the infections on time, spray chemicals conservatively and selectively to only the infected regions as well as time the sprayings precisely in order to reduce cost. As the laboratory-based electrochemical biosensor was developed with esterase, salicylate hydroxylase and tyrosinase for MeSA detection as introduced previously, commercialization of a portable device for plant disease detection became our goal. The underlying innovation for such a device could also be potentially used for other applications where early detection is necessary.

8.1.2 The importance of understanding customer needs

The proposed plant-disease detection device is intended to be developed for growers. Therefore, it becomes important to study the customer base and the market opportunity for such a device/technology. Though there is some information available in the literature about the need in the agricultural industry for technology such as the one being developed in this dissertation project, the information from the potential customers is still insufficient. And the end user need for a plant-disease detection device or technology was never validated against potential end-users (*i.e.* growers, food handlers and distributors, *etc.*) in the previous research. Thus, direct engagement with farmers and other end-users could be helpful in determining the demand, potential market size and commercialization potential for the aforementioned device. Moreover, the needs may differ broadly for different end users, and, therefore, a comprehensive understanding of the different customer segments is necessary for commercialization.

8.1.3 Research funded by NSF Innovation Corps (I-CorpsTM) program

The National Science Foundation (NSF) funded I-Corps program prepares scientist and engineers who lack knowledge and opportunities for commercialization in the academic field to

extend the focus beyond the technology towards technology transfer and commercialization, with the goal of broadening the economic and societal benefits of NSF-funded research projects. During the I-Corps program, the project teams learn to identify valuable product opportunities that can emerge from a fundamental research, and learn the entrepreneurship skills and business knowledge for technology transfer and commercialization. Key objectives of the program are to discover the product-market fit of the proposed product, its corresponding potential customer segment, and to convey the value propositions of the product / service to the customers. The program requires the project teams to carry out interviews, especially in-person interviews with the potential customers from different customer segments, in order to understand the customer needs.

During the interviews, the perceived issues and risks related to crop disease management practices were verified and/or validated through specific questions and surveys of potential customers of the device. Therefore, the problem of the customers and their need for the device can be clearly understood, and the development of the detection device can be improved based on the value propositions and customer segments accordingly before the start of the commercialization.

8.1.4 Interviews and anticipated output

During the I-Corps program in Los Angeles, CA, from October to December, 2014, the I-Corps team consisting Yi Fang as Entrepreneurial Lead (EL), Dr. Ramaraja Ramasamy as Principal Investigator (PI) and Mr. Stefan Schulze as mentor underwent an intense customer discovery exercise. Interviews of potential customers to determine product-market fit were conducted across the United States including California, Georgia, North Carolina and South Carolina as

well as in foreign countries, such as Brazil and Germany. Overall 105 potential customers were interviewed during this period, with over 91 in-person interviews.

A questionnaire as shown below was prepared. Questions related to basic profiling of the interviewee, their current methods for disease management, and their willingness to adopt a new technology were included in the questionnaire. The questions were related to:

- Basic information:
 - Company name, person name, position in the company (*e.g.* employee, technician, owner, manager)
 - Type of business (*e.g.* agricultural production, distribution, processor, lumbering industry, nursery)
 - Type of products (*e.g.* the type of vegetable, fruit, tree, flower)
 - The scale of the business (*e.g.* the average annual sales / revenue, size of the field)
- Current problems:
 - In their cultivation of plants (crops, vegetables, fruits, trees and nurseries), were they suffering from plant diseases caused by pathogens or pests?
 - If the answer is YES, what is their current approach to managing crop diseases?
Application of fungicide and pesticide
 - Is the currently used approach effective? What is the cost of the currently used approach?
- Market opportunity for the proposed device:
 - Would customers be interested in a device which provides them an early detection of plant diseases that allows for reduction in fungicide / pesticide usage?
 - What other characteristics and properties would they expect from such a device?

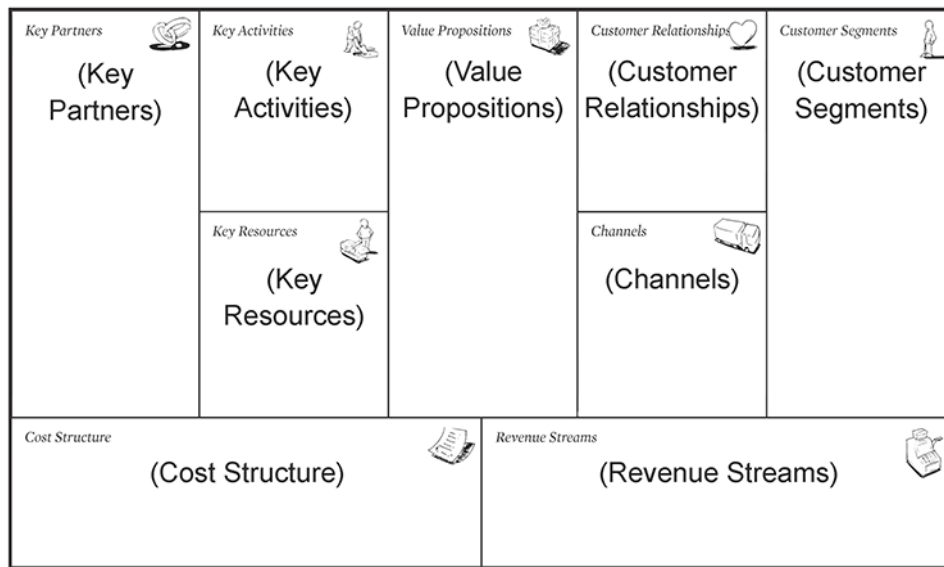
- How much would they be willing to pay for the device?

During each interview, the information collected from the interviewees was categorized based on the types and scale of business. The information was used for determining the value proposition and narrow down the customer segments.

8.2 DISCOVER THE CUSTOMER SEGMENTS AND VALUE PROPOSITIONS

8.2.1 Application of business model canvas

As introduced earlier, the key aspect of the I-Corps interview is to discover the product-market fit before real commercialization of the product is carried out. Business model canvas (Figure 8.1) was used to describe the rationale of how an organization creates, delivers and captures value and can be used to pivot the assumptions of both value proposition and customer segments during and after interview to find the best commercial model for product-market fit.



www.businessmodelgeneration.com

The templates here are made available on the same CC license terms as the original canvases.

Revised version with feedback from participants in the I-Corps program. © 2010-2011, Stanford University. All rights reserved.

Figure 8.1: The business model canvas used during I-Corps program to discover the best product-market fit.

Among all the nine building blocks of the business model canvas, the most important blocks are customer segments, which defines the groups of people or organizations an enterprise aims to serve, and the value propositions, which describes the bundle of products and services that create values for specific customer segments.

8.2.2 Customer segments and value propositions

At the very beginning of the I-Corps program, customer segments and value proposition were merely composed of assumptions about market opportunity. Six categories of potential customer segments were proposed, including vegetable/fruit handlers and distributors, crop growers, nursery wholesalers, nursery growers and forestry agents. The three value propositions were proposed including rapid detection of plant diseases, increase the productivity and minimize the fungicide/pesticide use as shown in the business model canvas below:

<p>Key Partners </p> <ul style="list-style-type: none"> • Food quality inspectors, USDA&FDA • Growers' association • Food industry Association • Crop growers of large Farms • Produce handlers & distributors • Medical doctors; Insurance companies • NIH; medical equipment makers 	<p>Key Activities </p> <ul style="list-style-type: none"> • Address and identify customer needs • R&D based on needs • Licensing; Regulatory approval • Manufacturing • Distribution thru Ag-companies extensions • Customer service <p>Key Resources </p> <ul style="list-style-type: none"> • Patents; IP; Licenses • Financial resources • Intellectual resources (human) 	<p>Value Proposition </p> <ul style="list-style-type: none"> • Rapid detection of plant diseases • Increase the productivity and minimize the fungicide/pesticide use • Rapid detection of cholesterol 	<p>Customer Relationships </p> <ul style="list-style-type: none"> • Commodity & Farmer Association • Seminars, Conferences • State extension unit meetings • Commodity groups • Ag-supply distributors • Gardening retailers <p>Channels </p> <ul style="list-style-type: none"> • Ag Comm., Assoc., Extensions & Exhibition • Farming equipment outlets 	<p>Customer Segments </p> <ul style="list-style-type: none"> • Vegetable/Fruit handlers & distributors • Crop growers • Nursery wholesalers • Nursery growers • Forestry
<p>Cost Structure </p> <ul style="list-style-type: none"> • Value-driven cost structure • (Fixed costs): Development; Capital; Licensing • (Variable costs): Manufacturing; Marketing 		<p>Revenue Streams </p> <ul style="list-style-type: none"> • (Assets sale): Sale/lease of equipment; sale of consumables; royalties (licensing) • (Pricing): Segment dependent pricing based on value proposition to a specific customer segment 		

Figure 8.2: Business model canvas (original version) proposed at the beginning of the I-Corps program.

During the interviews with potential customer segments, the value propositions were fully explained to the interviewees as described in the questionnaire and customer segments were narrowed down to eliminate the nursery wholesalers as a customer segment. This was because nurseries had a rapidly turn around, and any potential infection or disease do not directly affect the nurseries' business. We also narrowed down the vegetable/fruit handlers and distributors to those who have long storage time (longer than 1 week) and eliminated the fast-operating handlers and distributors. Furthermore, forestry was also removed from the customer segments in order to focus on only agricultural application. The value proposition was also revised and updated according to the customer needs. For example, rapid detection was quantitatively defined as less than 1 day, and productivity improvement was defined to be 10 % and fungicide / pesticide use reduction was defined to be 50 %. In addition, some potential customers require the shelf life prediction from the device, which requires the biosensor to provide quantitative information rather than just qualitative information (Figure 8.3).

<p>Key Partners </p> <ul style="list-style-type: none"> • Food quality inspectors, USDA&FDA • Growers' association • Food industry Association • Crop growers of large Farms • Produce handlers & distributors • Medical doctors; • Insurance companies • NIH; medical equipment-makers 	<p>Key Activities </p> <ul style="list-style-type: none"> • Address and identify customer needs • R&D based on needs • Licensing; Regulatory approval • Manufacturing • Distribution thru Ag-companies extensions • Customer service <p>Key Resources </p> <ul style="list-style-type: none"> • Patents; IP; Licenses • Financial resources • Intellectual resources (human) 	<p>Value Proposition </p> <ul style="list-style-type: none"> • Rapid detection (<1day) of plant diseases • Increase the productivity (at least 10%) and minimize the fungicide/pesticide use (at least 50%) • Rapid detection of cholesterol • Shelf life prediction 	<p>Customer Relationships </p> <ul style="list-style-type: none"> • Commodity & Farmer Association • Seminars, Conferences • State extension unit meetings • Commodity groups • Ag-supply distributors • Gardening retailers <p>Channels </p> <ul style="list-style-type: none"> • Ag Comm., Assoc., Extensions & Exhibition • Farming equipment outlets 	<p>Customer Segments </p> <ul style="list-style-type: none"> • Vegetable/Fruit handlers & distributors • Vegetable/Fruit handlers & distributors for long storage time >1 week • Crop growers • Nursery wholesalers • Nursery growers • Forestry
<p>Cost Structure </p> <ul style="list-style-type: none"> • Value-driven cost structure • (Fixed costs): Development; Capital; Licensing • (Variable costs): Manufacturing; Marketing 		<p>Revenue Streams </p> <ul style="list-style-type: none"> • (Assets sale): Sale/lease of equipment; sale of consumables; royalties (licensing) • (Pricing): Segment dependent pricing based on value proposition to a specific customer segment 		

Figure 8.3: Second version of business model canvas with forestry segment removed and vegetable/fruit handlers and distributors narrowed down.

In the later interviews within the potential customer segment of crop growers (including vegetable and fruit growers) and nursery growers, it was found that nursery growers were generally not interested in the proposition of the device due to lack of the described plant disease. Additionally, the scale of the nursery growers was generally small enough for the growers pay enough attention to spot the diseases rather than rely on the sensors. Coincidentally, crop growers were narrowed down to vegetable and fruit growers with large (> 100 acres) farms cultivating tomato, cucumber, squash, pumpkin and other high-value produce (Figure 8.4).

<p>Key Partners </p> <ul style="list-style-type: none"> • Food quality inspectors, USDA&FDA • Growers' association • Food industry Association • Crop growers of large Farms • Produce handlers & distributors 	<p>Key Activities </p> <ul style="list-style-type: none"> • Address and identify customer needs • R&D based on needs • Licensing; Regulatory approval • Manufacturing • Distribution thru Ag-companies extensions • Customer service <p>Key Resources </p> <ul style="list-style-type: none"> • Patents; IP; Licenses • Financial resources • Intellectual resources (human) 	<p>Value Proposition </p> <ul style="list-style-type: none"> • Rapid detection (<1day) of plant diseases • Increase the productivity (at least 10%) and minimize the fungicide/pesticide use (at least 50%) • Shelf life prediction 	<p>Customer Relationships </p> <ul style="list-style-type: none"> • Commodity & Farmer Association • Seminars, Conferences • State extension unit meetings • Commodity groups • Ag-supply distributors • Gardening retailers <p>Channels </p> <ul style="list-style-type: none"> • Ag Comm., Assoc., Extensions & Exhibition • Farming equipment outlets 	<p>Customer Segments </p> <ul style="list-style-type: none"> • Vegetable/Fruit handlers & distributors for long storage time >1 week • Crop-growers • Tomato, cucumber, squash, pumpkin growers with >100 acre farms • Nursery-growers
<p>Cost Structure </p> <ul style="list-style-type: none"> • Value-driven cost structure • (Fixed costs): Development; Capital; Licensing • (Variable costs): Manufacturing; Marketing 		<p>Revenue Streams </p> <ul style="list-style-type: none"> • (Assets sale): Sale/lease of equipment; sale of consumables; royalties (licensing) • (Pricing): Segment dependent pricing based on value proposition to a specific customer segment 		

Figure 8.4: Third version of business model canvas with nursery growers segment removed and crop growers narrowed down to vegetable/fruit growers with large farms.

8.3 MARKET OPPORTUNITY

8.3.1 Preliminary market research

Based on the information collected during the I-Corps program, our target market space, as narrowed down in the business model canvas (Figure 8.4) from the interviews, is the vegetative crop growers and handlers/distributors. Among them, the vegetable/fruit growers spending at least \$50,000 for chemical spraying annually are our archetypal customers whose primary concern is to protect the crops from pathogen infection and pest infestation during growing and harvesting seasons.

The potential customers indicated that pathogenic fungal infections cause numerous diseases such as white mold, grey mold, crown rot, leaf blight in varieties of cucurbit crops, grapes and strawberries. If not diagnosed, treated and controlled on time, these infections quickly spread to the entire field by wind, human or animal contact and splashed water; resulting in devastating damage to the crops. In addition to the growers, the vegetable handlers/distributors with long storage time also expressed similar concern about the disease and interest in the detection device. Although the produce is sold frequently to the food handler/distributor through mass distribution well before the infection and diseases appears, the hidden pathogens (if the crop is infected already) could break out at a later time and low the values of the vegetables and fruits.

The interview also indicated the frequency of the chemical spraying is from 4 days (grapes) to 15 days (cucurbit crops) depending on the crop type, weather and geography, and the average cost of the chemical sprayings is about \$200/acre/application and up to \$3,000/acre/season for some crops. One of our potential customers from Germany, owns a 3 acre greenhouse to grow tomatoes mentioned spending €30,000 annually on fungicide sprayings. Our potential customers typically take one of two options for chemical sprayings: (i) Unwilling to take risk of the crop losses, most vegetable/fruit growers adopt a preemptive spraying in which, chemicals, such as fungicide and pesticide, are applied to the entire crop field on a pre-determined schedule regardless of weather or the condition of infection. This type of customers spends much more on the chemical sprayings than what they are supposed to. (ii) Risk-takers, who are willing to take some risks by reducing costs of chemical sprayings, would rather wait for the onset of visual symptoms or bad weather that favors the diseases before applying chemical sprayings. But this option is not popular among most growers, except those who cultivate pumpkins which are not harvested as food. However, both types of growers expressed their interests in adopting a

solution that provides early detection of plant diseases which could further help them determine the single infectious 'plot' of the crop field to perform specific sprayings, which decreases the chemical expenses and maintain the standard of good agricultural practices (GAP) program.

8.3.2 Market size

The market size is estimated in this section based on how much direct economic value could be brought to the customers by means of reduced sprayings. The immediate market space is the agricultural industry that heavily relies on the chemical sprayings to contain and prevent pathogen infection / pest infestation. The worldwide fungicide spraying is estimated to be about \$9.2 billion in 2014 (total available market) of which \$1.375 billion was spend in the United States (service available market). If our value proposition is to reduce the spraying by at least 50 %, this could bring the benefit of up to ~ \$700 million annually (target market) to the agricultural industry (Figure 8.5). However, the data need further refinement based on the fungicide expenditures by regions and crop types, whose data are provided in the pie chart in Figure 8.5.

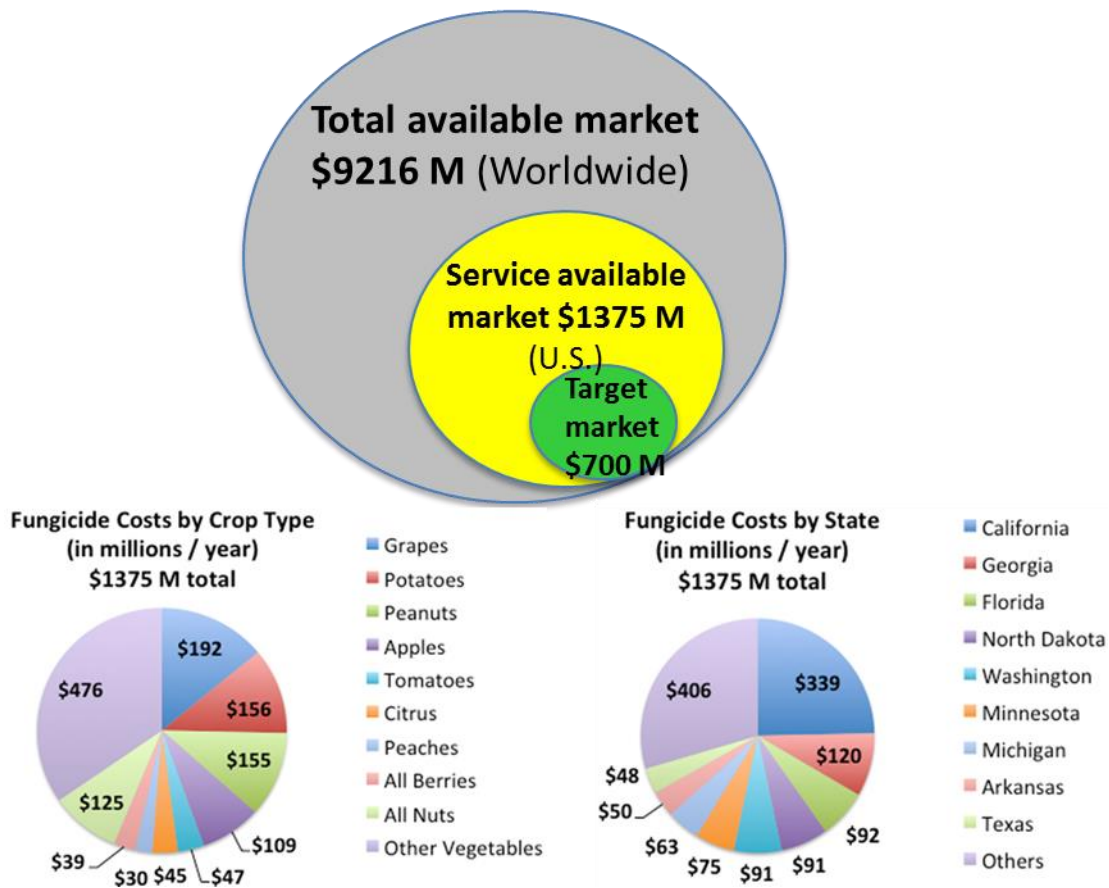


Figure 8.5: Total available, service available and target markets (above). Fungicide spraying costs by state and crop type (below).

The data shows that the fungicide expenditures in Georgia alone account for \$120 million and vine crops such as tomatoes and grapes constitute the largest consumption of fungicide. The data shown in Figure 8.5 indicated the current market that is available and our goal is to capture at least 10 % of our target market within the first 3 years of starting our business.

8.4 CONCLUSION

The NSF funded I-Corps program between the period of October and December of 2014 initiated our path towards commercialization of the biosensor-based early detection device for predicting plant diseases. In this program, the product-market fit with different types of customers was

studied and the business model canvas was updated every week through 8-week period during which potential customers were interviewed. The interviews we conducted with end-users, buyers and other recommenders suggest different attitudes towards the value propositions of our product. Through the interviews, we confined the potential customer segments to vegetable and fruit growers (*e.g.* tomatoes, strawberries, grapes, *etc.*) with large scale of farmlands (> 100 acres). And the value propositions provided by the early detection device was revalidated using interviews, which provides the motivations for the device development. From the requirements and interests of the potential customers, we learnt that a quantitative method for the prediction of vegetable / fruit shelf life is highly desired, suggesting the areas of focus for our future steps. In addition, the market size was also estimated based on the current fungicide expenditures for agricultural industry.

CHAPTER 9

CONCLUSIONS AND FUTURE DIRECTIONS

Although various methods including both direct detection methods for plant pathogens and pests and indirect detection methods for plant disease symptom have been developed for plant disease prediction, they either require expensive instruments or skilled operators to carry out the detection tests. Therefore, in dissertation research, an early detection method that is different from the traditional practices was developed using electrochemical biosensors through the measurement of volatile organic compounds that are released as chemical markers during a biotic stress event in plants. A multi-disciplinary approach to develop such biosensor could aid in proper disease management practices, including minimizing chemical spraying, improved cost savings, improved food quality and minimize environmental impact of the chemicals. Such efforts have been carried out in this dissertation research in three different dimensions:

(1) Electrochemical biosensors for volatile organic compounds

The research work reported in this dissertation is the illustration of electrochemical sensors for three volatile organic compounds that can be used as the biomarkers for the plant disease prediction – 4-ethylguaiacol, 4-ethylphenol and methyl salicylate. 4-Ethylguaiacol and 4-ethylphenol are produced by *Phytophthora cactorum* when infecting various plants, such as strawberries, and causes crown rot and can devastate the entire crop field. Detection of 4-

ethylguaiacol was realized in this project using metal oxide-modified (TiO_2 and SnO_2) screen printed electrodes, which generates good sensitivity and low limit of detection to nanomole scale. The detection of 4-ethylphenol was realized through the immobilization of enzyme tyrosinase on the glassy-carbon electrode by cross-linker PBSE. The analyte 4-ethyl-phenol was oxidized on the electrode to form 4-ethyl-1,2-benzoquinone by both monooxygenase activity (forming 4-ethyl-1,2-hydroquinone) and catechol activity (forming 4-ethyl-1,2-benzoquinone) from tyrosinase. 4-Ethyl-1,2-benzoquinone can be reduced on the electrode surface due to its electrochemical activity.

Detection of methyl salicylate, a common volatile organic compound that plays an important role in plant defense response was demonstrated using two methods. The first method involved the enzyme combination alcohol oxidase and horseradish peroxidase as recognition element. Although the approach was proven to be satisfactory, a second approach consisting of recombinant expressed salicylate hydroxylase and tyrosinase as recognition element was developed to achieve enhanced sensitivity ($30.6 \mu\text{A}\cdot\text{cm}^{-2}\cdot\mu\text{M}^{-1}$) and improved detection limits (13 nM). In addition to the noncovalent functionalization method for enzyme immobilization using PBSE, other cross-linking strategies based on N-(1-Pyrenyl) maleimide and poly-L-lysine were also explored as alternatives for enzyme immobilization on nanostructured electrodes.

In addition to the bi-enzymatic biosensor, an esterase was introduced in the system to make a tri-enzyme system for methyl salicylate detection without using the chemical method to hydrolyze methyl salicylate before detection. A screen-printed electrode was successfully prepared for methyl salicylate detection with a quasi-reference electrode. In addition, a computer controlled platform for automated collection of volatile organic compounds and temperature measurements was designed using MOSFET, allowing the control of a micro air pump through computer and

Arduino Uno to allow for the communication between a computer and the electronic device that contains the biosensor.

2) The mathematical modeling for bi-enzymatic reactions

In addition to the evaluation of bi-enzymatic (salicylate hydroxylase and tyrosinase) biosensors using electrochemical characterization tools, the mechanisms of the bi-enzymatic systems were also studied using enzyme assays. The initial reaction rates of both enzymes were measured using UV-Vis spectroscopy at different concentration of substrates. The Lineweaver-Burk plot generated from the initial reaction rate against substrate concentration indicated ternary-complex was formed in salicylate hydroxylase with salicylate and NADH, while the ping-pong reaction mechanism was observed in the oxygen utilization. The similar formation of ternary-complex in tyrosinase can also be demonstrated by the Lineweaver-Burk plot. In addition to the kinetic mechanisms, the enzyme kinetic parameters defined by Dalziel was derived and calculated from the Lineweaver-Burk plots, which in return, explained the biosensor linear range and can be used for the mathematical modelling. The electrochemical modeling including derivation of governing equations, initial conditions, boundary conditions and biosensor response equation were also discussed.

(3) Commercialization approaches by I-Corps program

Although the laboratory research work accounted for a majority of this dissertation research, the validation of assumptions about the biosensor device and its commercialization prospects were carried out to understand the product-market fit through the I-Corps program. The assumption validations include the existence of plant diseases in agriculture, current methods for plant disease prediction and prevention, and the necessity of the biosensor device. Based on the

interviews conducted during the program, a business model canvas was developed and later updated. During the I-Corps program, the potential customer segments were narrowed down to specific group of people, and the value proposition of the product (biosensor device) was revised. The project confirmed the existence of a commercial need for a biosensor device for early detection of plant diseases.

FUTURE DIRECTIONS:

- 1) The mathematical developed in chapter 8 will be rigorously solved in order to fully understand the biochemical kinetic and electrochemical reaction and transport mechanisms that govern the operation and performance of the biosensors for further optimization and improvement.
- 2) Improving enzyme stability could be an important goal for our future work as the enzyme stability determines the shelf life and operational duration of the biosensor. Other enzyme cross-linking strategy could be explored for better immobilization and stabilization of enzymes on the electrode. Lyophilization of enzymes could be explored for removing the solvent on the electrode when the enzyme is immobilized on the electrode for better shelf life.
- 3) Finally, real world application of the developed biosensor needs to be evaluated for the on-field detection. Different crops reported for MeSA generation could be our future target. In order to ensure the applicability of the biosensor at different temperature (which affects the enzyme activity), the developed biosensor will also be calibrated under different temperature before on-field test is carried out.

REFERENCES

- Akkara, J. A., K. J. Senecal and D. L. Kaplan (1991). "Synthesis and characterization of polymers produced by horseradish peroxidase in dioxane." Journal of Polymer Science Part A: Polymer Chemistry **29**(11): 1561-1574.
- Armbruster, D. A. and T. Pry (2008). "Limit of blank, limit of detection and limit of quantitation." Clin Biochem Rev **29**(Suppl 1): S49-52.
- Armstrong, N. R., A. W. Lin, M. Fujihira and T. Kuwana (1976). "ELECTROCHEMICAL AND SURFACE CHARACTERISTICS OF TIN OXIDE AND INDIUM OXIDE ELECTRODES." Analytical Chemistry **48**(4): 741-750.
- Bakker, E. (2004). "Electrochemical sensors." Analytical chemistry **76**(12): 3285-3298.
- Bard, A. J., L. R. Faulkner, J. Leddy and C. G. Zoski (1980). Electrochemical methods: fundamentals and applications, Wiley New York.
- Bernasconi, M. L., T. C. Turlings, L. Ambrosetti, P. Bassetti and S. Dorn (1998). "Herbivore-induced emissions of maize volatiles repel the corn leaf aphid, *Rhopalosiphum maidis*." Entomologia Experimentalis et Applicata **87**(2): 133-142.
- Boscan, L., W. Powrie and O. Fennema (1962). "Darkening of red beets, *Beta vulgaris*." Journal of Food Science **27**(6): 574-582.
- Brigati, J. R. and V. A. Petrenko (2005). "Thermostability of landscape phage probes." Analytical and bioanalytical chemistry **382**(6): 1346-1350.
- Bru, R., A. Sanchez-Ferrer and F. García-Carmona (1989). "Characteristics of tyrosinase in AOT–isooctane reverse micelles." Biotechnology and bioengineering **34**(3): 304-308.
- Buttery, R., R. Seifert, D. Guadagni and L. Ling (1969). "Characterization of some volatile constituents of bell peppers." Journal of Agricultural and Food Chemistry **17**(6): 1322-1327.
- Byrne, B., E. Stack, N. Gilmartin and R. O’Kennedy (2009). "Antibody-based sensors: principles, problems and potential for detection of pathogens and associated toxins." Sensors **9**(6): 4407-4445.
- Caboni, P., G. Sarais, M. Cabras and A. Angioni (2007). "Determination of 4-Ethylphenol and 4-Ethylguaiacol in Wines by LC-MS-MS and HPLC-DAD-Fluorescence." Journal of agricultural and food chemistry **55**(18): 7288-7293.
- Cai, H., J. Caswell and J. Prescott (2014). "Nonculture molecular techniques for diagnosis of bacterial disease in animals a diagnostic laboratory perspective." Veterinary Pathology Online **51**(2): 341-350.
- Candresse, T., H. Lot, S. German-Retana, R. Krause-Sakate, J. Thomas, S. Souche, T. Delaunay, M. Lanneau and O. Le Gall (2007). "Analysis of the serological variability of Lettuce mosaic virus using monoclonal antibodies and surface plasmon resonance technology." Journal of general virology **88**(9): 2605-2610.
- Cao, X., Y. Ye and S. Liu (2011). "Gold nanoparticle-based signal amplification for biosensing." Analytical biochemistry **417**(1): 1-16.
- Carpenter, J. H. (1965). "The Chesapeake Bay Institute technique for the Winkler dissolved oxygen method." Limnology and Oceanography **10**(1): 141-143.
- Chaerle, L., I. Leinonen, H. G. Jones and D. Van Der Straeten (2007). "Monitoring and screening plant populations with combined thermal and chlorophyll fluorescence imaging." Journal of Experimental Botany **58**(4): 773-784.

- Chitarra, L. G. and R. W. Van Den Bulk (2003). "The application of flow cytometry and fluorescent probe technology for detection and assessment of viability of plant pathogenic bacteria." European journal of plant pathology **109**(5): 407-417.
- Clark, M. F. and A. Adams (1977). "Characteristics of the microplate method of enzyme-linked immunosorbent assay for the detection of plant viruses." Journal of general virology **34**(3): 475-483.
- Clay, E. (2002). "Food security: concepts and measurement." Trade reforms and food security: Conceptualising the linkages: 25-34.
- Comninellis, C. and C. Pulgarin (1993). "Electrochemical oxidation of phenol for wastewater treatment using SnO₂, anodes." Journal of applied electrochemistry **23**(2): 108-112.
- Conway, G. (2012). One billion hungry: can we feed the world?, Cornell University Press.
- Cosnier, S. and C. Innocent (1993). "A new strategy for the construction of a tyrosinase-based amperometric phenol and o-diphenol sensor." Bioelectrochemistry and bioenergetics **31**(2): 147-160.
- Dalziel, K. (1957). "Initial steady state velocities in the evaluation of enzyme-coenzyme-substrate reaction mechanisms." Acta chem. scand **11**(1): 706-723.
- Dalziel, K. (1969). "The interpretation of kinetic data for enzyme-catalysed reactions involving three substrates." Biochemical Journal **114**(3): 547-556.
- Danner, H., G. A. Boeckler, S. Irmisch, J. S. Yuan, F. Chen, J. Gershenzon, S. B. Unsicker and T. G. Köllner (2011). "Four terpene synthases produce major compounds of the gypsy moth feeding-induced volatile blend of *Populus trichocarpa*." Phytochemistry **72**(9): 897-908.
- De Boer, J. G. and M. Dicke (2004). "The role of methyl salicylate in prey searching behavior of the predatory mite *Phytoseiulus persimilis*." Journal of chemical ecology **30**(2): 255-271.
- De Boer, J. G., M. A. Posthumus and M. Dicke (2004). "Identification of volatiles that are used in discrimination between plants infested with prey or nonprey herbivores by a predatory mite." Journal of chemical ecology **30**(11): 2215-2230.
- de Faria, R. O., V. Rotuno Moure, W. Balmant, M. A. Lopes de Almeida Amazonas, N. Krieger and D. A. Mitchell (2007). "The tyrosinase produced by *Lentinula boryana* (Berk. & Mont.) Pegler suffers substrate inhibition by L-DOPA." Food Technology and Biotechnology **45**(3): 334-340.
- de Lacy Costello, B., R. Ewen, P. Jones, N. Ratcliffe and R. Wat (1999). "A study of the catalytic and vapour-sensing properties of zinc oxide and tin dioxide in relation to 1-butanol and dimethyldisulphide." Sensors and Actuators B: Chemical **61**(1): 199-207.
- Delalieux, S., J. Van Aardt, W. Keulemans, E. Schrevens and P. Coppin (2007). "Detection of biotic stress (*Venturia inaequalis*) in apple trees using hyperspectral data: Non-parametric statistical approaches and physiological implications." European Journal of Agronomy **27**(1): 130-143.
- Dewey, F. and G. Marshall (1996). Production and use of monoclonal antibodies for the detection of fungi. British Crop Protection Council Symposium Proceedings. 1996.
- Dickert, F. L., O. Hayden, R. Bindeus, K.-J. Mann, D. Blaas and E. Waigmann (2004). "Bioimprinted QCM sensors for virus detection—screening of plant sap." Analytical and bioanalytical chemistry **378**(8): 1929-1934.
- Diebold, U. (2003). "Structure and properties of TiO₂ surfaces: a brief review." Applied Physics A: Materials Science & Processing **76**(5): 681-687.
- El-Ansary, A. and L. M. Faddah (2010). "Nanoparticles as biochemical sensors." Nanotechnology, science and applications **3**(1): 65-76.

- Ellis, M. and G. Grove (1983). "Leather rot in Ohio strawberries." Plant disease **67**(5).
- Enache, T. A. and A. M. Oliveira-Brett (2011). "Phenol and para-substituted phenols electrochemical oxidation pathways." Journal of Electroanalytical Chemistry **655**(1): 9-16.
- Espín, J. C., R. Varón, L. G. Fenoll, M. Gilabert, P. A. García-Ruíz, J. Tudela and F. García-Cánovas (2000). "Kinetic characterization of the substrate specificity and mechanism of mushroom tyrosinase." European Journal of Biochemistry **267**(5): 1270-1279.
- Eun, A. J.-C., L. Huang, F.-T. Chew, S. Fong-Yau Li and S.-M. Wong (2002). "Detection of two orchid viruses using quartz crystal microbalance-based DNA biosensors." Phytopathology **92**(6): 654-658.
- Eun, A. J.-C. and S.-M. Wong (2000). "Molecular beacons: a new approach to plant virus detection." Phytopathology **90**(3): 269-275.
- Fall, R. and A. A. Benson (1996). "Leaf methanol—the simplest natural product from plants." Trends in Plant Science **1**(9): 296-301.
- Fang, Y., Y. Umasankar and R. P. Ramasamy (2014). "Electrochemical detection of p-ethylguaiacol, a fungi infected fruit volatile using metal oxide nanoparticles." Analyst **139**(15): 3804-3810.
- Ghindilis, A. L., P. Atanasov and E. Wilkins (1997). "Enzyme-catalyzed direct electron transfer: Fundamentals and analytical applications." Electroanalysis **9**(9): 661-674.
- Godfray, H. C. J., J. R. Beddington, I. R. Crute, L. Haddad, D. Lawrence, J. F. Muir, J. Pretty, S. Robinson, S. M. Thomas and C. Toulmin (2010). "Food security: the challenge of feeding 9 billion people." science **327**(5967): 812-818.
- Gorris, M. T., B. Alarcon, M. M. Lopez and M. Cambra (1994). "Characterization of monoclonal antibodies specific for *Erwinia carotovora* subsp. *atroseptica* and comparison of serological methods for its sensitive detection on potato tubers." Applied and Environmental Microbiology **60**(6): 2076-2085.
- Granke, L. L., L. Quesada-Ocampo, K. Lamour and M. K. Hausbeck (2012). "Advances in research on *Phytophthora capsici* on vegetable crops in the United States." Plant Disease **96**(11): 1588-1600.
- Gurung, K. (2007). "Analysis of wintergreen oil." Ecology Agriculture and Rural Development Society, Dolakha, Nepal.
- Hakala, M. A., A. T. Lapveteläinen and H. P. Kallio (2002). "Volatile compounds of selected strawberry varieties analyzed by purge-and-trap headspace GC-MS." Journal of agricultural and food chemistry **50**(5): 1133-1142.
- Hijri, M. (2009). "The use of Fluorescent in situ hybridisation in plant fungal identification and genotyping." Plant Pathology: Techniques and Protocols: 131-145.
- Isidorov, V., I. Zenkevich and B. Ioffe (1985). "Volatile organic compounds in the atmosphere of forests." Atmospheric Environment (1967) **19**(1): 1-8.
- James, D. (1999). "A simple and reliable protocol for the detection of apple stem grooving virus by RT-PCR and in a multiplex PCR assay." Journal of Virological Methods **83**(1): 1-9.
- James, D. G. and T. S. Price (2004). "Field-testing of methyl salicylate for recruitment and retention of beneficial insects in grapes and hops." Journal of chemical ecology **30**(8): 1613-1628.
- Jansen, R. M., J. W. Hofstee, J. Wildt, F. W. Verstappen, H. Bouwmeester and E. J. van Henten (2009). "Induced plant volatiles allow sensitive monitoring of plant health status in greenhouses." Plant signaling & behavior **4**(9): 824-829.

- Jeleń, H., J. Krawczyk, T. Larsen, A. Jarosz and B. Gołębiak (2005). "Main compounds responsible for off-odour of strawberries infected by *Phytophthora cactorum*." Letters in applied microbiology **40**(4): 255-259.
- Katagiri, M., H. Maeno, S. Yamamoto, O. Hayaishi, T. Kitao and S. Oae (1965). "Salicylate hydroxylase, a monooxygenase requiring flavin adenine dinucleotide II. The mechanism of salicylate hydroxylation to catechol." Journal of Biological Chemistry **240**(8): 3414-3417.
- Kempf, V. A., K. Trebesius and I. B. Autenrieth (2000). "Fluorescent in situ hybridization allows rapid identification of microorganisms in blood cultures." Journal of clinical microbiology **38**(2): 830-838.
- Kesselmeier, J. and M. Staudt (1999). "Biogenic volatile organic compounds (VOC): an overview on emission, physiology and ecology." Journal of atmospheric chemistry **33**(1): 23-88.
- Kessler, A. and I. T. Baldwin (2001). "Defensive function of herbivore-induced plant volatile emissions in nature." Science **291**(5511): 2141-2144.
- Kliot, A., S. Kontsedalov, G. Lebedev, M. Brumin, P. B. Cathrin, J. M. Marubayashi, M. Skaljic, E. Belausov, H. Czosnek and M. Ghanim (2014). "Fluorescence in situ hybridizations (FISH) for the localization of viruses and endosymbiotic bacteria in plant and insect tissues." JoVE (Journal of Visualized Experiments)(84): e51030-e51030.
- Kobayashi, T., E. Kanda, K. Kitada, K. Ishiguro and Y. Torigoe (2001). "Detection of rice panicle blast with multispectral radiometer and the potential of using airborne multispectral scanners." Phytopathology **91**(3): 316-323.
- Kretzer, J. W., R. Lehmann, M. Schmelcher, M. Banz, K.-P. Kim, C. Korn and M. J. Loessner (2007). "Use of high-affinity cell wall-binding domains of bacteriophage endolysins for immobilization and separation of bacterial cells." Applied and environmental microbiology **73**(6): 1992-2000.
- Kruger, N. J. (1994). "The Bradford method for protein quantitation." Basic protein and peptide protocols: 9-15.
- Kruger, N. J. (2009). "The Bradford method for protein quantitation." The protein protocols handbook: 17-24.
- Leonard, P., S. Hearty, J. Brennan, L. Dunne, J. Quinn, T. Chakraborty and R. O'Kennedy (2003). "Advances in biosensors for detection of pathogens in food and water." Enzyme and Microbial Technology **32**(1): 3-13.
- Li, H., H. Wen and S. Calabrese Barton (2012). "NADH Oxidation catalyzed by electropolymerized azines on carbon nanotube modified electrodes." Electroanalysis **24**(2): 398-406.
- Li, H., K. E. Worley and S. Calabrese Barton (2012). "Quantitative analysis of bioactive NAD⁺ regenerated by NADH electro-oxidation." Acs Catalysis **2**(12): 2572-2576.
- Lian, P., X. Zhu, S. Liang, Z. Li, W. Yang and H. Wang (2011). "High reversible capacity of SnO₂/graphene nanocomposite as an anode material for lithium-ion batteries." Electrochimica Acta **56**(12): 4532-4539.
- Lievens, B., M. Brouwer, A. C. Vanachter, B. P. Cammue and B. P. Thomma (2006). "Real-time PCR for detection and quantification of fungal and oomycete tomato pathogens in plant and soil samples." Plant Science **171**(1): 155-165.

- Lindenthal, M. (2005). Visualisierung der Krankheitsentwicklung von Falschem Mehltau an Gurken durch Pseudoperonospora cubensis mittels Thermografie, Universitäts-und Landesbibliothek Bonn.
- Lindenthal, M., U. Steiner, H.-W. Dehne and E.-C. Oerke (2005). "Effect of downy mildew development on transpiration of cucumber leaves visualized by digital infrared thermography." Phytopathology **95**(3): 233-240.
- Loake, G. and M. Grant (2007). "Salicylic acid in plant defence—the players and protagonists." Current opinion in plant biology **10**(5): 466-472.
- Long, G. L. and J. Winefordner (1983). "Limit of detection. A closer look at the IUPAC definition." Anal. Chem **55**(7).
- López, M. M., E. Bertolini, A. Olmos, P. Caruso, M. T. Gorris, P. Llop, R. Penyalver and M. Cambra (2003). "Innovative tools for detection of plant pathogenic viruses and bacteria." International Microbiology **6**(4): 233-243.
- Luo, P., S. V. Prabhu and R. P. Baldwin (1990). "Constant potential amperometric detection at a copper-based electrode: electrode formation and operation." Analytical Chemistry **62**(7): 752-755.
- Mahlein, A.-K., E.-C. Oerke, U. Steiner and H.-W. Dehne (2012). "Recent advances in sensing plant diseases for precision crop protection." European Journal of Plant Pathology **133**(1): 197-209.
- Mandler, D. and S. Kraus-Ophir (2011). "Self-assembled monolayers (SAMs) for electrochemical sensing." Journal of Solid State Electrochemistry **15**(7-8): 1535.
- Martorell, N., M. Martí, M. Mestres, O. Busto and J. Guasch (2002). "Determination of 4-ethylguaiacol and 4-ethylphenol in red wines using headspace-solid-phase microextraction-gas chromatography." Journal of Chromatography A **975**(2): 349-354.
- Mason, M. (2013). Has urbanization caused a loss to agricultural land.
- Mc Grath, S. and D. van Sinderen (2007). Bacteriophage: genetics and molecular biology, Horizon Scientific Press.
- Mell, L. D. and J. Maloy (1975). "Model for the amperometric enzyme electrode obtained through digital simulation and applied to the immobilized glucose oxidase system." Analytical Chemistry **47**(2): 299-307.
- Nassuth, A., E. Pollari, K. Helmezy, S. Stewart and S. A. Kofalvi (2000). "Improved RNA extraction and one-tube RT-PCR assay for simultaneous detection of control plant RNA plus several viruses in plant extracts." Journal of Virological Methods **90**(1): 37-49.
- Neufeld, T., A. Schwartz-Mittelmann, D. Biran, E. Ron and J. Rishpon (2003). "Combined phage typing and amperometric detection of released enzymatic activity for the specific identification and quantification of bacteria." Analytical chemistry **75**(3): 580-585.
- Nieminen, T., P. Neubauer, S. Sivelä, S. Vatamo, P. Silfverberg and M. Salkinoja-Salonen (2008). "Volatile compounds produced by fungi grown in strawberry jam." LWT-Food Science and Technology **41**(10): 2051-2056.
- Nugaeva, N., K. Y. Gfeller, N. Backmann, M. Düggelin, H. P. Lang, H.-J. Güntherodt and M. Hegner (2007). "An antibody-sensitized microfabricated cantilever for the growth detection of *Aspergillus niger* spores." Microscopy and Microanalysis **13**(01): 13-17.
- Oerke, E.-C. (2006). "Crop losses to pests." The Journal of Agricultural Science **144**(01): 31-43.
- Oerke, E.-C., P. Fröhling and U. Steiner (2011). "Thermographic assessment of scab disease on apple leaves." Precision Agriculture **12**(5): 699-715.

- Oerke, E., U. Steiner, H. Dehne and M. Lindenthal (2006). "Thermal imaging of cucumber leaves affected by downy mildew and environmental conditions." Journal of experimental botany **57**(9): 2121-2132.
- Osiowy, C. (1998). "Direct detection of respiratory syncytial virus, parainfluenza virus, and adenovirus in clinical respiratory specimens by a multiplex reverse transcription-PCR assay." Journal of Clinical Microbiology **36**(11): 3149-3154.
- Ozimek, P., M. Veenhuis and I. J. van der Klei (2005). "Alcohol oxidase: a complex peroxisomal, oligomeric flavoprotein." FEMS yeast research **5**(11): 975-983.
- Palchetti, I. and M. Mascini (2008). "Electroanalytical biosensors and their potential for food pathogen and toxin detection." Analytical and bioanalytical chemistry **391**(2): 455-471.
- Pallisgaard, N., P. Hokland, D. C. Riishøj, B. Pedersen and P. Jørgensen (1998). "Multiplex reverse transcription-polymerase chain reaction for simultaneous screening of 29 translocations and chromosomal aberrations in acute leukemia." Blood **92**(2): 574-588.
- Park, S., H. Boo and T. D. Chung (2006). "Electrochemical non-enzymatic glucose sensors." Analytica Chimica Acta **556**(1): 46-57.
- Patel, R. N., C. Hou, A. Laskin and P. Derelanko (1981). "Microbial oxidation of methanol: properties of crystallized alcohol oxidase from a yeast, *Pichia* sp." Archives of biochemistry and biophysics **210**(2): 481-488.
- Perera, R. M., P. J. Marriott and I. E. Galbally (2002). "Headspace solid-phase microextraction—Comprehensive two-dimensional gas chromatography of wound induced plant volatile organic compound emissions." Analyst **127**(12): 1601-1607.
- Pickett, J. A., T. J. Bruce, K. Chamberlain, A. Hassanali, Z. R. Khan, M. C. Matthes, J. A. Napier, L. E. Smart, L. J. Wadhams and C. M. Woodcock (2006). "Plant volatiles yielding new ways to exploit plant defence." Chemical ecology: from gene to ecosystem: 161-173.
- Piesik, D., G. Lemńczyk, A. Skoczek, R. Lamparski, J. Bocianowski, K. Kotwica and K. J. Delaney (2011). "Fusarium infection in maize: Volatile induction of infected and neighboring uninfected plants has the potential to attract a pest cereal leaf beetle, *Oulema melanopus*." Journal of plant physiology **168**(13): 1534-1542.
- Pimentel, D., R. Zuniga and D. Morrison (2005). "Update on the environmental and economic costs associated with alien-invasive species in the United States." Ecological economics **52**(3): 273-288.
- Pollnitz, A. P., K. H. Pardon and M. A. Sefton (2000). "Quantitative analysis of 4-ethylphenol and 4-ethylguaiacol in red wine." Journal of Chromatography A **874**(1): 101-109.
- Premkumar, R. and N. Krishnamohan (2010). "Removal of methanol from waste gas using biofiltration." Journal of Applied Sciences Research(November): 1898-1907.
- Ramasamy, R. P., H. R. Luckarift, D. M. Ivnitski, P. B. Atanassov and G. R. Johnson (2010). "High electrocatalytic activity of tethered multicopper oxidase-carbon nanotube conjugates." Chemical Communications **46**(33): 6045-6047.
- Rassaei, L., J. Cui, E. D. Goluch and S. G. Lemay (2012). "Substrate-dependent kinetics in tyrosinase-based biosensing: amperometry vs. spectrophotometry." Analytical and bioanalytical chemistry **403**(6): 1577-1584.
- Rayne, S. and N. J. Eggers (2007). "4-ethylphenol and 4-ethylguaiacol in wines: estimating non-microbial sourced contributions and toxicological considerations." Journal of Environmental Science and Health Part B **42**(8): 887-897.

- Roberts, M. J., D. E. Schimmelpfennig, E. Ashley, M. J. Livingston, M. S. Ash and U. Vasavada (2006). The value of plant disease early-warning systems: a case study of USDA's soybean rust coordinated framework, United States Department of Agriculture, Economic Research Service.
- Ronkainen, N. J., H. B. Halsall and W. R. Heineman (2010). "Electrochemical biosensors." Chemical Society Reviews **39**(5): 1747-1763.
- Sadana, A. and J. R. Katzer (1974). "Involvement of free radicals in the aqueous-phase catalytic oxidation of phenol over copper oxide." Journal of Catalysis **35**(1): 140-152.
- Sadanandom, A. and R. M. Napier (2010). "Biosensors in plants." Current opinion in plant biology **13**(6): 736-743.
- Savary, S., A. Ficke, J.-N. Aubertot and C. Hollier (2012). "Crop losses due to diseases and their implications for global food production losses and food security." Food Security **4**(4): 519-537.
- Schaad, N. W. and R. D. Frederick (2002). "Real-time PCR and its application for rapid plant disease diagnostics." Canadian Journal of Plant Pathology **24**(3): 250-258.
- Schofield, D. A., C. T. Bull, I. Rubio, W. P. Wechter, C. Westwater and I. J. Molineux (2013). "'Light-tagged' bacteriophage as a diagnostic tool for the detection of phytopathogens." Bioengineered **4**(1): 50-54.
- Schulmeister, T. (1990). "Mathematical modelling of the dynamic behaviour of amperometric enzyme electrodes." Selective electrode reviews **12**(2): 203-260.
- Seskar, M., V. Shulaev and I. Raskin (1998). "Endogenous methyl salicylate in pathogen-inoculated tobacco plants." Plant Physiology **116**(1): 387-392.
- Settle, F. A. (1997). Handbook of instrumental techniques for analytical chemistry, Prentice Hall PTR.
- Shipway, A. N., E. Katz and I. Willner (2000). "Nanoparticle arrays on surfaces for electronic, optical, and sensor applications." ChemPhysChem **1**(1): 18-52.
- Shulaev, V., P. Silverman and I. Raskin (1997). "Airborne signalling by methyl salicylate in plant pathogen resistance.[Erratum: Apr 17, 1997, v. 386 (6626), p. 738.]." Nature.
- Siegbahn, P. E. (2004). "The catalytic cycle of catechol oxidase." JBIC Journal of Biological Inorganic Chemistry **9**(5): 577-590.
- Skottrup, P., H. Frøkiær, S. Hearty, R. O'Kennedy, J. Hejgaard, M. Nicolaisen and A. F. Justesen (2007). "Monoclonal antibodies for the detection of *Puccinia striiformis* urediniospores." mycological research **111**(3): 332-338.
- Skottrup, P., S. Hearty, H. Frøkiær, P. Leonard, J. Hejgaard, R. O'Kennedy, M. Nicolaisen and A. F. Justesen (2007). "Detection of fungal spores using a generic surface plasmon resonance immunoassay." Biosensors and Bioelectronics **22**(11): 2724-2729.
- Skottrup, P. D., M. Nicolaisen and A. F. Justesen (2008). "Towards on-site pathogen detection using antibody-based sensors." Biosensors and Bioelectronics **24**(3): 339-348.
- Sponsel, V. M. and P. Hedden (2010). Gibberellin biosynthesis and inactivation. Plant Hormones, Springer: 63-94.
- Stoll, M., H. R. Schultz, G. Baecker and B. Berkelmann-Loehnertz (2008). "Early pathogen detection under different water status and the assessment of spray application in vineyards through the use of thermal imagery." Precision agriculture **9**(6): 407-417.
- Suneesh, P., K. Chandhini, T. Ramachandran, B. G. Nair and T. S. Babu (2013). "Tantalum oxide honeycomb architectures for the development of a non-enzymatic glucose sensor with wide detection range." Biosensors and Bioelectronics **50**: 472-477.

- Sunesson, A., W. Vaes, C. Nilsson, G. Blomquist, B. Andersson and R. Carlson (1995). "Identification of volatile metabolites from five fungal species cultivated on two media." Applied and Environmental Microbiology **61**(8): 2911-2918.
- Thomas, S. G., A. L. Phillips and P. Hedden (1999). "Molecular cloning and functional expression of gibberellin 2-oxidases, multifunctional enzymes involved in gibberellin deactivation." Proceedings of the National Academy of Sciences **96**(8): 4698-4703.
- Torrance, L., A. Ziegler, H. Pittman, M. Paterson, R. Toth and I. Eggleston (2006). "Oriented immobilisation of engineered single-chain antibodies to develop biosensors for virus detection." Journal of virological methods **134**(1): 164-170.
- Ubeda, C., R. Callejon, A. Troncoso, J. Moreno-Rojas, F. Peña and M. Morales (2012). "Characterization of odour active compounds in strawberry vinegars." Flavour and fragrance journal **27**(4): 313-321.
- Ubeda, C., F. San-Juan, B. n. Concejero, R. M. Callejón, A. M. Troncoso, M. L. Morales, V. Ferreira and P. n. Hernández-Orte (2012). "Glycosidically bound aroma compounds and impact odorants of four strawberry varieties." Journal of agricultural and food chemistry **60**(24): 6095-6102.
- Umasankar, Y., G. C. Rains and R. P. Ramasamy (2012). "Electroanalytical studies on green leaf volatiles for potential sensor development." Analyst **137**(13): 3138-3145.
- Umasankar, Y. and R. P. Ramasamy (2013). "Catalytic Activity of Tyrosinase for Potential Biofuel Cell Application." ECS Transactions **45**(11): 9-14.
- Umasankar, Y. and R. P. Ramasamy (2013). "Highly sensitive electrochemical detection of methyl salicylate using electroactive gold nanoparticles." Analyst **138**(21): 6623-6631.
- Umasankar, Y. and R. P. Ramasamy (2013). "On the bio-electrocatalytic activity of tyrosinase for oxygen reduction reaction." Catalysis Science & Technology **3**(10): 2546-2549.
- Umasankar, Y. and R. P. Ramasamy (2014). "Enhanced Electron Transfer in Enzymatic Bioelectrodes by a Poly (vinyl alcohol) N-Methyl-4 (4'-formylstyryl) Pyridinium Methosulfate Acetal Cationic Polymer." ChemElectroChem **1**(11): 1834-1839.
- Veitch, N. C. (2004). "Horseradish peroxidase: a modern view of a classic enzyme." Phytochemistry **65**(3): 249-259.
- Vidal, J. (2007). "Global food crisis looms as climate change and fuel shortages bite." The Guardian **3**.
- Wang, L.-H. and S.-C. Tu (1984). "The kinetic mechanism of salicylate hydroxylase as studied by initial rate measurement, rapid reaction kinetics, and isotope effects." Journal of Biological Chemistry **259**(17): 10682-10688.
- White-Stevens, R. H. and H. Kamin (1972). "Studies of a flavoprotein, salicylate hydroxylase I. Preparation, properties, and the uncoupling of oxygen reduction from hydroxylation." Journal of Biological Chemistry **247**(8): 2358-2370.
- Williams, K., S. Blake, A. Sweeney, J. Singer and B. Nicholson (1999). "Multiplex reverse transcriptase PCR assay for simultaneous detection of three fish viruses." Journal of clinical microbiology **37**(12): 4139-4141.
- Yamamoto, S., M. Katagiri, H. Maeno and O. Hayaishi (1965). "Salicylate hydroxylase, a monooxygenase requiring flavin adenine dinucleotide I. Purification and general properties." Journal of Biological Chemistry **240**(8): 3408-3413.
- You, I.-S., D. Ghosal and I. C. Gunsalus (1991). "Nucleotide sequence analysis of the *Pseudomonas putida* PpG7 salicylate hydroxylase gene (nahG) and its 3'-flanking region." Biochemistry **30**(6): 1635-1641.

- You, I.-S., R. Murray, D. Jollie and I. Gunsalus (1990). "Purification and characterization of salicylate hydroxylase from *Pseudomonas putida* PpG7." Biochemical and biophysical research communications **169**(3): 1049-1054.
- Zeza, F., M. Pascale, G. Mulè and A. Visconti (2006). "Detection of *Fusarium culmorum* in wheat by a surface plasmon resonance-based DNA sensor." Journal of microbiological methods **66**(3): 529-537.
- Zhang, M., Z. Qin, X. Liu and S. L. Ustin (2003). "Detection of stress in tomatoes induced by late blight disease in California, USA, using hyperspectral remote sensing." International Journal of Applied Earth Observation and Geoinformation **4**(4): 295-310.
- Zhu, J. and K.-C. Park (2005). "Methyl salicylate, a soybean aphid-induced plant volatile attractive to the predator *Coccinella septempunctata*." Journal of chemical ecology **31**(8): 1733-1746.
- Zhuang, Z., X. Su, H. Yuan, Q. Sun, D. Xiao and M. M. Choi (2008). "An improved sensitivity non-enzymatic glucose sensor based on a CuO nanowire modified Cu electrode." Analyst **133**(1): 126-132.

APPENDICES

Appendix A

GenScript Sequence Information

Pseudomonas putida: *nahG* salicylate hydroxylase 1305bp original

```
atgaaaaaca ataaacttgg cttgcgcatac ggtatcgtcg gcggcggaat ttccggcggtt
gccttagcac tggaaactctg ccgctactcc catatccagg tacagctggt cgaggetgcg
ccggctttcg gtgaggtcgg tgccggcgctg tcctttggcc ccaacgcggt gcgcgccatt
gtcggcctgg gcttggggcga ggcctacctg cagggtgccc accgtacttc ggagccctgg
gaggacgtgt ggttcgaatg gcggcgcggc agcgatgcca gctatctggg agccaccatc
gctccggggc tgggcccagtc ctcggtacac cgggcggatt tcatcgacgc cctagtaact
cacctcccag aaggtatcgc ccaattcggg aagcgcgcca cccaggtcga gcagcagggg
ggcgaagtgc aagtgctggt caccgacggc acagagtacc gctgcgacct tctgatcggg
gccgacggaa tcaagtacgc gctccgtagc catgtgctgg aaggtcaggg gctggcccca
caagtgccgc gattcagcgg cacctgtgcc tatcggggga tggtcgacag cctgcatctg
cgagaagcct atcgggcccc tggcatcgac gagcacttgg tggacgtgcc gcagatgtac
ctagggctcg acggccatat cctcaccttt ccagtgagga atggcggcat catcaactgt
gtggctttca tctccgaccg tagcgagccg aagccgacct ggcctgcgga tgccccctgg
gtgctgtgag cgagccagcg cgagatgctc gatgccttcg cgggttgggg ggatgcgcgcg
cgcgccctgc tggagtgcac cccggcacca actctctggg cactgcatga cctggcggag
ctgcccgggct acgtgcacgg tcgggtcgtc ctgatcggcg acgcagctca cgccatgctg
ccgcaccaag gtgcccgtgc tggccaaggg cttgaggacg cctacttctt cgcccgcctg
ttgggcgata cgcaggccga tgccggcaac ctccgagcgc tgcttgaagc ctacgacgac
ctgcccgcgc ctgctgctcg tcgctgtcag caaacctcct gggagaccgg cgagttatac
gagttgcgcg accccgtcgt cgggtgcgaa gagcagctgc tgggggaaaa cctggcgacc
cgcttcgact ggctgtggaa ccacgacctc gacactgacc tggccgaggg ccgtgcgcgg
ctgggttggg agcatggtgg cgggggtgcg ctacgtcaag ggtga
```

Optimized

```
ATGAAAAACAATAAACTGGGTCTGCGTATCGGCATCGTGGGTGGCGGCATCTCGGGCGTTGCTCTGGCTC
TGGAAGTGTGTGCGTACTCACATATTCAGGTGCAACTGTTTGAAGCAGCACCGGCTTTTCGGTGAAGTTGG
TGCAGGTGTCTCGTTTTGGCCGAACGCAGTGCCTGCTATCGTTGGCCTGGGTCTGGGCGAAGCATATCTG
CAGGTGGCTGACCGCACCTCAGAACCCTGGGAAGATGTTTGGTTTCGAATGGCGTCGCGGTAGTGATGCAT
CCTACCTGGGTGCAACGATTGCACCGGGTGTGGCCAAAGCTCTGTGCATCGTGCAGACTTTATTGATGC
CCTGGTCACCCACCTGCCGGAAGGTATCGCCAGTTCGGCAAACCGCAACGCAAGTTGAACAGCAAGGC
GGTGAAGTGCAGGTTCTGTTTACCGATGGTACGGAATATCGTTGCGACCTGCTGATTGGTGTGATGGCA
TCAAGAGCGCGCTGCGCTCTCACGTTCTGGAGGGTCAAGGTCTGGCACCGCAAGTCCCAGCTTTTCAGTGG
TACCTGTGCCTATCGCGGCATGGTGGATTCCCTGCATCTGCGTGAAGCATAACCGCGCTCATGGCATCGAC
GAACACCTGGTTCGATGTGCCGCAGATGTACCTGGGTCTGGATGGCCACATTCTGACCTTTCCGGTGCCTA
ACGGCGGTATTATCAATGTGGTTGCGTTTCATCTCAGACCGTTTCGGAACCGAAACCGACGTGGCCGGCAGA
TGCTCCGTGGGTTTCGTGAAGCAAGCCAGCGCGAAATGCTGGACGCGTTTGCAGGTTGGGGTGATGCAGCT
CGTGCACCTGCTGGAATGCATTCCGGCACCGACCCTGTGGGCTCTGCATGACCTGGCGGAACTGCCGGGTT
ATGTGCACGGTTCGTGTGCTGCTGATCGGTGATGCAGCACATGCAATGCTGCCGCACCAGGGTGCAGGTGC
TGTTCAAGGCTTGAAGATGCGTACTTCTGGCAGCTGTGGTGGTGCACCCAGGCAGATGCAGGCTAAC
CTGGCAGAACTGCTGGAAGCATATGATGACCTGCGTGCCTCGCCGCGTGCATGTGCTGTTTCAGCAACCTCTT
GGGAAACGGGCGAACTGTACGAACTGCGTGACCCGGTTGTGGTCCAACGAACAGCTGCTGGGCGAAAA
TCTGGCAACCCGCTTTGATTGGCTGTGGAATCATGATCTGGACACGGATCTGGCGGAAGCTCGTGTCTGT
CTGGGCTGGGAACATGGTGGTGGCGGTGCTCTGCGTCAAGGCTAA
```

Original

MetKNNKLGLRIGIVGGGISGVALALELCRYSHIQVQLFEAAPAFGEV GAGVSFGPN
AVRAIVGLGLGEAYLQVADRTSEPWEDVWFWRGSDASYLGATIAPGVGQSSV
HRADFDALVTHLPEGIAQFGKRATQVEQQGGEVQVLFTDGTEYRCDLLIGADGIK
SALRSHVLEGQGLAPQVPRFSGTCAYRG **Met**VDSLHLREAYRAHGIDEHLVDVPQ
MetYLGLDGHILTFPVRNGGIINVVAFISDRSEPKPTWPADAPWVREASQRE **Met**LD
AFAGWGDAARALLECIPAPTLWALHDLAELPGYVHGRVVLIGDAAHA **Met**LPHQG
AGAGQGLEDAYFLARLLGDTQADAGNLAELLEAYDDLRRPRACRVQQT SWETGEL
YELRDPVVGANEQLLGENLATRFDWLWNHDLDTDLAEARARLGWEHGGGGALR
QG **Stop**

Optimized

MetKNNKLGLRIGIVGGGISGVALALELCRYSHIQVQLFEAAPAFGEV GAGVSFGPN
AVRAIVGLGLGEAYLQVADRTSEPWEDVWFWRGSDASYLGATIAPGVGQSSV
HRADFDALVTHLPEGIAQFGKRATQVEQQGGEVQVLFTDGTEYRCDLLIGADGIK
SALRSHVLEGQGLAPQVPRFSGTCAYRG **Met**VDSLHLREAYRAHGIDEHLVDVPQ
MetYLGLDGHILTFPVRNGGIINVVAFISDRSEPKPTWPADAPWVREASQRE **Met**LD
AFAGWGDAARALLECIPAPTLWALHDLAELPGYVHGRVVLIGDAAHA **Met**LPHQG
AGAGQGLEDAYFLARLLGDTQADAGNLAELLEAYDDLRRPRACRVQQT SWETGEL
YELRDPVVGANEQLLGENLATRFDWLWNHDLDTDLAEARARLGWEHGGGGALR
QG **Stop**

Appendix B

Primer design for PCR amplification

1. C-terminus

a. Forward primer: GGGAAA**GGATCC**ATG**AAAA**CAATAAACTGGGTCTGC

b. Reverse primer: GGGAAA **AAGCTT****TTA**ATGATGATGATGATGATG**GCCTT**GACGCAGAGCAC

2. N-terminus

a. Forward primer: GGGAAA**GGATCC**ATG**CACCATCACCATCACCAC**

ATGAAAAACAATAAACTGGGTCTGCG

b. Reverse primer: GGGAAA**AAGCTT****TTA**GCCTTGACGCAGAGCA

- Note: red – restriction sites, blue – start and stop codons, green – histidine tag, yellow – structural gene sequence

Appendix C

Primer dilution # 1 for PCR:

Refer to operon datasheet on each primer for correct dilution to 100 μM with primers and DI water

Primer dilution # 2 for PCR (from dilution # 1):

Forward primer	2 μL
Reverse primer	2 μM
DI water	16 μM
Total	20 μM

PCR system:

Polymerase	0.5 μL
pUC57- <i>nahG</i> (template)	1 μL
Primer dilution # 2	5 μL
DMSO	5 μL
dNTPs	5 μL
5 \times Phusion buffer	10 μL
DI water	23.5 μL
Total	50 μL

Restriction enzyme digestion:

BSA diluted 10 \times	5 μL
Buffer	5 μL

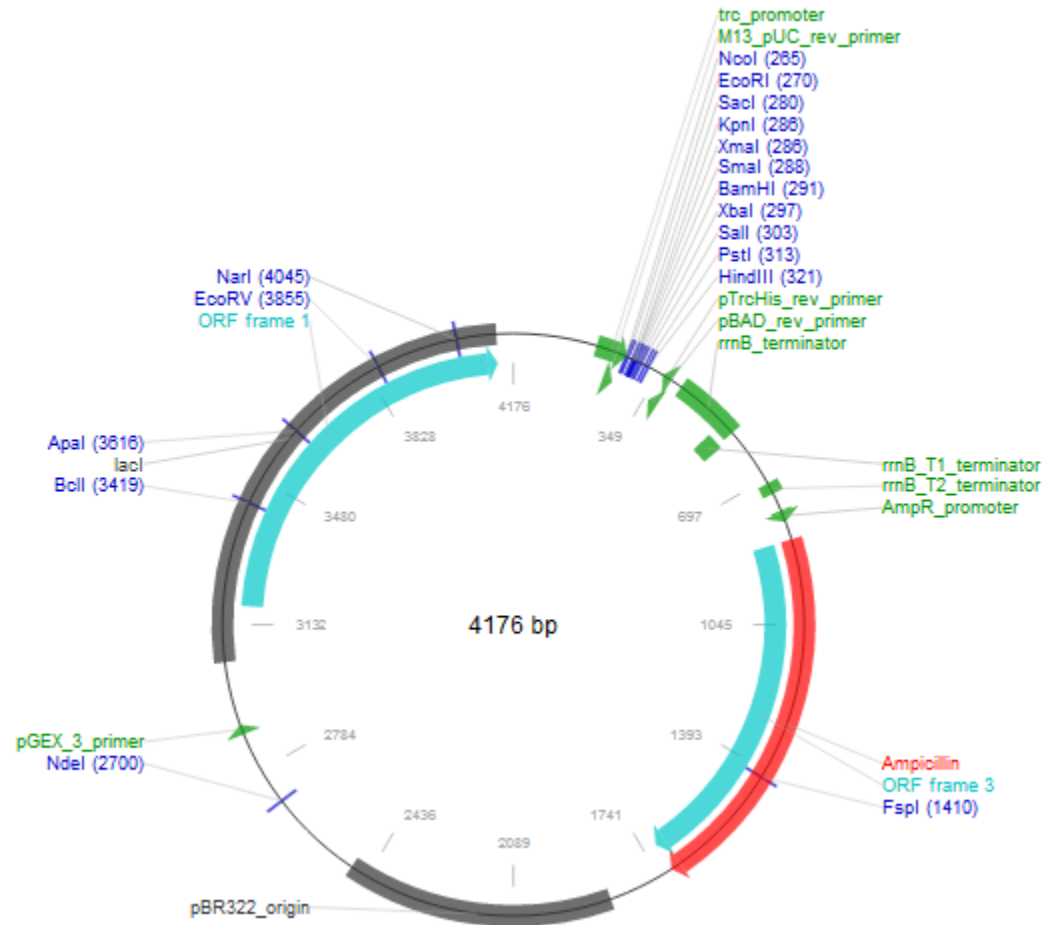
<i>nahG</i> -His-tag (DNA)	14 μ L
BamHI	2 μ L
HindIII	2 μ L
DI water	22 μ L
Total	50 μ L

Ligation:

DNA (<i>nahG</i> -His-tag)	1 μ L
pTrc99A	1 μ L
Ligase	1 μ L
Ligation buffer 2 \times	10 μ L
DI water	7 μ L
Total	20 μ L

Appendix D

The plasmid map of pTrc99A



Appendix E

Enzyme assay for salicylate hydroxylase from crude extract of *E.coli*

	Volume of experimental (μL)	Volume of control (μL)
20 mM Phosphate buffer	180	180
0.1 mM FAD	67	67
1 mM sodium salicylate	100	-
1 mM NADH	160	160
Crude extract of <i>E.coli</i>	5	5
Water	488	588
Total	1000	1000

Enzyme assay for purified salicylate hydroxylase

	Volume of experimental (μL)	Volume of control (μL)
20 mM Phosphate buffer	180	180
0.1 mM FAD	67	67
1 mM sodium salicylate	100	-
1 mM NADH	160	160
Crude extract of <i>E.coli</i>	10	10
Water	483	583
Total	1000	1000

Appendix F

Code of computer controlling system for automatic VOC collection (2 h) and temperature measurement

```
const int temperaturePin = 0;
void setup() {
  // put your setup code here, to run once:
  pinMode (13,OUTPUT);
  pinMode (12,OUTPUT);
  pinMode (11,OUTPUT);
  Serial.begin(9600);
  digitalWrite (12,HIGH);
  digitalWrite (13,HIGH);
  delay(5000);
  digitalWrite (12,LOW);
  digitalWrite (13,LOW);
  delay(1000);
  digitalWrite (11,HIGH);
}

void loop() {
  // put your main code here, to run repeatedly:
  float voltage, degreesC, degreesF;
  voltage = getVoltage(temperaturePin);
  degreesC = (voltage - 0.5) * 100.0;
  degreesF = degreesC * (9.0/5.0) + 32.0;
  Serial.print("voltage: ");
  Serial.print(voltage);
  Serial.print(" deg C: ");
```

```
Serial.print(degreesC);  
Serial.print(" deg F: ");  
Serial.println(degreesF);  
delay(1000);  
}  
  
float getVoltage(int pin) {  
    return (analogRead(pin) * 0.004882814);  
}
```

Appendix G

Enzyme assays of salicylate hydroxylase and tyrosinase

Salicylate hydroxylase assays with different salicylate concentrations (10, 20 and 50 μM) at given concentration of NADH (10, 20 and 50 μM):

	[NADH]=50 μM	[NADH]=20 μM	[NADH]=10 μM
Water	334/329/314	349/344/329	354/349/334
Buffer	100	100	100
0.1 mM FAD	34	34	34
Salicylate hydroxylase	2	2	2
1 mM NADH	25	10	5
1 mM sodium salicylate	5/10/25	5/10/25	5/10/25
Total	500	500	500

Salicylate hydroxylase assays with different salicylate concentrations (10, 20 and 50 μM) at concentration of NADH of 100 μM purged with nitrogen, air and oxygen:

	[NADH]=100 μM
Water	309/304/289
Buffer	100
0.1 mM FAD	34
Salicylate hydroxylase	2
1 mM NADH	50
1 mM sodium salicylate	5/10/25
Total	500

For tyrosinase with different catechol concentrations (10, 20 and 100 μ M):

	Experimental (μ M)	Control (μ M)
Water	390/385/345	395/390/350
0.1 M Phosphate buffer	100	100
1 mM Catechol	5/10/50	5/10/50
Tyrosinase (5 mg/mL)	5	-
Total	500	500

Appendix H

Winkler Titration method for dissolved oxygen measurement

Reagents for Winkler titration:

	Chemicals	Concentration
Reagent I	Manganese (II) chloride	3 M
Reagent II	Sodium iodide	4 M
	Sodium hydroxide	8 M
Reagent III	Sulfuric acid	50 % (v/v)

Winkler titration procedure:

1. Sample 25 mL of assay solution (water and phosphate buffer solution) in the volumetric flask.
2. Add 1 mL of Reagent I into the volumetric flask.
3. Add 1 mL of Reagent II into the volumetric flask. The brownish precipitation (MnO_2) appears. Shake the flask well for oxygen fixation.
4. Add 1 mL of Reagent III into the volumetric flask. Shake the flask well and wait until all the precipitation (MnO_2) disappeared and turned to clear yellowish (I_2) solution.
5. Transfer the solution from the volumetric flask to the conical flask. Titrate the solution using 0.018 M $\text{Na}_2\text{S}_2\text{O}_3$ until the yellowish color turns pale.
6. Add 1 % starch indicator and the solution turns blue.
7. Titrate the solution using 0.018 M $\text{Na}_2\text{S}_2\text{O}_3$ until the blue color disappeared.